Institut für Physik und Astronomie der Universität Potsdam
Physik weicher Materie

Responsive Polymers for Optical Sensing Applications

Dissertation

zur Erlangung des akademischen Grades

"*doctor rerum naturalium*" (Dr. rer. nat.)

in der Wissenschaftsdisziplin Experimentalphysik

eingereicht an der

Mathematisch-Naturwissenschaftlichen Fakultät

der Universität Potsdam

von

Sahika Inal

Potsdam, im Oktober 2013

Published online at the
Institutional Repository of the University of Potsdam:
URL http://opus.kobv.de/ubp/volltexte/2014/7080/
URN urn:nbn:de:kobv:517-opus-70806
http://nbn-resolving.de/urn:nbn:de:kobv:517-opus-70806

Abstract

LCST-type synthetic thermoresponsive polymers can reversibly respond to certain stimuli in aqueous media with a massive change of their physical state. When fluorophores, that are sensitive to such changes, are incorporated into the polymeric structure, the response can be translated into a fluorescence signal. Based on this idea, this thesis presents sensing schemes which transduce the stimuli-induced variations in the solubility of polymer chains with covalently-bound fluorophores into a well-detectable fluorescence output. Benefiting from the principles of different photophysical phenomena, i.e. of fluorescence resonance energy transfer and solvatochromism, such fluorescent copolymers enabled monitoring of stimuli such as the solution temperature and ionic strength, but also of association/disassociation mechanisms with other macromolecules or of biochemical binding events through remarkable changes in their fluorescence properties. For instance, an aqueous ratiometric dual sensor for temperature and salts was developed, relying on the delicate supramolecular assembly of a thermoresponsive copolymer with a thiophene-based conjugated polyelectrolyte. Alternatively, by taking advantage of the sensitivity of solvatochromic fluorophores, an increase in solution temperature or the presence of analytes was signaled as an enhancement of the fluorescence intensity. A simultaneous use of the sensitivity of chains towards the temperature and a specific antibody allowed monitoring of more complex phenomena such as competitive binding of analytes.

The use of different thermoresponsive polymers, namely poly(N-isopropylacrylamide) and poly(meth)acrylates bearing oligo(ethylene glycol) side chains, revealed that the responsive polymers differed widely in their ability to perform a particular sensing function. In order to address questions regarding the impact of the chemical structure of the host polymer on the sensing performance, the macromolecular assembly behavior below and above the phase transition temperature was evaluated by a combination of fluorescence and light scattering methods. It was found that although the temperature-triggered changes in the macroscopic absorption characteristics were similar for these polymers, properties such as the degree of hydration or the extent of interchain aggregations differed substantially. Therefore, in addition to the demonstration of strategies for fluorescence-based sensing with thermoresponsive

polymers, this work highlights the role of the chemical structure of the two popular thermoresponsive polymers on the fluorescence response. The results are fundamentally important for the rational choice of polymeric materials for a specific sensing strategy.

Zusammenfassung

Als Reaktion auf bestimmte äußere Stimuli ändern bestimmte wasserlösliche Polymere reversibel ihren physikalischen Zustand. Dieser Vorgang kann mithilfe von Fluorophoren, die in die Polymerstrukturen eingebaut werden und deren Fluoreszenzeigenschaften vom Polymerzustand abhängen, detektiert werden. Diese Idee ist der Ausgangspunkt der vorliegenden Arbeit, die sich damit beschäftigt, wie äußerlich induzierte Änderungen der Löslichkeit solcher Polymere mit kovalent gebundenen Fluorophoren in Wasser in ein deutlich messbares Fluoreszenzsignal übersetzt werden können. Dazu werden photophysikalische Phänomene wie Fluoreszenz-Resonanzenergietransfer und Solvatochromie ausgenutzt. In Kombination mit einem responsiven Polymergerüst wird es möglich, verschiedene Stimuli wie Lösungstemperatur oder Ionenstärke, oder auch Assoziation-Dissoziation Reaktionen mit anderen Makromolekülen oder biochemische Bindungsreaktionen über die Änderung von Fluorezenzfarbe bzw. –Intensität autonom mit bloßem Auge zu detektieren. Unter anderem wurde ein wässriger ratiometrischer Temperatur- und Salzsensor entwickelt, der auf der komplexen supramolekularen Struktur eines thermoresponsiven Copolymers und eines thiophenbasierten konjugierten Polyelektrolyts beruht. Die Anbindung solvatochromer Fluorophore erlaubte den empfindlichen Nachweis einer Temperaturänderung oder des Vorhandenseins von Analyten. Komplexere Phänomene wie das kompetitive Anbinden von Analyten ließen sich hochempfindlich steuern und auslesen, indem gleichzeitig die Sensitivität dieser Polymeren gegenüber der Temperatur und spezifischen Antikörpern ausgenutzt wurde.

Überraschenderweise wiesen die hier untersuchten thermoresponsiven Polymere wie poly-N-isopropylacrylamid (pNIPAm) oder poly-Oligoethylenglykolmethacrylate (pOEGMA) große Unterschiede bzgl. ihrer responsiven optischen Eigenschaften auf. Dies erforderte eine ausführliche Charakterisierung des Fluoreszenz- und Aggregationsverhaltens, unter- und oberhalb des Phasenübergangs, im Bezug auf die chemische Struktur. Ein Ergebnis war, dass alle drei Polymertypen sehr ähnliche temperaturabhängige makroskopische Absorptionseigenschaften aufweisen, während sich die Eigenschaften auf molekularer Ebene, wie der Hydratisierungsgrad oder die intermolekulare Polymerkettenaggregation, bei diesen

Polymeren sehr unterschiedlich. Diese Arbeit zeigt damit anhand zweier sehr etablierter thermoresponsiver Polymere, nämlich pNIPAm und pOEGMA, das die chemische Struktur entscheidend für den Einsatz dieser Polymere in fluoreszenzbasierten Sensoren ist. Diese Ergebnisse haben große Bedeutung für die gezielte Entwicklung von Polymermaterialien für fluoreszenzbasierte Assays.

List of Abbreviations and Symbols

AB	Anti-DEAC antibody	ΔH_{mix}	Enthalpy of mixing
C_p	Cloud point	ΔS_{mix}	Entropy of mixing
$CHCl_3$	Chloroform	ΔG_{mix}	Gibbs free energy of mixing
CPE	Conjugated polyelectrolyte	ε	Molar extinction coefficient
DMF	Dimethylformamide	δ_t	Hansen solubility parameter of solvents at 25 °C
DP	Nominal number average of monomer repeat units per chain	δ_d	Dispersive term of δ_t
DSC	Differential scanning calorimetry	δ_p	Polar term of δ_t
EG	Ethylene glycol	δ_h	Hydrogen-bonding term of δ_t
FRET	Fluorescence resonance energy transfer	k_r	Radiative decay constant
IR	Infrared	k_{nr}	Non-radiative decay constant
LCST	Lower critical solution temperature	k_T	Rate of FRET
LLS	Laser light scattering	$\lambda^{abs}{}_{max}$	Wavelength of absorbance peak
MEO_2A	2-(2'-methoxyethoxy)ethyl acrylate	$\lambda^{PL}{}_{max}$	Wavelength of maximum emission intensity
MEO_2MA	2-(2'-methoxyethoxy)ethyl methacrylate	M_n^{app}	Apparent number-average molecular weight (from SEC)
NC	Average number of chromophores per chain	M_w^{app}	Apparent mass-average molecular weight (from SEC)
NMR	Nuclear magnetic resonance	$M_{w,app}$	Apparent molecular weight (from SLS)
NOE	Nuclear Overhauser Effect	N_{agg}	Aggregation number
NOESY	2D ^{1}H-^{1}H Nuclear Overhauser Effect Spectroscopy	ρ	Chain density
OEG	Oligo(ethylene glycol)	R_g	Radius of gyration
P3TMAHT	Poly[3-(6-trimethylammoniohexyl)thiophene bromide]	φ	Fluorescence quantum yield
PBS	Phosphate buffered saline	τ	Fluorescence lifetime
PDI	Polydispersity index	τ_{amp}	Amplitude-weighted fluorescence lifetime

pEG	Poly(ethylene glycol)
PL	Photoluminescence
pNIPAm	Poly(N-isopropylacrylamide)
pNIPMAm	Poly(N-isopropylmethacrylamide)
pOEGA	Poly(oligo(ethylene glycol)methyl ether acrylate)
pOEGMA	Poly(oligo(ethylene glycol)methyl ether methacrylate)
PS	Polystyrene
pVCL	Poly(N-vinylcaprolactam)
pVME	Poly(vinylmethylether)
SDS	Sodium dodecyl sulfate
SEC	Size exclusion chromatography
SLS	Static light scattering
UCST	Upper critical solution temperature
UV-VIS	Ultraviolet-visible

τ_{int}	Intensity-averaged fluorescence lifetime
T_g	Glass transition temperature
T_θ	θ temperature

Table of Contents

1 Introduction

1.1 Thermoresponsive Polymers for Fluorescence-Based Sensing

Certain water soluble polymers respond to very weak global or local external stimuli with a substantial change of their physical state or in chemical properties.[1] Fundamentally, most of the macromolecules of living systems, e.g. nucleic acids, proteins, and polypeptides, have the ability to adopt their structures specific to their surroundings as they perform in physiological processes.[2,3] With their nonlinear and bulk response, synthetic responsive polymers are therefore considered to be biomimetic and have the potential to match nature's performance.[4-7] Depending on the physical form of the polymeric material, the response might manifest itself in various ways, e.g., as an alteration in aqueous solubility, self assembly behavior, volume or in surface characteristics (Scheme 1-1).[4,8,9] A change in temperature,[6,10] pH,[11] ionic strength,[12,13] light,[14] or in electrical or magnetic field,[15,16] the presence of certain chemical species,[17] or a combination of these have been reported so far to trigger the response mechanism. Moreover, once the stimulus is withdrawn, the polymer chains return back to their original state.[18] The reversibility is the key feature due to which these materials can mimic classical patterns known from engineering applications. As the response is an intrinsic property, i.e. not imparted to the polymer by an additional moiety, responsive polymers are also termed as *smart polymers*.

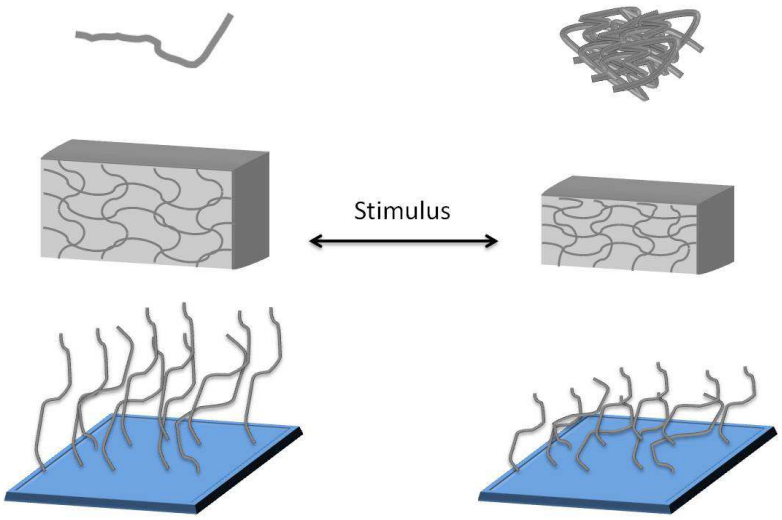

Scheme 1-1: Schematic representation of a stimuli-responsive polymer in different physical forms, including an aqueous solution, a macro- or micro-gel, and a surface attached comb-like structure immersed in water. The polymer responds reversibly to the applied stimulus with a change in its physical structure. In this work, the responsive polymers are investigated in their aqueous solutions.

Since the discovery of synthetic responsive polymers, a considerable amount of work has focused on understanding the processes involved in the response mechanism. The gained knowledge is then employed to develop strategies applying these materials in emerging technologies. Due to their compatibility with biological systems,[19] research activities biased towards the bio-related applications including targeted drug delivery,[20,21] tissue engineering,[22] bio-separation (chromatography),[23] and physical, chemical or biological sensing.[24,25] For the latter, responsive polymers are particularly attractive because it is the relatively small perturbations at the molecular scale which can bring about dramatic transformations in macroscopic properties of the material.[2] Achieving such (high) level of sensitivity has been the driving force of the sensor research for several decades. Given its facile and remote operation, ***fluorescence*** is by far the most applied method to monitor an environmental parameter.[26] Also, depending on the fluorophore and on the detection technique, the read-out signal appears in variety of forms such as the lifetime, intensity or anisotropy of fluorescence. As many of the conventional small molecular probes suffer from limitations such as poor water solubility, low quantum yield, and low structural stability,[24] fluorescent dyes are typically integrated within polymer scaffolds. For this reason, when used as the polymeric material, in addition to its active participation in the sensing event, the responsive polymer provides structural support to the dye, as well.[24]

Since pathological activities are typically associated with abnormal temperatures, accurate monitoring of an increase in temperature is important for the diagnosis of certain

diseases.[27] In the last few decades, quite a few fluorescent temperature probes with a considerable structural variety have been developed benefitting from the intrinsic response of ***thermoresponsive*** polymers.[24,28,29] Thermoresponsive polymers demix from the homogenously mixed aqueous phase when heated to temperatures above their *lower critical solution temperature* (LCST). This (LCST-type) phase transition is associated with the transformation of polymer chains from a hydrated and expanded state to a relatively more hydrophobic and collapsed one (cf. Scheme 1-1). Typically, incorporating fluorescent probes that are amenable to a change in character, e.g. charge, polarity, or solvency,[2,3] along the polymer backbone allows remote monitoring of these temperature-induced changes in chain conformation through fluorescence characteristics.[24,28] Different fluorophore-based concepts, e.g. solvatochromism, fluorescence resonance energy transfer (FRET), charge transfer, aggregation-induced emission, or excimer/exciplex formation, can be exploited to obtain an optical signal.[28] A simplified representation of fluorometric detection platforms based on two prevalent fluorescence concepts, namely *FRET* and *solvatochromism*, is depicted in Scheme 1-2.

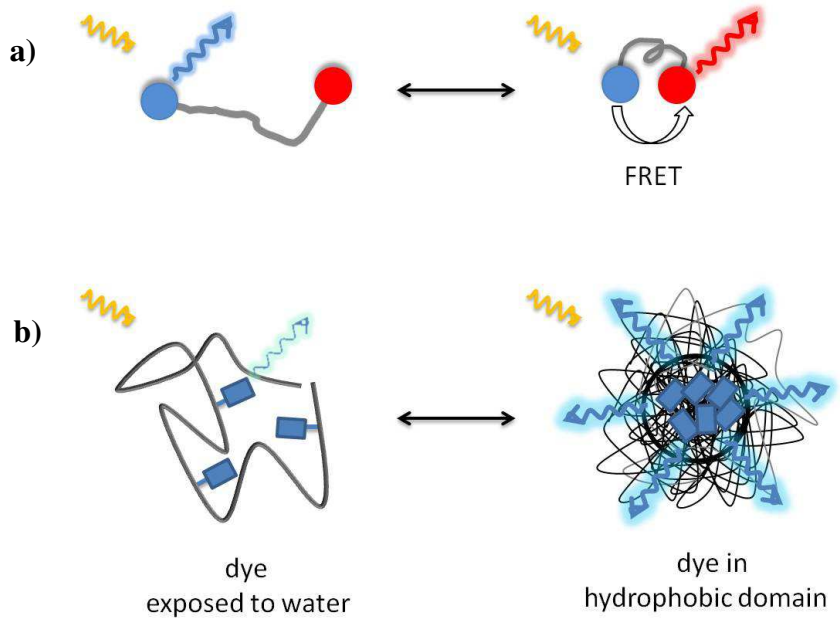

Scheme 1-2: Schematic representation of dye-labeled thermoresponsive polymer-based sensing platforms relying on **a)** the changes in FRET efficiency, **b)** the intrinsic sensitivity of a solvatochromic dye to the micro-environment.

In the first approach, a single thermoresponsive chain is labeled with a FRET donor and acceptor at the two terminals.[30] An increase in temperature triggers the dehydration and subsequent collapse of the chain, which is initially in an extended conformation. This brings the FRET pair in close proximity. Since the efficiency of FRET increases as the distance between the two dyes is reduced; the emission of the donor dye is quenched and its energy is

transferred to the (fluorescent) acceptor dye. Consequently, increasing the solution temperature above the LCST, i.e. switching between "open" and "closed" states of a chain, can be monitored via the fluorescence spectrum of the solution, ideally as a change of the emission color. The same principle would apply as a swollen gel shrinks, surface-grafted chains collapse, or multiple chains aggregate into globular structures.

The second approach takes advantage of the optical properties of solvatochromic dyes readily sensitive to the nature of their micro-environment. Such dyes change color and/or their fluorescence yield in response to changes of the environmental polarity.[31] Attached to the thermoresponsive chain, the fluorophore is well exposed to water molecules before the transition takes place (Scheme 1-2b). Heating the solution above the LCST leads to the formation of multi-chain aggregates of dehydrated chains, i.e., mesoglobules[*].[1] Within these polymer-rich domains, the dye´s surrounding is relatively nonpolar, which alters its fluorescence properties. The polymer therefore acts as a probe for temperature. Since the response is reversible, such temperature sensing platforms offer continuous detection and quantification. Moreover, the thermoresponsive polymer can easily be furnished with other functionalities, for instance by copolymerization of monomers with different stimuli-responsiveness, providing opportunities for the development of multifunctional materials.[24,32] Also, adjustable properties of polymers such as porosity, biocompatibility, or mechanic strength make the polymer based systems ideal candidates for specific detection purposes. This practically enables their use in various media.[26]

Apart from changes in temperature, fluorescent thermoresponsive polymers can signal the presence of certain metal ions, e.g. Hg^{2+} or Cu^{2+}, which alter the emission properties of the fluorophores that they bind to.[33-36] In such sensing strategies, the intrinsic polymer response is utilized to endow a second functionality,[24] or to modulate the detection efficiency in terms of selectivity and sensitivity by tuning the spatial arrangement of the sensing components.[34] Alternatively, for chemo-sensing purposes, an additional receptor moiety, i.e. a functional group interacting with chemically relevant species, can be integrated into the responsive polymer. These interactions affect the hydrophilicity-hydrophobicity balance of the chains, and thereby their aqueous solubility, meaning that the polymer exhibits responsive behavior at isothermal conditions when exposed to certain chemical/biological molecules. This approach is therefore a form of biomimicry since many biomacromolecules are known to alter their conformation and degree of self-assembly in response to the presence of specific chemical

[*] Adjusted by the solution concentration, the polymer chains above the LCST can form stable dispersions of aggregates, named "mesoglobules" with sizes in the 50 nm up to lower µm range.

species in their surroundings.[2] An example of such analyte-induced change in chain solubility is given in Scheme 1-3.

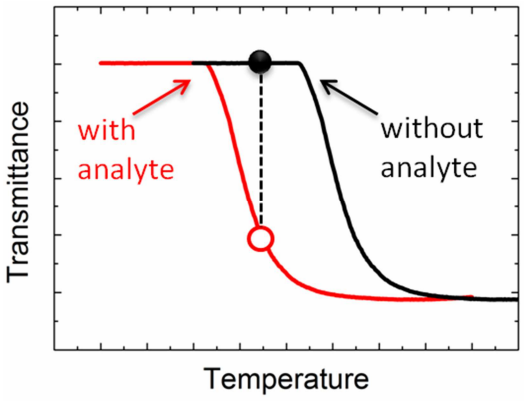

Scheme 1-3: Schematic representation of a change in the aqueous solubility of a thermoresponsive polymer upon its interaction with an analyte. The black curve is the turbidity profile of the polymer and the red one represents that after binding of the analyte.

Judging by the transparency of the solution, the chains are well soluble at the designated point before the addition of the analyte. In the example above, as the target analyte interacts with the polymer, the increase in the overall hydrophobicity leads to the collapse of the chains, resulting in the increased scattering. In other words, the recognition event shifts the LCST of the polymer to lower temperatures. The binding of the analyte might as well cause an opposite effect and elevate the LCST. As for temperature, these analyte-induced changes in chain conformation/aggregation behavior can be observed as alterations in the fluorescence properties of the dye. This means that the molecular recognition event *isothermally* triggers a fluorometric response.[37-41] For instance, thermoresponsive N-isopropylacrylamide (NIPAm) based micro-gels bearing phenylboronic acid groups and CdS quantum dots swell upon recognition of the analyte, glucose, by phenylboronic acid moieties.[37] The swelling of the network is due to an increase in the number of anionic boronate groups, which then brings about interfacial states quenching the emission of the quantum dots. This decrease in fluorescence intensity is directly correlated with the increase in glucose concentration. A fluorogenic ion sensor based on NIPAm units, an ion-receptor, and an environmentally sensitive dye works in the opposite way: Upon interaction of the receptor with target ions, the polymer coils undergo a three-dimensional conformational change to a globular form due to increased inter-polymer interactions, leading to an enhanced fluorescence signal.[38] Such molecular recognition events might also proceed via analyte specific-chemical reactions. However, despite being very selective, this type of sensing is not reusable due to the irreversible nature of such reactions.[24]

The approaches summarized above offer a possibility to switch and/or manipulate the emission signal by a physical stimulus or by a recognition event; they therefore render the use of water soluble responsive polymers quite inspiring and attractive for physical/chemical sensing applications. So far, the majority of the materials used in such sensing schemes have been based on poly(N-isopropylacrylamide) (pNIPAm).[24] Despite its wide popularity, pNIPAm has some disadvantages, such as the inadequate reversibility of the response, toxic amines produced during hydrolysis and unspecific interactions with proteins.[42,43] This triggered investigations on other type of polymers, which exhibit a LCST-type phase transition. The recent decade has therefore seen an expansion in the number of reports on poly(meth)acrylates bearing oligo(ethylene glycol) (OEG) side chains, a few of which were about such fluorescence-based sensing platforms.[30,31,44] The LCST of these polymers is easily tuned either by changing the length of OEG units of the (meth)acrylate-derived macromonomer or by copolymerization of macromonomers bearing different number of EG units[*], advantageous to build probes working at various temperature ranges. Also, the transition exhibits better reversibility than that of pNIPAm,[45] crucial for accurate and reliable probes.[28] Owing to the well-established non-toxicity and the resistance to nonspecific protein adsorption and to cell adhesion that the poly(ethylene glycol)s (pEGs) feature, these polymers are suggested to be well suited for bio-related applications.[46]

However, for a particular sensing scheme, such as the ones depicted in Scheme 1-2, to work efficiently, the responsive polymer needs to fulfill certain properties other than simply being thermoresponsive or possessing the envisaged chemical structure, e.g., the accurate position of donor-acceptor dyes along the chain or a particular initial distance between them. For instance, for the solvatochromic approach, if the globules formed are not dense with the polymeric material, a significantly large solvatochromic shift does not occur. Similarly, for the FRET approach, if chains do not efficiency dehydrate and collapse, it is unlikely to observe a ratiometric fluorescence change. Such outcome is related to the chemical structure/architecture of the polymer, and is however subtle at a macroscopic scale and cannot be anticipated beforehand solely from the chemical structure. For instance, the solutions of most thermoresponsive polymers become comparably turbid above the LCST-type transition, evidenced by temperature-transmission profiles such as the one shown in Scheme 1-3. However, recent studies on the basis of temperature dependent nuclear magnetic resonance (NMR) and infrared (IR) spectroscopy show that the mechanisms involved in the solubility

[*] For instance, thermoresponsive copolymer p(MEO_2MA-*co*-OEGMA) was prepared by random copolymerization of 2-(2'-methoxyethoxy)ethyl methacrylate (MEO_2MA) monomer which bears 2 EG units with oligo(ethylene glycol)methyl ether methacrylate (OEGMA) monomer which has 8-9 units of EG. By changing the ratio of these macromonomers, the LCST can be tuned between 28 and 90 °C [80].

transition of different polymers, e.g. pNIPAm, p(MEO_2MA-*co*-OEGMA) (the copolymer of 2-(2'-methoxyethoxy)ethyl methacrylate (MEO_2MA) with oligo(ethylene glycol)methyl ether methacrylate (OEGMA)), or poly(N-vinylcaprolactam) (pVCL), feature certain peculiarities.[42] For instance, although pNIPAm chains exhibit a strong precontraction process, the phase transition of p($MEO_2MA_{0.95}$-*co*-$OEGMA_{0.05}$)* is found to arise mostly from multiple chain aggregations.[42,47] Also, the changes in the conformation of p(MEO_2MA-*co*-OEGMA) chains start sharply at temperatures below the LCST and continue gradually above the LCST.[44] With this behavior, the copolymer is reported to be similar to pVCL, but in contrast with pNIPAm. The pVCL chains expel water molecules continuously upon increasing temperature, while pNIPAm mesoglobules do not exhibit a distribution of water molecules ranging from a hydrophobic core to a hydrophilic surface and the water content therein is relatively stable against further heating.[48] Moreover, the results of fluorescence anisotropy and excimer formation/disruption studies probing the LCST transition of pVCL suggest that the transition of pVCL is not as sharp or as intense as that observed for pNIPAm.[49]

Although particularly useful, a possible influence of the chemical structure of the polymeric material on the performance of these fluorescent sensors has not yet been elaborated. However, there are implications of the importance of such structural considerations elsewhere. For instance, just recently, Gibson *et al*. reported two responsive polymers based on p(MEO_2MA-*co*-OEGMA) and pNIPAm which were functionalized at one of the chain ends with pyridyl disulfide.[50] Selective cleavage of these disulfide linked end-groups by glutathiones led to coil-to-globule collapse at isothermal conditions. The LCST transition was evidenced from the enhanced turbidity of the aqueous polymer solutions. Interestingly, although both polymers exhibited such collapse and aggregation triggered by an increase in the local glutathione concentration, OEGMA-based copolymer showed a "slower" response. This was attributed to a difference in the accessibility of the end groups as a function of polymer side chain length. Moreover, at the end of experimental time, the change in turbidity was "greater" for pNIPAm.[50] This reflects differences in the scattering intensity of any aggregates formed. Consequently, the different response qualifies a main incompatibility of OEGMA-based polymers for such specific methodology.[51]

If the nature of the structural adaptations is governed by the chemical and the topological structure of the polymer, the efficiency of a fluorescence-based sensing event must also be specific to the polymer. An evolution of the aggregation properties of the chains

* This is a copolymer of MEO_2MA and of OEGMA, which contains 95 mol% and 5 mol% of each monomer, respectively.

before and after the LCST-type transition and of the structural features that determine these properties may therefore be the key for a good understanding of the performance of fluorescence-based sensing with responsive polymers. By controlling such structure-property relationship, it is possible to design really *smart* and efficient systems for optical sensing applications.

1.2 The Aim and Outline of this Thesis

This work was conducted within the project "Taschentuchlabor", the ultimate goal of which has been to develop platforms for fast diagnostics of certain pathogens with an optical read-out. Therefore, the *main aim* of this work was to evaluate proof of concept sensing schemes based on fluorescent thermoresponsive copolymers. In the previous section, I exemplified some basic sensing schemes that rely on the LCST transition. By using such photophysical phenomena, we envisaged to translate changes in chain conformation/aggregation properties into an optical output signal. In this way, one could monitor association/disassociation mechanisms of polymer assemblies (Chapter **3**), a change in solution temperature (Chapter **3**-**4**-**5**) or in ionic strength (Chapter **3**), and ultimately the presence of biological macromolecules (Chapter **5**) through a well-detectable fluorescence signal, i.e., a change in emission color, intensity, or lifetime.

After a brief introduction to the topics of importance, i.e. the phase transition of thermoresponsive polymers, conjugated polyelectrolytes (CPEs) and photophysical aspects of sensing with fluorophores (**Chapter 2**), I will present a promising candidate towards an aqueous dual-color probe for temperature and salts, benefiting from the *FRET* approach but in an alternative way than what is described above (**Chapter 3**). Instead of a dual-dye labeled chain, a supramolecular assembly formed between a dye-labeled thermoresponsive copolymer and a thiophene-based CPE performs the sensing event. The signal transduction in this system relies on the "unspecific" interactions between the non-ionic p(MEO_2MA-*co*-OEGMA) being the FRET donor and the cationic CPE as the acceptor. These inter-polymer interactions result in efficient FRET at room temperature, i.e., well below LCST. However, heating of the mixture weakens the interactions, the extent of which is simultaneously monitored as a decrease of FRET efficiency. Interestingly, the efficiency of temperature sensing depends strongly on the presence of salts, caused by the fact that the inter-polymer interactions are salt-tunable, rendering this assembly with double-stimuli sensitivity. Presenting the potential of this system to be a dual-sensor, the chapter includes a comprehensive discussion on the thermoresponsive behavior of the OEGMA-based copolymer in the presence of alkali chlorides and of a charged macromolecule, studied with ultraviolet-visible (UV-VIS) absorbance, fluorescence, ^{1}H NMR, and laser light scattering methods.

While evaluating the performance of the sensing approach depicted in Scheme 1-2b, I observed a clear dependency of the sensitivity on the chemical structure of the host polymer. This identified the *secondary goal* of this work, i.e., to understand the optical properties of these systems under consideration of the specific polymer structure and to highlight structural considerations for the specific case of sensing with a fluorescence response. This topic is addressed particularly in **Chapter 4** which demonstrates the differences in the temperature-regulated fluorescence response of a *solvatochromic* probe (a naphthalimide dye) attached to three different thermoresponsive polymers. The polymers in comparison are based on either NIPAm or on (meth)acylate backbone bearing OEG side chains. While the NIPAm-based copolymer acts as a molecular sensor for temperature, temperature has no specific effect on the emission properties of OEG-based copolymers. Through a combination of photophysical and light scattering studies, these findings are ascribed to substantial differences in the solubility behavior of each polymer.

The following **Chapter 5** presents a novel multi-functional polymer which can adapt its structure not only in response to temperature but also to a specific protein. Using copolymers based on either pNIPAm or p(MEO_2MA-*co*-OEGMA), the sensing strategy is the same as in Chapter **4**, but with a different *solvatochromic* dye, an amino coumarin derivative (DEAC). Besides its ability to detect changes in solution temperature, the fluorescence properties of the NIPAm-based copolymer change remarkably in the presence of the protein, namely an anti-DEAC antibody. The recognition event proceeds through the specific binding of the antibody to the fluorophores, which can be facilely monitored also via the turbidity profile. The chapter furthermore demonstrates how to control the molecular recognition and monitor competitive binding events by utilizing the intrinsic response of the polymer to temperature. Also, as with the naphthalimide case of the previous chapter, whether the polymer exhibits a fluorescence response to the applied stimuli depends on its chemical structure.

Lastly, I will summarize the main conclusions of this work in **Chapter 6**, and an overview of the sample preparation methods and experimental techniques is provided in **Chapter 7**.

2 Fundamentals

This chapter gives a brief introduction into the basic concepts of the phase transition phenomenon of thermoresponsive polymers, the use of conjugated polyelectrolytes, and of photophysical phenomena employed in fluorescence-based sensing schemes. A more detailed consideration of processes relevant for the understanding of a certain type of sensing strategy can be found in the respective chapter.

2.1 Phase Transition of Thermoresponsive Polymers

The solubility of all synthetic and natural polymers depends on temperature.[1] In other words, a polymer which is molecularly dissolved in a solvent can become insoluble and precipitate from the solution upon increasing or decreasing the temperature.[52] As the temperature increases, the polymers which become miscible with the solvent display an upper critical solution temperature (UCST), while those that demix from the solution, the reverse case, exhibit a LCST.[53] Such temperature-induced reduction in the solubility of polymer chains results in the formation of two phases which contain a higher amount of either of the components; the polymer or the solvent molecules.[52] The phase separation is typically described with an isobaric *phase diagram* in which temperature is plotted against polymer concentration (Figure 2-1). These diagrams are constructed on the basis of the free energy of mixing of two components. For polymers, the relevant theory explaining the solubility behavior and their phase diagrams is the *Flory-Huggins lattice theory* which considers the combinatorial entropy (number of molecular arrangements during mixing) and the interaction energy between different segments. Appendix A summarizes the basic equations of this theory.

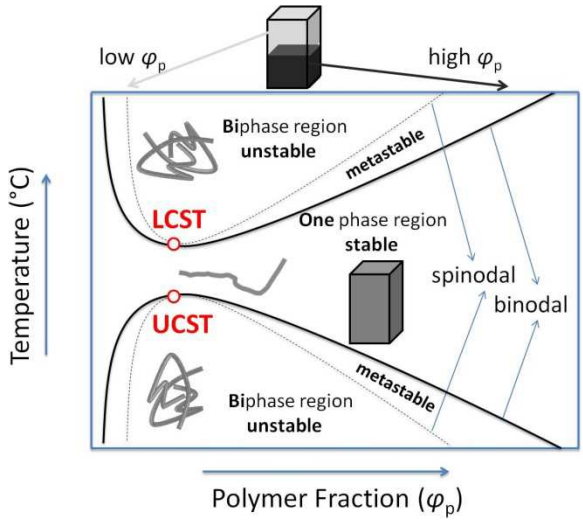

Figure 2-1: Schematic phase diagram (polymer fraction *vs*. temperature) of a polymer solution exhibiting LCST- or UCST-type behavior.[1,52,54]

In phase diagrams, the **binodal** (coexistence) curve represents the equilibrium separation boundary between the one- and the two-phase region.[1] In one phase region, the polymer is homogenously dissolved, thereby forming a single liquid phase. Across the binodal, the transition is from complete miscibility to conditions where the solution is metastable or stable. The **LCST** or **UCST** above which this reversible demixing or mixing transition occurs is designated as the minimum or the maximum of the binodal curve and can therefore be found at a distinct critical concentration.[7,54] For other concentrations, the temperature at which the phase separation occurs, i.e. the phase transition temperature, is a point on the binodal curve. The curve that merges the binodal at the critical point is called the **spinodal**. The spinodal curve separates the metastable region from the unstable region in the biphasic solution. The distinct compositions in these regions are relevant to the mechanism of phase separation. For instance, in the unstable region bounded by the spinodal, the system phase separates spontaneously instead of uniformly by nucleation and growing, promoted by small concentration fluctuations. In contrast, in the metastable region, the phase separation occurs similar to crystallization, i.e., relatively large concentration fluctuations must take place with a large energy cost.[55]

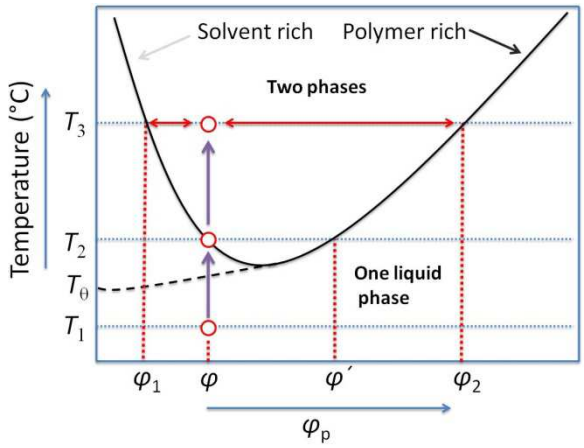

Figure 2-2: An idealized phase diagram (polymer fraction *vs*. temperature) of a polymer solution exhibiting a LCST-type behavior.[1,52,54] The composition of the coexisting phases at a given temperature can be found by drawing a tie-line between the two branches of the binodal curve.[54]

Considering a strictly binary polymer solution, the binodal is employed to determine the composition of each phase, i.e. the polymer-rich and the solvent-rich, at a designated temperature. In Figure 2-2, at temperature T_1 with an overall polymer concentration of φ in the solution, the polymer is completely miscible with the solvent. As the temperature of the solution is raised to T_2, which is the phase transition temperature for this concentration, phase separation sets in.[54] Further increase of the temperature to T_3 results in the formation of two phases, one of which contains a higher fraction of the polymer (φ_2) than the other (φ_1). For the construction of typical phase diagrams, see Appendix B.

Also depicted in Figure 2-2 is the θ-temperature (T_θ) which is the extrapolated minimum of the binodal of a polymer of an infinite molar mass.[54] According to *Flory theory*, as the length of the polymer chain increases, the solubility of the polymer decreases and the upper or lower critical solution temperature shifts towards zero polymer composition in the solvent-rich region. The asymmetry of binodal, as the one exemplified in Figure 2-1, is indicative of the dissimilarity between the sizes of mixing components. Nevertheless, not all thermoresponsive polymers follow this trend and three types of LCST behavior can be distinguished according to the critical miscibility behavior.[56] The polymers, such as pVCL, which are in accordance to the Flory theory, are classified as Type I. Type II polymers have the LCST independent of the chain length and a typical example is pNIPAm. Finally, Type III polymers are characterized by two critical points for low and high polymer concentrations corresponding to the Type I and Type II behaviors, respectively, an example for such is poly(vinylmethylether) (pVME).[1] The shape of phase diagrams is furthermore informative about the phase transition behavior. For instance, for polymers exhibiting a LCST behavior that is only weakly concentration dependent, the binodal has a flat minimum. If the binodal

extends far into the polymer-rich region, it is expected that the phases that are formed are dense.[54] For example, pNIPAm includes 52 wt% water in the polymer-rich phase at 40 °C above its phase transition temperature (=31 °C).[57] Polymers exhibiting effective phase separation, i.e. almost pure composition of each phase, are suggested to have a low glass transition temperature (T_g).[1,58]

Both LCST and UCST phenomena happen according to energetic considerations, driven by entropic and enthalpic gain.[1] For the miscibility of a polymer in a solvent, the change in the free energy of the components must always have a negative value. Gibbs free energy of mixing (ΔG_{mix}), i.e. the difference between the enthalpic (ΔH_{mix}) and the entropic (ΔS_{mix}) contribution, is given as:

$$\Delta G_{\mathrm{mix}} = \Delta H_{\mathrm{mix}} - T\Delta S_{\mathrm{mix}} \qquad \textit{Equation 2-1}$$

According to Equation 2.1, sufficiently positive entropy of mixing or a negative heat of mixing lowers the ΔG_{mix}. In most cases the attractive forces between similar repeat units are stronger than those between different units, enabling that $\Delta H_{mix}>0$. On the other hand, ΔS_{mix} is larger than zero with a strong dependence on the chain length.* At lower temperatures this unfavorable energy effect predominates over the positive entropic term and phase separation occurs.[59] This is typical for the UCST behavior, for which the solubility increases with the increase in temperature.

LCST-type polymers are miscible with water due to the presence of polar groups involved in hydrogen-bonding interactions. However, the polymer structure also includes segments that are not favorably in contact with water. In addition to the specific ordering of water due to attractive interactions with hydrophilic moieties, these hydrophobic segments enforce water molecules to organize into an ordered structure, which is known as the "hydrophobic effect".[1] Being in such a structural order, water molecules lack of orientational freedom. In these conditions, ΔS_{mix} has a low negative magnitude, while due to hydrogen-bonding interactions ΔH_{mix} is negative, too.[59] Therefore, there is a delicate boundary between solubility and insolubility, which can be modulated by the other variable in the equation: temperature. As temperature increases, constrained water molecules gain more mobility and break the hydrogen bonds with the polar moieties of the polymer. This is why LCST-type phase separation is an entropy driven process.[10] For both ΔH_{mix} and ΔS_{mix} being negative, ΔG_{mix} becomes positive as $|T\Delta S_{\mathrm{mix}}| > |\Delta H_{\mathrm{mix}}|$ and phase separation occurs. This means that

* For polymers exhibiting an UCST-type transition, as combinatorial entropy always favors mixing, it is the energetic interactions between mixing components, which governs whether a homogenous mixture is formed. Nevertheless, due to the long chain character of polymers, the entropic contribution to mixing is very small.

attractive interactions between or within polymer chains become more favorable than their interactions with water. Rather than a complete change from a hydrophilic to hydrophobic state,[60] the polymer chains minimize encounters with water molecules and eventually collapse above the LCST.

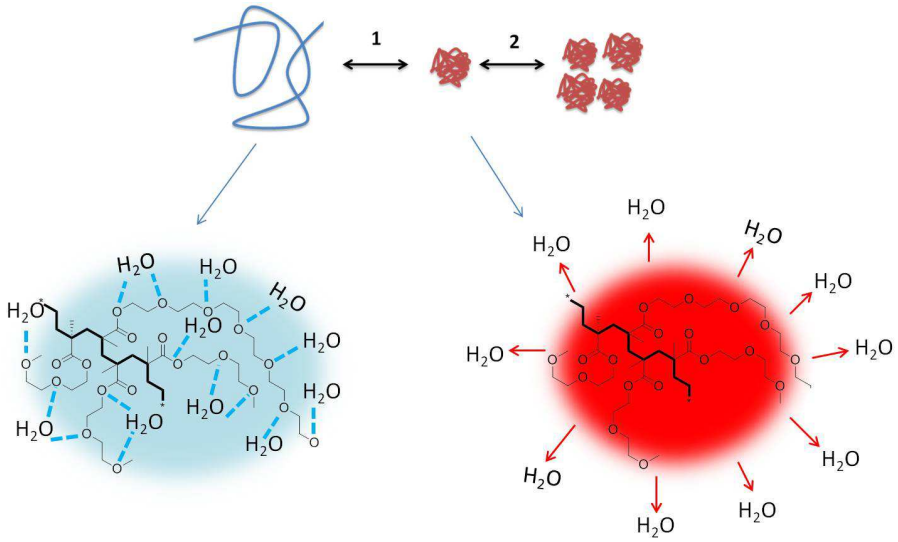

Scheme 2-1: Upper panel: the temperature induced changes triggered in the conformation of an OEG-bearing thermoresponsive polymer chain, 1: Coil-to-globule transition, 2: Subsequent aggregation of globules into mesoglobules. Lower panel: favorable hydrogen bonds with water are disrupted and water is expelled from the structure in the collapsed state.

This temperature-induced change in solubility of polymer chains is known as "coil-to-globule transition" (cf. Scheme 2-1), and can be experimentally observed, e.g. by laser light scattering, for very dilute solutions of thermoresponsive polymers.[47] For more concentrated solutions, the association of these globules into multi-chain aggregates follows the coil-to-globule transition, leading to two phases. However, in most cases, instead of precipitation and formation of macroscopic phases, solutions above the LCST consist of colloidally stable aggregates, the so-called "mesoglobules", in the size of 50 nm up to lower micrometer range.[61-68] Studies showed that particles which are relatively fluid right after phase transition temperature do merge and grow as the solution is heated up to a certain temperature, above which rigid stable spheres are formed.[61] Different theories about how this stability is maintained have been proposed and possible reasons have been comprehensively discussed.[69] Electrostatic repulsions between the aggregates, due to a small number of solution ions accumulating on the globules or due to the presence of ionic groups in case of the intrinsically ionic polymers, were held responsible to prevent colloidal coalescence.[61,66,70,71] For non-ionic polymers, Aseyev *et al.* attributed the formation of stable dispersions of mono-disperse spherical particles to steric stabilization provided by rather hydrophilic segments of the

polymer preferentially accumulating at the surface of globules.[62] Others have reasoned the lack of association between mesoglobules to a viscoelastic effect.[65] The time required for a chain of a globule to establish permanent entanglements with another globule is proposed to be longer than the contact time of the globules upon collision, leading ineffective connections.[72] This is promoted if the polymer-rich phase vitrifies partially above the LCST, slowing down chain motion and enhancing resistance toward merging.[66,73]

Note that what is shown in Scheme 2-1 is an idealized picture for the dehydration and inter-aggregation mechanisms. Typically, the LCST-type transition behavior depends on the type of the polymer,[42] but also on factors such as the thermal history.[61,74] For instance, the rate of heating can effectively modulate the influence of intrachain collapse and interchain association mechanisms and govern the dominance of one over the other.[72,74] Such factors were reported to affect the structure, e.g. the size and the weight, of the mesoglobules.[61,62,67]

2.1.1 Probing the Phase Transition

The phase transition of LCST-type polymers can be probed by a variety of methods including laser light scattering, UV-VIS, differential scanning calorimetry (DSC), NMR, viscosity, and fluorescence techniques. Since each method probes the changes of a different polymer property, they provide complementary information. For the same reason, the phase separation temperature which is deduced from each technique might differ. The most common method is to record the transmission of the solution while its temperature is gradually changed. Due to the formation of polymer-rich aggregates, the originally transparent solution becomes turbid after passing the LCST. From a turbidity profile such as the one shown in Figure 2-3, the beginning of the demixing process, i.e. the onset of solution clouding, known as the “cloud point” can be determined. The broadness of the profile might be indicative of how long and strongly the phase separation proceeds. It might also give an idea about the polymer´s polydispersity, if the phase separation temperature depends on the chain length, or about a copolymer´s homogeneity in terms of its composition.[75] A broad transition window range was also attributed to the partial pre-aggregation of chains before the phase transition sets in.[76]

Generally, in the reverse cycle, i.e. cooling the solution down below the cloud point (C_p), a hysteresis is seen. Hysteresis occurs due to differences in the kinetics of collapse-aggregation and of dissolution-deentanglement, resulting in mismatches of the value of C_p observed upon heating and upon cooling. The rate of dissolution is slower if hydrogen bonds are formed within and between polymer chains in the collapsed state.[77-79] These bonds act as

crosslinking points for dehydrated chains and retard their dissolution. Also, partial vitrification of the polymer-rich phase was suggested to slow down re-mixing.[68,73]

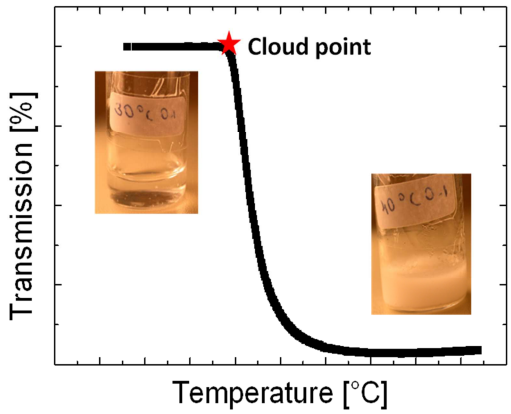

Figure 2-3: Temperature *vs*. transmission profile of a LCST-type aqueous polymer solution. As the temperature increase, phase separation takes place. The cloud point (C_p) is designated as the initial drop of transparency. The pictures are taken for a solution well below and above its C_p.

As thermoresponsive polymers form macromolecular associates or aggregates in aqueous solutions, typically triggered by changes in solution temperature, laser light scattering has been a popular technique to probe the phase transition. By measuring the amount of the scattered light from the polymer solution during a heating/cooling cycle as a function of the scattering angle, the evolution of the particle size can be deduced. A combination of static and dynamic light scattering measurements gives more structural information, such as the density, the polydispersity, the weight of the structures, and the number of accumulated chains in a multi-chain aggregate. On the other hand, as it is a thermodynamical phenomenon, the phase transition can be probed by DSC. The LCST transition is characterized by an endothermic peak in the temperature *vs*. heat flux curves, corresponding to the destruction of the ordered hydration layer surrounding the polymer chain.[1]

2.1.2 Chemical Structure of Thermoresponsive Polymers

The structures of some of the most common LCST-type thermoresponsive (homo) polymers, including the repeat units which form the basis of the ones that are used in this work, are shown in Scheme 2-2.

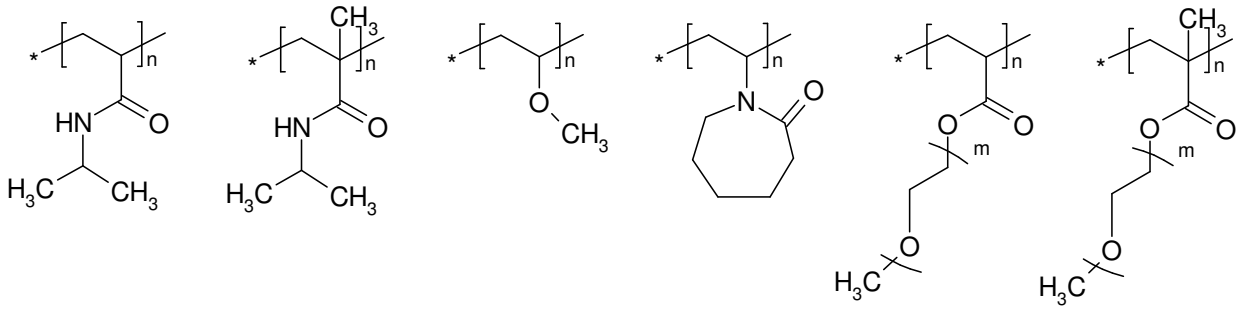

Scheme 2-2: Some of the most common LCST-type thermoresponsive polymers including the structures used in this work. From left to right: poly(N-isopropylacrylamide) pNIPAm, poly(N-isopropylmethacrylamide) pNIPMAm, poly(vinylmethylether) (pVME), poly(N-vinylcaprolactam) (pVCL), poly(oligo(ethylene glycol)methyl ether acrylate) (pOEGA), and poly(oligo(ethylene glycol)methyl ether methacrylate) (pOEGMA). The structures underlined are studied in this work.

Having a closer look onto repeat units of common thermoresponsive polymers, we see that all of them are of amphiphilic nature. For instance, the currently most studied thermoresponsive polymer, pNIPAm, comprises hydrophilic amide groups and the hydrophobic backbone and isopropyl groups. Similarly, pEG exhibits LCST-type behavior at ambient pressure only when it is attached to a hydrophobic backbone. Typically, if the polymer structure contains more chemical units that are capable of forming hydrogen bonds with water, e.g. amide, hydroxyl or ether, the transition to insolubility takes place at higher temperatures. The reverse case holds true, as well. For instance, the C_p of pOEGMA (cf. Scheme 2-2) increased from ca. 27 °C (m=2) to ca. 90 °C (m=9) with the increase in the number of EG groups of the side chains.[*80,81] Likewise, the presence of hydrogen-bonding units on the *N*-substituted groups of polyacrylamides can elevate the LCST, while an increase in the number of carbon atoms at this part can decrease it.[53] Replacement of the methyl groups at the end of the pendant pEG chains of pOEGMA with hydroxyl units enhanced the hydrophilicity of the macromolecule so that the polymer was soluble over the entire temperature range of water.[82] Similarly, charged groups in the structure are expected to shift the LCST to higher temperatures due to repulsions between neighbouring segments hindering chain aggregations. On the other hand, if the structure allows attractive intra/interchain interactions or if it sterically obstructs hydrogen-bonding, the LCST will drop. For instance, polymethacrylates bearing OEG side chains were reported to be less hydrophilic than their acrylate analogues.[52] Also, the C_p of pOEGMAs was modulated with regard to the type of the terminal groups at either side of the chains, more significantly for low molar mass polymers.[83]

[*] These values depend on the concentration and molar mass.

These *general* trends associated with the chemical units building the homopolymers also apply for copolymers. The introduction of hydrophilic or hydrophobic co-monomers can cause the LCST of the copolymer to increase or decrease, respectively.[84] For instance, the C_p of the random copolymers of MEO_2MA and OEGMA (M_n = 475 g mol^{-1}, m~9) showed a direct correlation with the co-monomer ratio,[83] i.e., increasing the content of the OEGMA from 5 to 15 mol% in the composition increased the C_p from 32 to 44 °C.[80] Besides fine tuning of the LCST, copolymerization gives also the possibility to incorporate additional functionalities, e.g. ionizable groups, recognition units, sensitivity to other stimuli, or fluorescent dyes, into the thermoresponsive structure.[52] Apart from the effect of chemical units, the phase transition temperature of the most thermoresponsive polymers is known to be sensitive to molecular weight,[85] molecular architecture,[76,86] and the polymer concentration.[87] The presence of a cosolvent, salts, or additives like ionic or non-ionic molecules/polymers also modifies the LCST because they perturb the balance of interactions between water-polymer and polymer-polymer molecules.

So far, as for most of the thermoresponsive polymer-based sensor designs, pNIPAm has been the accepted prototype for the majority of fundamental research and the choice of "smart" polymer for the development of functional systems.[61,75] This is partly because pNIPAm inherently has a LCST of ca. 32 °C (close to human body temperature) over a relatively broad concentration range and the transition is sharp and well defined.[53] However, the LCST of pNIPAm is not only sensitive to factors like the solution ionic strength or molecular weight,[45] but also the transition characteristically exhibits a marked hysteresis[*].[47] The latter is not beneficial considering applications relying on a fast response to temperature changes.

In the last decade, there has been an expansion of reports on (meth)acrylate copolymers bearing OEG side chains due to some of their superior properties in comparison to pNIPAm. Besides their stimuli-responsive nature, they are attractive for biomedical applications owing to the non-toxic EG groups which exhibit also low tendency for unspecific interactions. This bio-repellent property is a trivial advantage in comparison with the polyacrylamides which might form hydrogen bonds with other polyamides such as proteins.[43,46,88] The copolymers, especially when they are prepared via controlled radical polymerization techniques, exhibit relatively homogenous chain-to chain compositions and well-defined turbidity profiles with reduced hysteresis (cf. pNIPAm).[46] However, the phase transition temperature is sensitive to changes in concentration (especially in the dilute regime) and in solution ionic strength,

[*] This is associated with the amide groups forming intra- and inter-molecular hydrogen bonds which persist in the globule-to-coil transition.

crucial for their compatibility with the target area of application.[89] Overall, good reversibility, antifouling behavior, low cytotoxicity and easy adjustment of the LCST enable these polymers particularly advantageous for biological applications.

2.2 Concepts for Fluorescence Sensing

As introduced above, the stimuli-driven changes in the conformation of polymer chains have been studied by a wide range of experimental techniques. In this respect, fluorescent techniques have been commonly used due to their robustness, invasiveness, sensitivity, and ease of use in addition to the broad range of molecular information that can be extracted from different photophysical phenomena.[24,28,32,61,90-93] Also, an attractive aspect of fluorescence techniques is that a combination of them, such as the steady-state and time-resolved fluorescence spectroscopy, gives complementary results. Reporter dyes can be covalently attached to chains either during the polymerization process as a co-monomer or as an initiator, or after the polymerization is completed, for instance, via click reactions. These fluorophores embedded into the responsive polymer structure report about their immediate surroundings, the properties of which are changed by molecular events. This renders such a material particularly useful as a molecular sensor. The solubility-insolubility transition is translated into a fluorescence signal and this output is a direct measure of the stimulus leading to the transition.[24,28,32,52,94-101] As this thesis includes sensing approaches exploiting the principles of two fluorescence concepts, namely FRET and solvatochromism, the fundamentals of these are briefly discussed in the following.

2.2.1 Fluorescence resonance energy transfer (FRET)

Fluorescence (or Förster) resonance energy transfer is one of the most applied fluorescence concepts in biological imaging, diagnostics, and sensing. It is effective over long distances, typically in the range of 1-10 nm, and therefore contains different (molecular) information as compared to what other fluorescence methods can provide. As the efficiency depends strongly on the distance between the two reporter dyes (a FRET pair), it is the favored approach when it comes to probing molecular interactions, binding between two moieties, conformational changes of macromolecules, and diffusion processes.[102]

As an electrodynamic phenomenon, FRET can be explained considering dipole-dipole interactions.[103] It occurs between an energy donor (*D*) fluorophore in its electronically excited state and an energy acceptor (*A*) chromophore in the ground state. In a semi classical picture, the oscillating dipole of the excited donor molecule enforces the electron of the acceptor to oscillate as well, via Coulombic interactions. If the donor emission frequency is in resonance

with the absorption transition of the acceptor, energy is transferred radiationless from the donor to the acceptor. FRET does not include the emission of donor photons which are then absorbed by the acceptor; it is a non-radiative process. Indeed, reabsorption does not depend on molecular distances, but are rather consequences of how the sample is placed with respect to the excitation source or to the detector, and of probe concentration and its geometry. The energy transferred to the acceptor brings the molecules into the excited state and if emissive, the transfer event can be observed from the enhanced emission of the acceptor (Scheme 2-3).

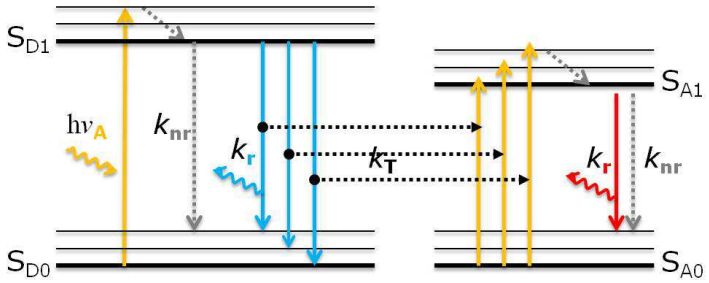

Scheme 2-3: A simplified Jablonski diagram for the processes of the donor absorption ($h\nu_A$), donor relaxation (radiative transition (k_r)-solid line, non-radiative transition (k_{nr})-dashed lines) and energy transfer between donor excitation and acceptor emission (the rate of transfer=k_T). The transferred energy is transformed into the emission of the acceptor taking place radiatively or non-radiatively.[103,104]

Besides the frequency match, certain conditions should be fulfilled for FRET to happen efficiently. These factors can be understood by considering at which rate the transfer proceeds between a single donor-acceptor pair separated by a distance r:[102,103]

$$k_T(r) = \frac{k_r \kappa^2}{r^6}\left(\frac{9000(\ln 10)}{128\pi^5 N_A n^4}\right)J(\lambda) \qquad \textit{Equation 2-2}$$

The rate of the transfer (k_T) is proportional to the radiative decay rate of the donor (k_r), the extent of the spectral overlap between the emission spectrum of the donor and the absorption spectrum of the acceptor (J), and the orientation factor (κ). The latter is 2/3 after averaging the donor and acceptor transition dipoles oriented randomly or rotating rapidly during the lifetime of the donor. In practice, in order to calculate k_r, the donor quantum yield (φ_D) and its lifetime (τ_D) in the absence of the acceptor should be known ($k_r = \varphi_D/\tau_D$). Most importantly, the rate decreases with the sixth power of r. In the equation, n is the refractive index of the medium, and N_A is Avogadro's number. The spectral overlap J is defined as:

$$J(\lambda) = \int_0^\infty F_D(\lambda)\varepsilon_A(\lambda)\lambda^4 d\lambda \qquad \textit{Equation 2-3}$$

The overlap is calculated from the optical spectra of the FRET pair by considering the normalized fluorescence spectrum of the donor (F_D) (so that $\int_0^\infty F_D(\lambda)d\lambda$=1) and the extinction coefficient of the acceptor (ε_A) as a function of the wavelength (λ). Equation 2-2 is often expressed as:

$$k_T(r) = \frac{1}{\tau_D}\left(\frac{R_0}{r}\right)^6 \qquad \textit{Equation 2-4}$$

where R_0 is known as the Förster distance and given by $R_0 = 0.211\left(\kappa^2 \varphi_D n^{-4} \int_0^\infty F_D(\lambda)\varepsilon_A(\lambda)\lambda^4 d\lambda\right)^{1/6}$ in units of Å. Once R_0 is estimated, it is possible to calculate the efficiency of the transfer for the pair at a certain distance. The energy transfer efficiency (Φ) is then defined as the ratio of the transfer rate to the sum of all rates depopulating the excited state of the donor:

$$\Phi = \frac{k_T(r)}{{\tau_D}^{-1} + k_T(r)} \qquad \textit{Equation 2-5}$$

Note that ${\tau_D}^{-1}$ corresponds to k_D which is the sum of non-radiative (k_{nr}) and radiative decay rates (see Scheme 2-3). Using the expression for k_T in Equation 2-4, the efficiency of energy transfer is found as:

$$\Phi = \frac{{R_0}^6}{{R_0}^6 + r^6} \qquad \textit{Equation 2-6}$$

Due to this power law, the efficiency has a strong dependency on the separation distance between the donor and the acceptor. When r corresponds to R_0, the transfer rate is the inverse of the excited state lifetime of the donor and Φ is 50%. As r decreases below R_0 or gets greater than that, Φ rapidly increases to unity or decreases to zero, respectively. Using Equation 2-6, the distance between an immobilized donor and acceptor pair can be calculated from the experimental data, which makes FRET a unique concept for fluorescence based probes. Since energy transfer is a deactivation channel for the excited donor molecules, in the absence of other quenching mechanisms, one could quantify Φ from the decrease of fluorescence intensity or lifetime of the donor:

$$\Phi = \frac{F_D - F_{DA}}{F_D} = \frac{\tau_D - \tau_{DA}}{\tau_D} \qquad \textit{Equation 2-7}$$

Here, the subscript $_{DA}$ refers to the measured donor property in the presence of the acceptor. Alternatively, if the acceptor is fluorescent, Φ can be measured from the increase of its emission intensity and enhanced lifetime. In the FRET system studied within this work,

more than one single donor-acceptor pair is present in the solution, i.e., there is a distribution of distances (cf. Chapter 3). In such cases, depending on the dimension of the media, more complex equations are necessary to describe the energy transfer. Considering multiple acceptors and neglecting homo-transfer between the donors, the intensity decay of the donor in the presence of acceptor ($I_{DA}(t)$) is described as:[103]

$$I_{DA}(t) = {I_D}^0 exp\left(-{}^{t}/_{\tau_D} - 2\gamma\sqrt{{}^{t}/_{\tau_D}}\right) \qquad \textit{Equation 2-8}$$

where ${I_D}^0$ defines the initial fluorescence intensity of the donor. The first part of the exponential function describes the depopulation of the excited state via radiative and non-radiative channels (the decay function in the absence of acceptors) and the second part represents the competing FRET pathway. The term γ describes the strength of transfer and is calculated for randomly distributed acceptors in three dimensions as in a homogenous solution according to:

$$\gamma = \frac{\sqrt{\pi}}{2} C \left(\frac{4}{3}\pi {R_0}^3\right) \qquad \textit{Equation 2-9}$$

with C being the acceptor concentration in the solution. From this, the efficiency of quenching of the steady-state donor emission intensity by FRET can be calculated as:

$$\Phi = \sqrt{\pi}\gamma exp(\gamma^2)(1 - \mathrm{erf}(\gamma)) \qquad \textit{Equation 2-10}$$

In this expression, the error function *erf* (γ) is defined as:

$$erf(\gamma) = \frac{2}{\sqrt{\pi}} \int_0^{\gamma} exp(-x^2)\, dx \qquad \textit{Equation 2-11}$$

Equation 2-10 shows that the degree of donor quenching by desolved acceptors depends only on the concentration of acceptor molecules. The acceptor concentration must be high enough to ensure that an acceptor molecules is statistically within a distance of R_0 to the donor.[103]

2.2.2 Solvatochromism

Fluorophores are called solvatochromic, typically when their emission properties, e.g. spectral shape, fluorescence lifetime and its quantum yield, are sensitive to the nature of the surrounding solvent molecules.[105] It is often observed that as the solvent polarity increases, the maximum of the emission spectrum exhibits a red-(bathochromic) or blue-(hypsochromic)

shift, known as positive or negative solvatochromism, respectively.[106] In reality, the photophysical properties of the fluorophore are not only affected by the polarity but a result of the complex interplay between a variety of interactions with the solvent stabilizing its ground and excited state.[106,107] These might involve nonspecific dielectric interactions (due to the average polarizibility and the permanent dipole moment of each component) and specific interactions such as hydrogen-bonding.[106] Typically, for many fluorophores a redistribution of electrons upon electronic excitation results in a larger dipole moment in the excited state (μ_E) than that in the ground state (μ_G). The solvent molecules reorient around these excited state dipoles and lower the energy of the excited state (Scheme 2-4), the extent of which is directly correlated with the polarity and viscosity of the solvent. This leads to the red-shift in the emission spectrum. This solvent relaxation-mediated spectral shift takes place only when solvent dipoles move at a time scale faster than the excited-state lifetime of the fluorophore.

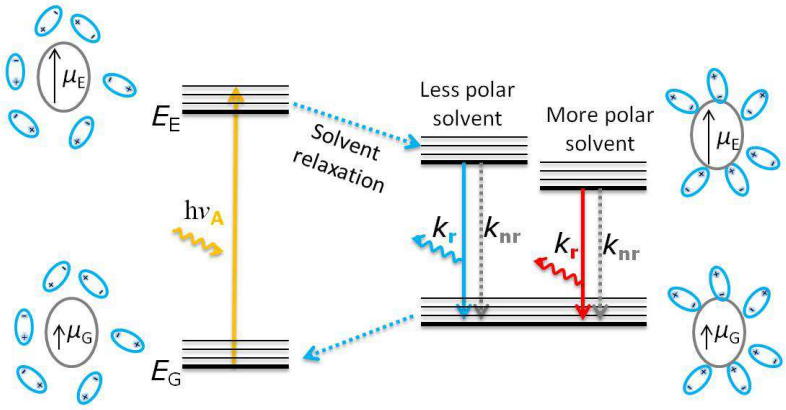

Scheme 2-4: The fluorophore dipole moment (μ_G and μ_E) in the ground (E_G) and excited state (E_E) surrounded by solvent dipoles. Solvent dipoles reorient and relax around the excited state, lowering its energy.[103]

A basic expression for the relationship between the spectral properties of a solvatochromic fluorophore and the solvent polarity is given by the *Lippert–Mataga* relation.[106] Solvent properties are defined by the refractive index (n) and dielectric constant (ε) of the solvent and the spectral shift is attributed solely to the reorientation of the solvent dipoles. The solvatochromic shifts for absorption and emission in wavenumber ($\bar{\nu}_A$ and $\bar{\nu}_F$) are given as:

$$\bar{\nu}_A = -\frac{2}{hc}\mu_G(\mu_E - \mu_G)a^{-3}\Delta f$$
$$\bar{\nu}_F = -\frac{2}{hc}\mu_E(\mu_G - \mu_E)a^{-3}\Delta f$$

Equation 2-12

where h is Planck's constant, c is the velocity of light, and a is the radius of the cavity wherein the chromophore is. Here, Δf (orientation polarizability) relates the shift to the solvent property (n and ε) and is defined as:

$$\Delta f = \frac{\varepsilon - 1}{2\varepsilon + 1} - \frac{n^2 - 1}{2n^2 + 1} \qquad \textit{Equation 2-13}$$

Consequently, the Stokes shift ($\Delta\bar{\nu} = \bar{\nu}_{\mathrm{A}} - \bar{\nu}_{\mathrm{F}}$) can be related to solvent polarity and the magnitude of the charge transfer dipole moment:

$$\Delta\bar{\nu} = \frac{2}{hc}(\mu_{\mathrm{E}} - \mu_{\mathrm{G}})^2 a^{-3} \Delta f \qquad \textit{Equation 2-14}$$

Since this equation relates the shift only and directly to solvent polarity, deviations from linearity in a plot of $\Delta\bar{\nu}$ of a fluorophore measured in various solvents as a function of Δf reveal other effects changing the spectra. These can be the presence of intermolecular interactions other than dipole-dipole interactions or other peculiarities from the chemical structure such as ion- or viscosity-sensitivity. Solvatochromic dyes are therefore widely used to obtain information about the target environment.

Some fluorophores exhibit exceptional sensitivity to solvent polarity. These probes typically possess an electron donor and acceptor group separated by a linker. Upon excitation, due to the push-pull mechanism, the internal charge transfer (ICT) leads to large changes of the dipole moment.[107] In some cases, certain groups of the fluorophore rotate upon excitation and a twisted ICT (TICT) state is formed. The formation of TICT is facilitated in polar solvents and affected strongly by the viscosity of the environment. The relaxation from a TICT state is generally non-radiative,[103] and competes with the emission from the non-distorted ICT state.[108-110] Therefore, when the environment is rigid, the TICT state is suppressed, which is typically detected as an increased yield of emission or a change in fluorescence anisotropy.

2.3 Conjugated Polyelectrolytes (CPEs)

Conjugated polyelectrolytes (CPEs) combine the aqueous solubility of conventional polyelectrolytes with the unique photophysical properties of conjugated polymers. The conjugated backbone built from alternating single and double bonds results in extended π-molecular orbitals. Charge carrier transport is possible by hopping of charges between these delocalized orbitals. Besides the charge transport ability, tuning the band gap with the length of the effective conjugation length renders these polymers useful components of

optoelectronic devices.[111] Different primary backbones, e.g. poly(thiophene)s (PTs), poly(p-phenylenevinylene)s (PPVs), polyfluorenes, and poly(phenylene ethynylene)s (PPEs), have been used in CPE structures.[111] The conjugated backbone is typically substituted with a side chain including the ionic groups which promote solubility in water. Some examples of CPEs are demonstrated in Scheme 2-5.

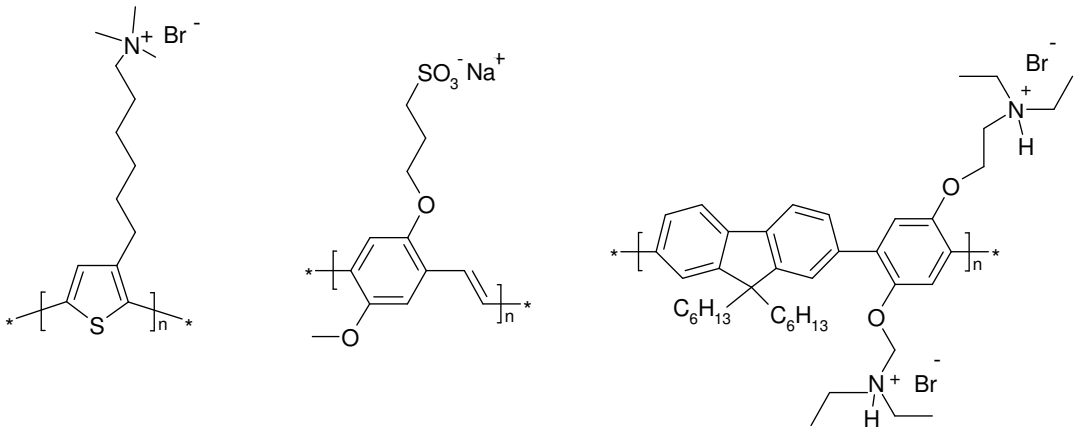

Scheme 2-5: Selected examples of CPE structures. From left to right: poly[3-(6-trimethylammoniohexyl)thiophene bromide], poly[5-methoxy-2-(3-sulfopropoxy)-1,4-phenylenevinylene], and poly[2,5-bis[3-(N,N-diethylamino)-1-oxapropyl]-1,4-phenyl-co-alt-2,7-(9,9-dihexylfluorene)]

The polyelectrolyte-like behavior, i.e. the charged nature, allows their interaction with various charged molecules in water. Therefore, with their profound optical properties, CPEs are particularly advantageous for optical sensing of chemical and biological molecules. The large binding energy of charge-charge interactions and the possibility to arrange the ionic groups in the CPEs in a specific way allows sensitive detection of biomolecules.[112-120] In comparison with small molecule fluorescent probes, the highly electron-delocalized backbones enable larger absorption extinction coefficients and more efficient intramolecular/intermolecular energy transfer.[121] They are also better bio-compatible than quantum dots. Moreover, the possibility to functionalize the structure with specific recognition groups enables selective detection of analytes. The utilization of CPEs as a sensing element in the field of bio/chemo sensing has been demonstrated with a large variety of detection strategies, and such schemes have been the focus of excellent reviews.[111,113,117,121-124] Two types of transduction mechanisms are typically used in these CPE-based sensors: fluorescence quenching via FRET or electron transfer, and the analyte-induced aggregation and conformational changes of CPE chains.[111,122,125] The following summarizes the basic principles of these approaches.

2.3.1 Sensing Based on Electron Transfer or FRET

This type of sensing strategy takes advantage of the migration of excitation energy along the conjugated backbone. Upon excitation of the CPE, the energy of the exciton generated at an arbitrary site can be quenched by an acceptor (FRET or electron acceptor) molecule residing in another site. What makes these assays efficient is the intensity of the read-out signal, i.e., the quenching or the enhancement of the CPE fluorescence. This is due to the fact that when they are bound, only one quencher or energy acceptor molecule is sufficient to trap almost all of the exciton energy along the CPE backbone.[111] In other words, it is the fluorescence of the entire backbone which is quenched.

In the simplest case, the analyte is labeled with an oppositely charged quencher/acceptor molecule (alternatively, the analyte might intrinsically act as a quencher).[126] The CPE fluorescence is quenched due to its interactions with the analyte. This reduction of PL is directly correlated with the amount of target molecules in the solution interacting with the CPE. Another well-exploited proof of concept design relies on the fact that free quencher molecules interact more favorably with the targeted analyte than the CPE.[127] As a result of this, the quencher is pulled away from the CPE sites by the target and an increase in CPE fluorescence is observed. If the quencher is an (emissive) energy acceptor, one can also observe a change of the acceptor emission, rendering ratiometric detection. Overall, this fluorescence "superquenching" effect associated with the efficient transfer of excitation energy between the conjugated segments enables signal amplification and an enhanced sensitivity of sensing with CPEs.[123,128]

2.3.2 Sensing Based on Aggregation or Conformational Changes

CPEs exhibit a rich self-assembly behavior in aqueous solutions with a strong tendency to aggregate.[116,117,119,129-131] This is reasoned with the amphiphilic nature of the polymer structure, i.e., the relatively hydrophobic backbone will orient in a certain way to limit the water exposure.[124] Depending on factors such as the type of backbone, the nature of ionic groups, molecular weight, or length of side chains, aggregation properties differ. Also, the effect of environmental factors such as concentration, temperature, solution ionic strength and presence of surfactants on the aggregation properties was reported.[132] Most importantly, the conformation and aggregation behavior of the chains govern the effective conjugation length, and therefore the polymer´s optical properties. For instance, when CPE chains exist as molecularly dissolved (non-interacting) entities, the fluorescence spectrum of the polymer exhibits sharp, structured and narrow features with a relatively small Stokes shift. As chains

aggregate, both the absorbance and emission spectra undergo a red-shift, while fluorescence appears as a broad structureless band.[124] Aggregation, in most cases, lowers the quantum yield due to the formation of non-radiative defect sites. Moreover, twisting of the conjugate backbone leads to a decrease of the effective conjugated length, changing the absorbance maxima.[117] These properties are exploited in this type of sensing.

Typically, upon complexation with other molecules bearing charged units, e.g. DNA, proteins, or surfactants, the conformation of the CPE chains changes.[111,122,123,133] For instance, for rigid PT-based structures, complexation with analytes mostly alters the conformation of the backbone. A change from a random-coil conformation to a planar (highly conjugated) conformation is manifested by a red-shifted absorption wavelength, and the extent of the shift can be correlated with the concentration of inter-polyelectrolyte complexes.[113,117,134] A relevant characteristic of this strategy is its ability to relay information from the change of solution color by simple visual inspection.[111,135]

Alternatively, electrostatic interactions between an oppositely charged analyte and a CPE can lead to a change in aggregation properties of the CPE chains.[136,137] If the CPE contains donor and acceptor units, analyte-induced aggregations of these chains bring (more of) the FRET pairs in close contact, monitored visually by a change in emission color. The inverse case is as well possible, for which the formation of an electrostatic complex with the analyte breaks up the CPE aggregation and thereby reduces the efficiency of FRET. For regular CPEs, such analyte induced aggregations typically bring about a quenched fluorescence intensity and lifetime.

3 Supramolecular Assembly of a Thermoresponsive Polymer and a CPE: a Route to Temperature/Chemical Sensing*

3.1 Background

As a common tool for resolving molecular distances and conformation changes,[102] FRET has been favorably exploited for the investigations of the molecular processes taking place during the LCST-type phase transition.[61,90,91,138-140] For sensing applications, FRET is advantageous particularly when the acceptor label is fluorescent. Otherwise, quenching of donor emission reduces the intensity of the read-out; however this signal alone is not practically useful. Moreover, the decrease in intensity with time is commonly observed for most fluorophores and several factors other than FRET can quench the emission signal. These interfering facts can severely complicate the interpretation of results. Therefore, two emissive species can together feature self calibration, enhancing the sensitivity of the detection event.[141,142] A ratiometric change is the desired read-out, enabling detection and quantification even only by visual examination of the emission color.

In this context, various design concepts for sensors integrating thermoresponsive polymers have been based on the modulation of FRET efficiency.[24,32] The main approach has been the site-specific incorporation of FRET pairs into polymer chains. In the ideal case, similar to protein folding studies, collapse or extension of the chain changes the spatial distance between the fluorophores modulating the efficiency of FRET (cf. Scheme 1-2a).[30,143] This dual-labeling concept has been applied within different architectures, examples being pNIPAm micro-gels bearing two types of quantum dots acting as a donor-acceptor pair,[144] NIPAm-based core/shell micro-gels labeled in the core with donor and in the shell with acceptor moieties,[145] and double hydrophilic copolymers consisting of fluorescent NIPAm

* Published in part: S. Inal *et al*., "Temperature-Regulated Fluorescence Characteristics of Supramolecular Assemblies Formed by a Smart Polymer and a Conjugated Polyelectrolyte" *Macromolecular Chemistry and Physics* **2013**, *214*, 435 and S. Inal *et al*., "Temperature-Regulated Fluorescence and Association of an Oligo(ethyleneglycol)methacrylate-based Copolymer with a Conjugated Polyelectrolyte- The Effect of Solution Ionic Strength" *the Journal of Physical Chemistry B* **2013** DOI: 10.1021/jp408864s

and OEGMA blocks.[36] In an original work, a single thermoresponsive chain was labeled with one donor and two pH-switchable acceptor dyes, at the middle and end of the chain, respectively, resulting in a dual-probe for pH and temperature.[146] Benefiting from the solubility changes induced by recognition events, detection of specific molecules, e.g., glucose or K^+ ions, through a FRET signal has as well been reported.[39,40]

However, such sensing concepts face the common challenge that the change in the donor-acceptor proximity needs to be quite drastic, in order to change the emission color effectively.[30,147] Considering the demanding synthetic procedures required for such nano-sized control of the location of fluorophores (along individual chains or within a restricted geometry in a gel), supramolecular assemblies of donor and acceptor moieties are promising candidates for the generation of new types of functional systems.[148] Also, concepts that can allow further functionalities and are flexible for modifications are certainly more attractive. In this chapter, I will present such an assembly, i.e. a dye-functionalized thermoresponsive copolymer and a cationic CPE-based FRET system, as a fluorescent probe for aqueous solution temperature as well as for solution ionic strength. The assembly relies on the "unspecific" interactions between a non-ionic OEGMA-based copolymer bearing the donor dye and a thiophene-based CPE as the fluorescent acceptor. Such inter-polymer interactions lead to efficient FRET at room temperature. However, as the temperature of the solution is raised above the C_p, a structural re-organization process results in increased donor-acceptor separation distances, decreasing the FRET efficiency. As a result, the phase transition is reported with a well visible change of the emission color. Also, the change in FRET efficiency covers a broad temperature range. The first part of the chapter presents the investigations on this FRET-based system detecting the **temperature** of a *buffer* solution.

Similar to the effect of temperature, interactions between the thermoresponsive polymer and water can be modulated by changing the ionic strength of water. This should thereby give an opportunity to modify the mechanism of self assembly. The second part focuses on this response of the macromolecular assembly to the presence of **salt**s, for which the concentration and also the type of the cation was varied. The thermo-regulated fluorescence characteristics presented earlier are found to depend strongly on the ionic strength of the solution. Moreover, the inter-polymer interactions are salt-tunable at room temperature, rendering the assembly with double-stimuli sensitivity with the most efficient temperature sensing occurring around physiological salt concentration. To elucidate the reasons behind such thermo-and ion-sensitive fluorescence characteristics, the effect of salts, in particular of NaCl, on the association behavior of the macromolecules before and after the polymer phase transition is investigated by a combination of UV-VIS, fluorescence, ^{1}H NMR, and light scattering

measurements. As various results contribute to our understanding, a separate section for discussions will appear before the conclusions.

3.2 Materials*

The CPE of this work is the poly[3-(6-trimethylammoniohexyl)thiophene bromide] (P3TMAHT). The apparent number-average molecular weight (M_n^{app}) of P3TMAHT is 5000 g mol^{-1} as determined for the non-ionic polycation precursor with bromohexyl side groups by size exclusion chromatography (SEC).[120] The non-ionic fluorescent thermoresponsive copolymer, here denoted as CLP, is a statistical copolymer synthesized by free radical copolymerization of three methacrylate monomers namely OEGMA, MEO_2MA, and a coumarin-functionalized methacrylate (ca. 1 wt%). The chemical structures of the CLP and P3TMAHT are shown in Scheme 3-1.

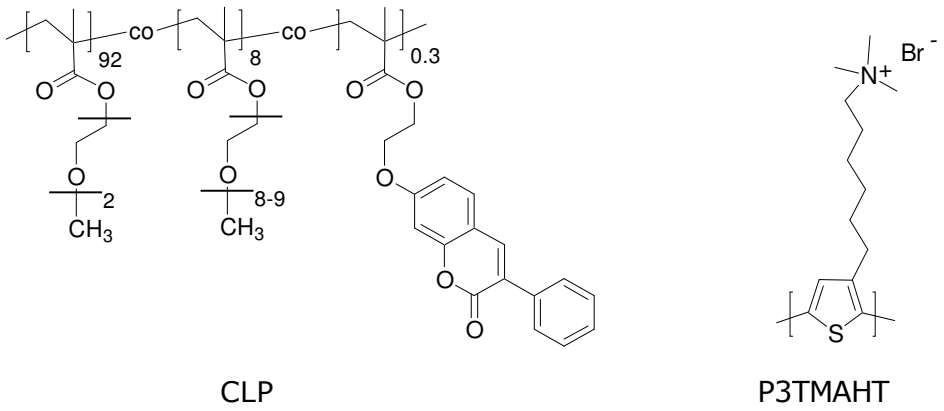

Scheme 3-1: Chemical structures of the thermoresponsive copolymer CLP (ternary copolymer of OEGMA, MEO_2MA, and a coumarin functionalized methacrylate) and of the polycation P3TMAHT.

The chemical similarity of the co-monomers results in almost the same copolymerization reactivity. This avoids a compositional drift during the copolymerization and assures a random distribution of the monomers in the chemical structure.[120] The incorporation of the dye into the copolymer was quantified via UV-VIS spectroscopy. CLP has a M_n^{app} of 21000 g mol^{-1}, and the dye content corresponds roughly to 1 chromophore per 3 chains in average. The polymer has a polydispersity index (PDI) of 3 determined by SEC in dimethylformamide (DMF) solution, using polystyrene (PS) standards.

Upon incorporation into the polymeric structure, optical properties of the coumarin are well preserved (Figure 3-S1a). Moreover, the fluorescence intensity of CLP is rather insensitive to heating to temperatures above the C_p (Figure 3-S1b). This is advantageous

* Thermoresponsive polymers were provided by *Jonas D. Kölsch* from the *University of Potsdam*. The CPEs were synthesized by *Mario Kraft* from the *University of Wuppertal*.

considering that the polymer is used as a FRET donor, the emission of which should ideally vary only due to changes in the donor-acceptor proximity. Note that all experiments shown in the first part of the chapter were performed for solutions prepared in the phosphate buffered saline (PBS).

3.3 Temperature Responsive Mixtures

The temperature-turbidity profile of the CLP solution and of its mixture with P3TMAHT in PBS is shown in Figure 3-1. Addition of P3TMAHT does not suppress the thermal sensitivity of the polymer, but shifts its C_p to slightly higher temperatures.

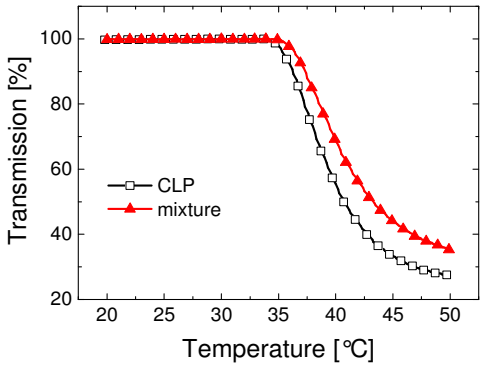

Figure 3-1: Transmittance of CLP solution (0.8 mM with respect to repeat units) and its mixture with P3TMAHT (0.09 mM with respect to repeat units) in PBS as a function of temperature.

In order to elucidate the origin of the C_p shift, turbidity profiles of mixtures of CLP with different amounts of P3TMAHT are recorded. The results are summarized in Figure 3-2.

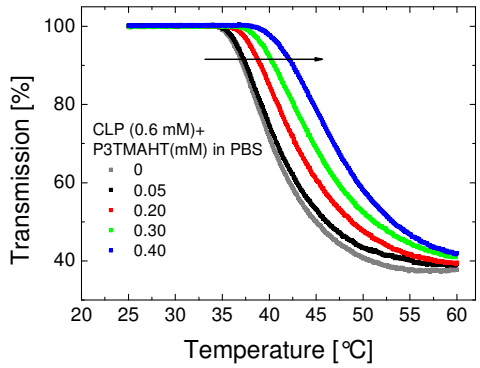

Figure 3-2: Transmittance of pure CLP (0.6 mM) solution or its mixture with P3TMAHT at different concentrations (0.05, 0.20, 0.30, 0.40 mM). The direction of the arrow shows the increase in P3TMAHT concentration.

Although the solvent quality changes when P3TMAHT is added to water, the increase of C_p with polyelectrolyte concentration might be ascribed to the inter-polymer

interactions.[149] In this respect, a comparable system may be the mixture of pNIPAm with sodium dodecyl sulfate (SDS). The adsorption of SDS on the pNIPAm chains shifts the C_p to higher temperatures associated with the increased solubility of the polymer.[150] For a gel network, Wu *et al*. observed that addition of SDS raises the collapse temperature of poly (N-vinylcaprolactam-*co*-sodium acrylate) micro-gels due to electrostatic repulsions between the anionic chains accumulating inside the network.[151] Likewise, the polyelectrolyte might integrate the CLP as a part of a charged complex and the inter-aggregate repulsions retard the phase transition.

3.3.1 Photophysical Properties

The absorption and photoluminescence (PL) spectra of aqueous solutions of P3TMAHT and CLP measured at room temperature (well below the C_p) are shown in Figure 3-3. The optical spectra of P3TMAHT exhibit a broad absorption band with its maximum at 415 nm and a red-shifted emission, in good agreement with published data.[119] Note the large spectral overlap between the CLP emission and the P3TMAHT absorbance, which promises a high efficiency of FRET*.

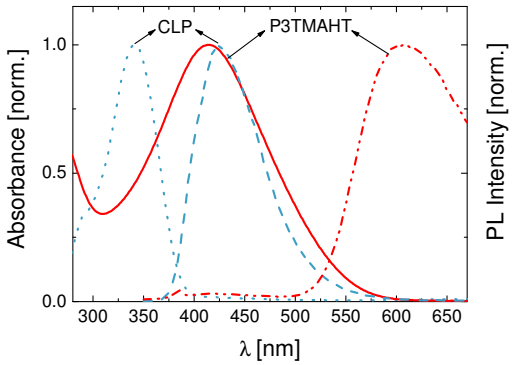

Figure 3-3: Normalized absorbance and PL spectra of CLP (0.8 mM in PBS, dotted and dashed blue line, respectively) and of P3TMAHT (0.09 mM in PBS, solid and dashed-dotted red line, respectively). The excitation wavelength was 340 nm.

Energy transfer from the coumarin labels of the CLP (donor) to the P3TMAHT (acceptor) was investigated by mixing the CLP at a constant concentration of 0.6 mM with increasing amounts of the polyelectrolyte (0.04 mM to 0.30 mM) in PBS. The steady-state and time-resolved emission spectra of these mixtures at room temperature are displayed in Figure 3-4, together with the pure P3TMAHT emission recorded under identical conditions. Over the concentration range studied here, as the shape of the optical spectra of CPE is constant and the scaling of the intensity values of the absorption with the concentration of the

* Using this spectrum, the Förster distance R_0 is calculated to be 4.9 nm.

polymer follows *Beer-Lambert law*, the degree and nature of self-association of the chains must be independent of concentration. For the absorbance spectra of these mixtures, see Figure 3-S2.

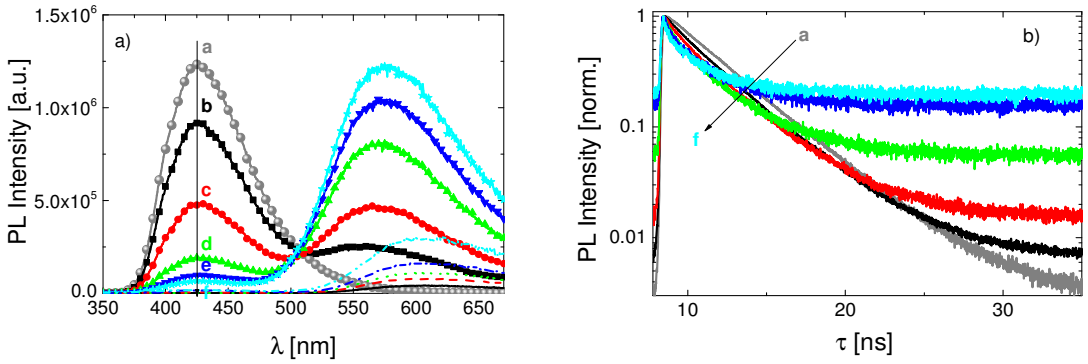

Figure 3-4: **a)** Steady-state emission spectra and **b)** normalized PL decay traces of mixtures of CLP (0.6 mM) with P3TMAHT at increasing concentrations at 20 °C: a) 0 mM b) 0.04 mM c) 0.08 mM d) 0.18 mM e) 0.26 mM f) 0.30 mM. The arrows indicate the increase in acceptor concentration. Thin lines in a) are the emission of the acceptor at the given concentrations, measured under otherwise identical conditions. The decay curves in b) were collected for the emission at 425 nm (maximum of the donor PL). The excitation wavelength was 340 (360) nm for steady-state (time-resolved) measurements.

Upon increasing the concentration of P3TMAHT in the mixture, the intensity of CLP emission is severely reduced, while the acceptor's fluorescence is enhanced markedly. Quenching of the donor fluorescence at 20 °C is also evident from the shortening of the donor lifetime. These findings are consequences of efficient energy transfer from the coumarin to the polythiophene. Although P3TMAHT absorbs the excitation light at 340 nm, the emission increased additionally up to fourfold[*] in the presence of the donor. Within the concentration range studied, these spectral changes are continuous. Notably, compared to the pure P3TMAHT spectrum, the wavelength of maximum emission intensity (λ^{PL}_{max}) of the acceptor exhibits a marked blue-shift in the presence of the CLP. The interplay between the two polymers is evident also from the absorbance spectrum of the mixtures, which does not match the linear combination of the spectra of the individual components (Figure 3-5).

[*] The interactions of P3TMAHT with EG groups of CLP might lead to reduced conformational disorder of its chains and thereby contribute to the enhancement of its emission intensity. CPEs are known to display hydrophobic interactions with nonionic surfactants. For instance, Burrows *et al.* and Monkman *et al.* studied the effect of n-dodecyl pentaoxyethylene glycol ether ($C_{12}E_5$) on the spectral properties of the anionic CPE and of a cationic one in aqueous solutions, respectively [154,156,129]. Their results showed that the presence of $C_{12}E_5$ enhanced the PL quantum yield by the breaking up of polymer aggregates or by incorporating the polymer chain into micelles (above a certain concentration of the surfactant). Such a structural change eliminated the interchain quenching sites.

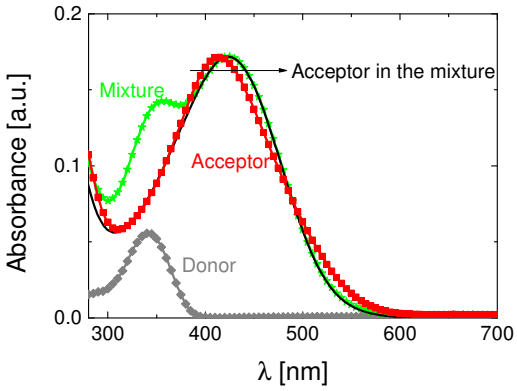

Figure 3-5: Absorbance spectra of the CLP (0.8 mM), of the P3TMAHT (0.09 mM), of their mixture. Also shown is the absorbance of the acceptor obtained by subtracting the donor contribution from the mixture spectrum. The arrow indicates the shift of the P3TMAHT absorbance peak when going from the pure solution to the mixture.

The slightly red-shifted and narrowed absorption of P3TMAHT in the mixtures suggests a more planar conformation of the conjugated chains, i.e., a longer conjugation length.[117,152] Since CLP does not carry charged groups and even if so, the presence of buffer ions would minimize a contribution from electrostatic interactions, the inter-polymer interactions seem to be of hydrophobic origin. Such forces were responsible for the association of CPEs with non-ionic surfactants,[129,153-156] and for their complexation with proteins, e.g. histones.[157,158] Further evidence on the type of the interactions can be obtained by examining the effect of CLP on photophysical characteristics of the thiophene-based CPEs which are not cationic. The absorbance spectra of such analogous CPEs and of their mixtures with CLP are illustrated in Figure 3-6.

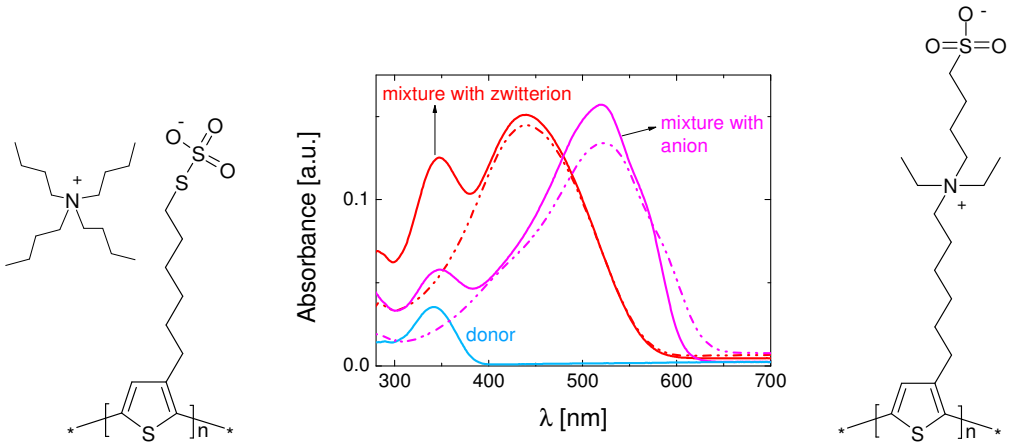

Figure 3-6: Absorbance spectra of aqueous solution of CLP (blue solid line), of the zwitterionic/anionic thiophene (red/magenta dashed line), and of their mixture (red/magenta solid line) in PBS. Also shown are the chemical structures of the CPEs.

Figure 3-6 shows that the shape of the "anionic" CPE spectrum differs when it is mixed with the CLP which, on the other hand, does not affect the absorbance spectrum of the "zwitterionic" thiophene. The PL spectrum of the latter is as well insensitive to the CLP and although the value of R_0 of this couple (3.2 nm) is comparable to what is measured for P3TMAHT and CLP (4.9 nm), no energy transfer takes place (Figure 3-S3a). On the contrary, the emission of CLP is strongly quenched by the anionic polythiophene (Figure 3-S3b). These facts indicate that the zwitterionic CPE do not have inter-molecular contacts with the CLP. Due to its enhanced ionic nature, this polymer is expected to be well-dissolved in water.* It can, therefore, be inferred that the weak aqueous solubility of anionic or cationic CPEs leads their search for other hydrophobic segments such as the CLP chains and that the unspecific interactions are responsible for the efficient FRET at room temperature.

3.3.2 Fluorescence Response to Phase Transition

When the solution temperature is increased from 20 °C to 50 °C (well above the C_p), the PL spectra of the mixtures undergo remarkable changes: the intensity and the lifetime of donor fluorescence partially recovers while the acceptor emission becomes weaker as if in the absence of CLP (Figure 3-7).

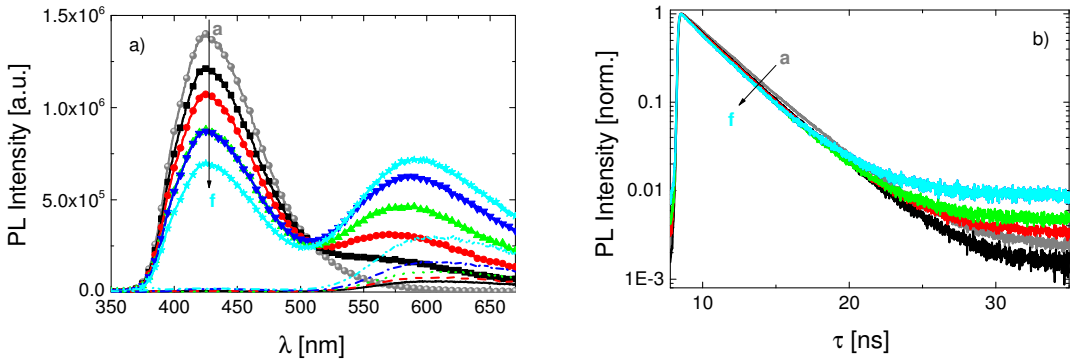

Figure 3-7: **a)** Steady-state emission spectra and **b)** normalized PL decay traces of mixtures of the CLP (0.6 mM) and the P3TMAHT at increasing concentrations measured at 50 °C. The arrows indicate the increase in acceptor concentration: a) 0 mM b) 0.04 mM c) 0.08 mM d) 0.18 mM e) 0.26 mM f) 0.30 mM. Thin lines in a) are the emission from P3TMAHT at the given concentrations in PBS, measured under otherwise identical conditions. The emission in b) was detected at 425 nm (maximum of the donor PL). The excitation wavelength of the steady-state (time-resolved) measurements was 340 (360) nm.

Importantly, heating the solutions of the pure components to 50 °C has negligible effect on the shape or the intensity of the optical spectra (cf. Figure 3-S1b and S4). This means that

* Based on the visual inspection on these polymers, I suggest that the zwitterion exhibits much better solubility in PBS than the other two types of thiophene, i.e., P3TMAHT and the thiosulfate-functionalized CPE. Anionic CPE has a M_n^{app} of 8450 g mol^{-1} while zwitterion one has 15400 g mol^{-1}.

the temperature induced-alterations of the emission involve changing interactions between the two polymers. Weakening of inter-polymer interactions is evidenced also from the smaller blue-shift of λ^{PL}_{max} of the acceptor at 50 °C (cf. Figure 3-7). The extent of FRET observed at 20 °C and its temperature sensitivity are significantly more pronounced in comparison to another FRET system relying on changing interactions between a pNIPAm and hydrophobized polymers.[159] The temperature-induced changes in the emission spectra can readily be observed by visual inspection (cf. Figure 3-8) and they are reversible, i.e., the two polymers re-interact as the mixture is cooled down to room temperature. Exhibiting relatively high detection sensitivity, such a polymer assembly can, therefore, be useful as a fluorescent sensor for temperature.

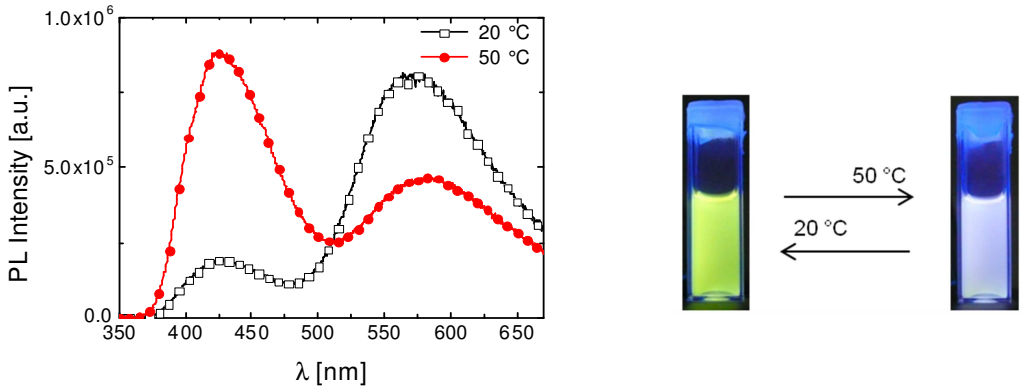

Figure 3-8: Changes in the fluorescence properties upon heating a mixture of CLP (0.6 mM) and P3TMAHT (0.18 mM) above its C_p. PL spectra were recorded at an excitation wavelength of 340 nm while the photographs were taken under UV illumination at 365 nm.

Typically, the C_p of thermoresponsive copolymers is affected by the polymer concentration, i.e., the onset of the phase transition is detected at higher temperatures for lower concentrations. On the basis of this consideration, in order to find out whether the observed changes are a result of a purely temperature-activated de-assembly or of the LCST-type transition, I compared the temperature-induced PL spectra of two mixtures containing an equal amount of P3TMAHT, but differing in CLP concentration. Figure 3-9 shows that changes in PL spectra set in at a lower temperature for the mixture including more CLP molecules. Characteristically, the onset temperature for the decrease in FRET efficiency (expressed as the ratio of the maximum emission intensity of the acceptor to that of the donor, i.e. $I_{Acceptor}/I_{Donor}$, determined after convolution of the mixture spectra) agrees qualitatively with the C_p of each mixture. These findings suggest that the temperature-induced changes in emission properties are governed by the phase transition of the thermoresponsive polymer. Apparently, the nature of inter-polymer interactions changes continuously and accordingly with the ongoing insolubility transition.

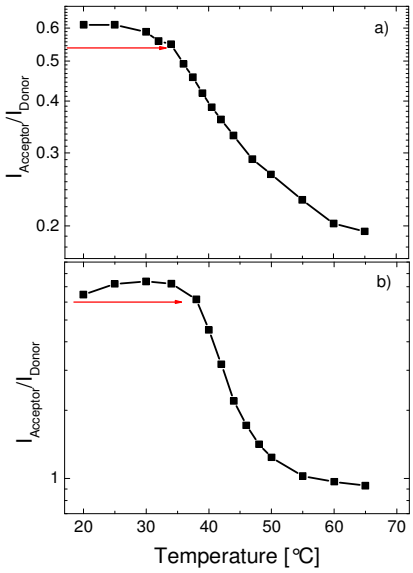

Figure 3-9: The ratiometric response (ratio of the peak intensity of the acceptor to that of the donor) of 0.08 mM P3TMAHT mixed with **a)** 0.8 mM of **b)** 0.1 mM of CLP at various temperatures.

Figure 3-4 showed that both the intensity and the lifetime of CLP emission were strongly quenched at room temperature. As explained in Section 2.2.1, in classical FRET, the through-space transfer of excitation energy from the donor to the acceptor depopulates the excited state of the donor, thus affecting both its quantum yield and PL lifetime (dynamic quenching). Additional mechanisms, such as formation of a non-fluorescent ground-state complex* to the acceptor, might substantially reduce the steady-state emission, while not affecting the apparent lifetime of the emissive donor molecules (static quenching). In order to address this point, Figure 3-10 demonstrates the efficiency of donor quenching as a function of acceptor concentration determined from the time-resolved and from the steady-state fluorescence experiments both below and above the C_p. (cf. Figure 3-4 and 3-7). When determining the quenching efficiency from the fluorescence decay curves, I considered FRET to multiple acceptors in a homogenous three dimensional solution of donors and acceptors, neglecting the fact that the acceptor molecule does not form a point dipole.

* Known also as "contact quenching", this mechanism requires strong coupling between a quencher and the fluorescent molecule. The process does not reduce the lifetime because the properties of the fluorophores which are not complexed are not affected.

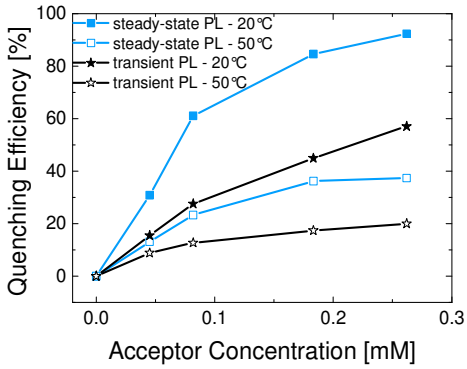

Figure 3-10: Efficiency of quenching of the CLP emission at 20 °C and 50 °C as a function of acceptor concentration, as calculated from transient fluorescence data by use of *Eq.* 2-10, and determined by applying *Eq.* 2-7 to the steady-state emission spectra. The bi-exponential fits performed on the decay curves of the CLP in the absence of P3TMAHT are demonstrated in Figure 3-S5.

Figure 3-10 demonstrates the strong quenching of the donor emission, continuous as more acceptor molecules are present in the mixtures at 20 °C, in contrast to the considerably low quenching efficiencies at 50 °C. Notably, for both temperatures and at each acceptor concentration, the quenching efficiency determined from the PL transients is smaller than the steady-state value[*], meaning that processes, which cannot be detected by the time-resolved PL set-up, contribute to donor emission quenching. This is possibly related to a rapid excitation transfer and formation of non-luminescent states. According to Equation 8-10, if FRET solely accounts for the observed quenching, a higher acceptor concentration would be necessary in order to account for the measured efficiency. For instance, with R_0=3 nm, an acceptor concentration of 7 mM is required to rationalize the reduction in the decay time and the related Φ of 50%. The discrepancy between the actual acceptor concentrations and those extracted from the decay fit confirms the preferential positioning of the thiophenes in the mixture close to the donor chromophores.

3.3.3 Aqueous Solubility and Aggregation[†]

Laser light scattering is a powerful tool to study the association/aggregation behavior of polymer chains in solution.[160-164] Figure 3-11 displays the intensity autocorrelation functions $g^{(2)}(\tau)$ recorded for the donor, acceptor and their mixture before and after the solubility transition.

[*] Inner filter effects were negligible due to the short path length of the cuvettes (1 mm) used in steady-state measurements. This limits the contribution from the trivial energy transfer processes which would artificially enhance the quenching efficiency. On the other hand, transient spectra are impervious to this effect.

[†] Light scattering measurements were performed by *Leonardo Chiappisi* in the *Stranski-Laboratory for Physical and Theoretical Chemistry of Technische Universität Berlin*.

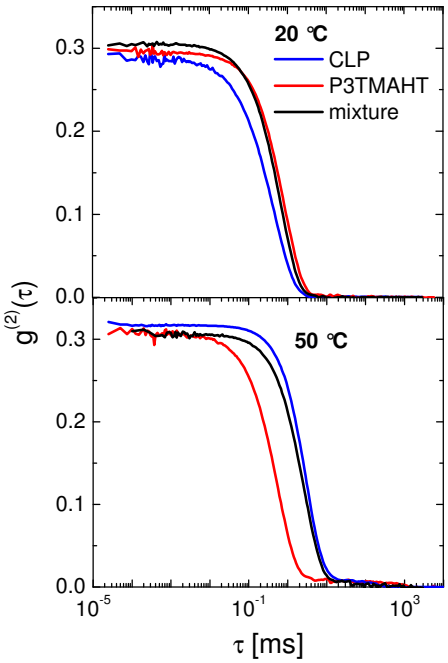

Figure 3-11: Behavior of the intensity-time autocorrelation function recorded for the donor CLP (0.6 mM), acceptor P3TMAHT (0.08 mM), and their mixture in PBS at 20 °C and at 50 °C, all showing a mono-modal decay.

The analysis of the scattering intensity values available from these data provides insight on the aggregation properties of the polymers. This structural information can then be correlated with the findings of fluorescence measurements. The values of the radius of gyration R_g, apparent molecular weight $M_{w,app}$, chain density ρ, and aggregation number N_{agg} are summarized in Table 3-1. For the determination of these parameters, see Chapter 7, section 2.4.

Table 3-1: Laser light scattering results of CLP (0.6 mM), P3TMAHT (0.08 mM), and of their mixture in PBS

Polymer	T [°C]	R_g [nm]	$M_{w,app}$ [10^6 g mol^{-1}]	ρ [10^{-3} g cm^{-3}]	N_{agg}
CLP	20	55	2.1	2.3	33
P3TMAHT	20	115	30.7	3.7	3800
Mixture	20	90	9.9	2.5	
CLP	50	140	690.0	46.4	10950
P3TMAHT	50	125	33.1	3.1	4100
Mixture	50	135	481.0	36.0	

The solution of OEGMA based copolymer (0.12 g L^{-1}) contains structures exhibiting a much higher molecular weight (corresponding to an aggregation number of ca. 30) and a larger R_g (55 nm) than expected for a swollen single chain. The apparent chain density of these "associates" is very low (about 0.2% of the dry polymer) indicating that the chains forming the loose associates are in a fully hydrated state and hold a large amount of water

molecules. This pre-aggregation has not been observed in earlier DLS studies of analogous copolymers. The aqueous solutions (1 g L^{-1}) of the p($MEO_2MA_{0.9}$-*co*-$OEGMA_{0.1}$) (containing 90 mol% MEO_2MA and 10 mol% of OEGMA) included small particles with a hydrodynamic radius (R_h) of ca. 3 nm and larger aggregates of ca. 150 nm while the latter represents less than 0.01% of the polymer chains.[165] Therefore, the chains were suggested to adopt mostly a coiled conformation in water.* Nevertheless, examples for intermolecular association of pEG-based structures are not rare in literature. For example, pEG chains formed micelles in water,[166] or hydroxy-capped comb-like OEG chains attached to a methacrylate backbone showed a spontaneous aggregation into highly order structures, such as vesicles.[167] Moreover, the low value of ρ of CLP corresponds to densities observed for aqueous solutions of slightly hydrophobic pNIPAm, and of pEG containing block copolymers before their insolubility transition.[61,160,168] Such pre-aggregation has also been observed for aqueous mixtures of pVME.[62]

For P3TMAHT, the observed aggregation (N_{agg}=3800) is not surprising as these chains in D_2O were found to form charged aggregates ordered in a 3-D array at room temperature via small angle neutron scattering studies.[119] The scattering features were assigned to interacting and predominantly spherical polymer particles.[169] In this two-component mixture, the values of structural parameters are intermediate of those of the CLP and the P3TMAHT. Interestingly, the correlation function of the mixture is mono-modal, pointing to the presence of only one type of aggregate (cf. Figure 3-11). Apparently, the hydrophobic interactions between the two polymers link them without precipitation at 20 °C. The mobility of the acceptor and donor units seems to be sufficiently high for an efficient FRET process.

The conformational change of thermoresponsive polymer chains induced by the increased temperature is reflected in the slower decay of the correlation curve in Figure 3-11. While CLP solution consists of larger, much denser and heavier aggregates at 50 °C, almost no difference for $M_{w,app}$ is observed in the aggregation behavior of the pure acceptor chains. The latter finding is expected for this non-thermoresponsive polymer. Upon heating the mixture above the C_p, $M_{w,app}$ and ρ increase strongly and attain values only slightly smaller than those measured for the pure CLP solution under the same conditions. This means that the CLP undergoes a solubility transition with subsequent formation of large globules, which reduces the number of interacting sites available for P3TMAHT. Importantly, as at 20 °C, the decay of the mixture exhibits a single relaxation, suggesting that P3TMAHT chains are

* This copolymer was synthesized via atom transfer radical copolymerization which provided better defined co-polymers with controlled molecular weight, composition and molecular weight distribution than free radical copolymerization [165]. It has a M_n^{app} of 20100 g mol^{-1} and a PDI of 1.35. Moreover, it is possible that the observed differences are due to the different experimental conditions and the measurement set-up.

involved in CLP globules (cf. Figure 3-11). Local segregation of the components in these large hydrophobic globules, possibly in combination with a limited chain mobility,[61] seems to be the reason for the drastic decrease in FRET efficiency.

3.3.4 The Nature of Intermolecular Interactions

As introduced in Section 2.3.2, CPE chains change their conformation or the association behavior as a result of interactions with other charged molecules. Similar to previous reports,[119] the absorbance and fluorescence properties of aqueous solutions of P3TMAHT are severely affected by complexation with the anionic surfactant SDS.

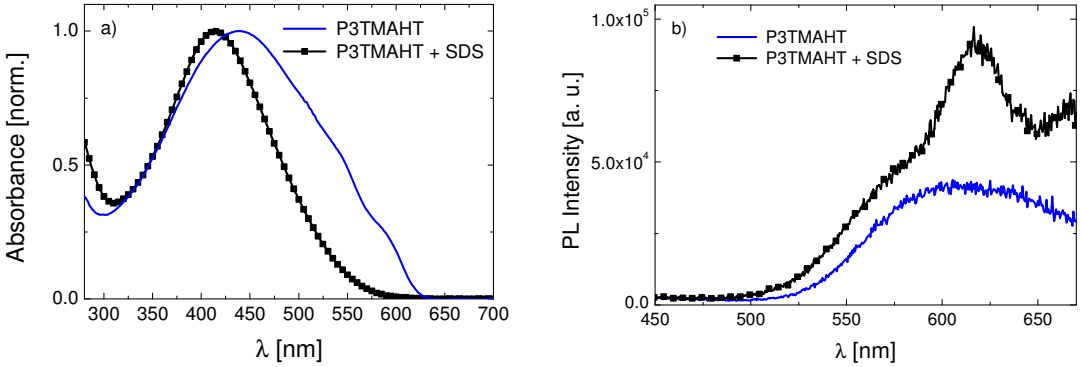

Figure 3-12: Modified absorbance **a)** and emission **b)** spectra of P3TMAHT (0.03 mM) upon addition of SDS (0.4 mM) at 20 °C.

As the two molecules interact, the broad absorbance of P3TMAHT becomes narrower and its maximum shifts to lower wavelengths (Figure 3-12a). Besides, the featureless PL spectrum is now structured with a peak with two shoulders (Figure 3-12b). These distinct features that SDS evokes can be used to qualify the strength of interactions between P3TMAHT and CLP. As SDS molecules are injected into the mixture of CLP with P3TMAHT, $I_{Acceptor}/I_{Donor}$ decreases from 0.39 to 0.07, i.e., FRET from CLP to P3TMAHT is almost fully suppressed (Figure 3-13). The structuring at the longer wavelengths resembles Figure 3-12b, evidencing the specific interactions with SDS. Note that the SDS concentration in the stock solution (4.5 mM) is below its critical micellization concentration*.

* This is the concentration of a surfactant solution above which self assembled structures named "micelles" are formed.

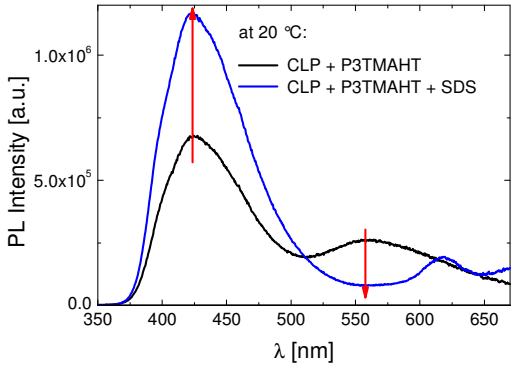

Figure 3-13: Changes in the fluorescence spectrum of the mixture of CLP (0.4 mM) and P3TMAHT (0.03 mM) upon addition of SDS (0.4 mM) at 20 °C. PL spectra were recorded at an excitation wavelength of 340 nm. The arrows point towards suppressed FRET in the presence of the surfactant.

Although the non-ionic CLP might as well interact with the surfactant, such an association in the present concentration range must be rather weak as it would have otherwise prevented the phase transition of the CLP or retarded the C_p. The modified PL spectrum of the mixture, therefore, suggests that the charged complexes formed between the two electrolytes disable the interactions of P3TMAHT with CLP. This fact indicates the importance and the priority of electrostatic interactions between oppositely charged species in aqueous media.

3.3.5 Conclusions

In contrast to most of the binary systems, the sensing strategy presented here relies on the unspecific interactions between the thiophene-based cationic CPE (P3TMAHT) and the OEGMA-based non-ionic fluorescent copolymer (CLP). Efficient energy transfer from the CLP to the CPE with the alterations in the shape of the P3TMAHT optical spectra evidences that the macromolecules interact at room temperature. Such interactions are modulated by increasing the solution temperature which leads to drastic changes in the solution structure. Above the C_p of the responsive polymer, large globules which comprise both donor and acceptor polymers are formed as deduced from the increased scattering values and mono-modal decay curves. From the reduced FRET efficiency at this temperature, these globules are suggested to have an inhomogeneous structure with domains of rather pure donor and pure acceptor sites. Overall, with an undemanding copolymerization strategy lacking of precise control on the location of fluorescent moieties, temperature-sensitive self-assembly of these macromolecules enabled the visualization of the solution temperature. The fact that P3TMAHT interacts with certain type of molecules, such as the SDS shown here, might pave the way for chemo-sensing based on this assembly.

3.4 Response to Ionic Strength

The temperature sensing approach introduced in Section 3.3 relies on the interactions between water and the CLP, which become relatively unfavorable by increasing the temperature. The ionic strength of the solution is an environmental parameter which modulates the solubility of the copolymer in a somehow similar fashion. In fact, specific ion effects on the aqueous solubility referred to the "salting in" and "salting-out" behavior, and their relation to the Hofmeister series* have been investigated not only for standard polymers such as the pNIPAm,[150,170-174] and pEG,[96,175-179] but also for copolymers of OEGMA-based macromonomers.[74,89,180,181] The ion-induced change in aqueous solubility of EGs has traditionally been reasoned with perturbations of the water structure.[96] In particular, the salting-out phenomenon was associated with the competition between the salt anions and the ether oxygens for hydration water,[175,182] and with the removal of the polarized water from the hydration shell. Both of these mechanisms render segmental (polymer-polymer) interactions more favorable.[96,177] For OEGMA-based copolymers, the effect of solution ionic strength was more severe than for pNIPAm when both were confronted by the same type and concentration of salts.[170,171,180] This sensitivity was attributed to the EG-rich side chains impacting solvation and leading to a strong structuring of water. Although these findings allowed at least qualitatively a prediction of the direction and the extent of the LCST shift with regard to the type of ionic species and to their concentration, the effect of ions on the aqueous solution structure and on the phase transition behavior has only been examined in parts. With the aim of showing the potential of this system to be a salt-sensitive fluorescent probe, the following discussion will therefore give particular consideration to the LCST-transition of the copolymer in the presence of NaCl and of the polycation.

3.4.1 Photophysical Properties

Firstly, in order to elucidate the effect of different monovalent salts on the temperature-dependent solubility behavior of CLP and of its mixture with P3TMAHT, I recorded the transmission of the solutions as a function of temperature. Increasing the amount of NaCl from 0 to 1 M in aqueous solutions of CLP gives rise to a strong salting-out effect, as evident from the shift of the C_p to lower temperatures in Figure 3-14a.

* A series of salts that leads to a consistent trend on the solubility and conformational stability of proteins, named after the discovery of F. Hofmeister. The theory initially reasoned this trend with the type of the changes created in water structure, either making or breaking the water structure. Anions appear to have a larger effect than cations.

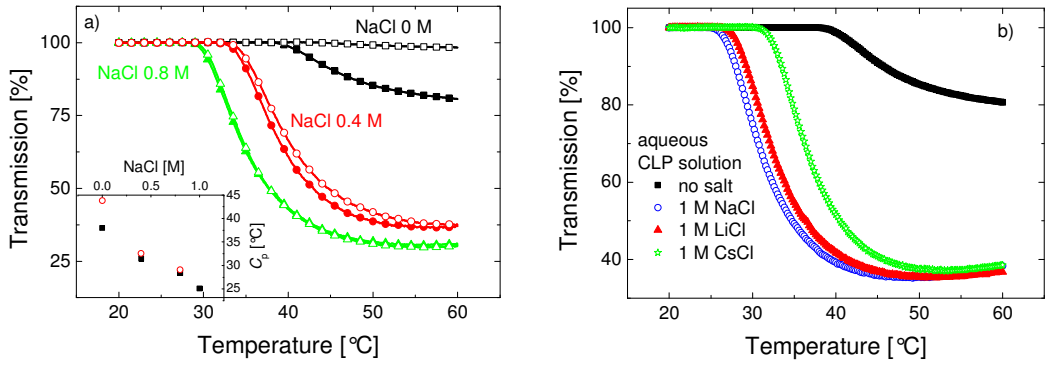

Figure 3-14: **a)** Temperature-transmission profiles of an aqueous solution of CLP (0.66 mM-full symbols), and its mixture with P3TMAHT (0.08 mM-hollow symbols) at various concentrations of NaCl (0 M, 0.4 M, 0.8 M as squares, circles, and triangles, respectively). The inset depicts the cloud point of these solutions as a function of NaCl concentration (full squares: CLP, hollow circles: mixture) **b)** Turbidity curves of aqueous solutions of CLP (0.66 mM) in the presence of NaCl (1 M), of LiCl (1 M) and of CsCl (1 M).

The salting-out effect is not limited to NaCl, but the C_p is shifted to lower temperatures also in presence of LiCl or CsCl (Figure 3-14b).* This rules out that the shift is governed by specific interactions between the Na^+ ions and the pEG chains. With the addition of NaCl, the C_p of the mixtures is suppressed as well (Figure 3-14a, hollow symbols). Compared with that of the pure CLP solutions, the transition of the mixtures occurs at higher temperatures. For the mixtures in PBS (0.15 M), such a shift was recorded and attributed to direct interactions of CLP with P3TMAHT (cf. Figure 3-2). Here, one can see that the presence of salt affects the magnitude of this polyelectrolyte-induced elevation of the LCST: it is most prominent in the case of the salt-free mixture, while it becomes negligible at higher salt concentrations.

The effect of salt on the interactions between the macromolecules and on the spatial proximity of FRET pairs can be probed with PL measurements summarized as in the following (Figure 15a).

* The shift is less pronounced for LiCl and even less for CsCl, so this system is not directly following the Hofmeister series. For cations: $Cs^+ > Na^+ > Li^+$ (the order is for salting out effect)

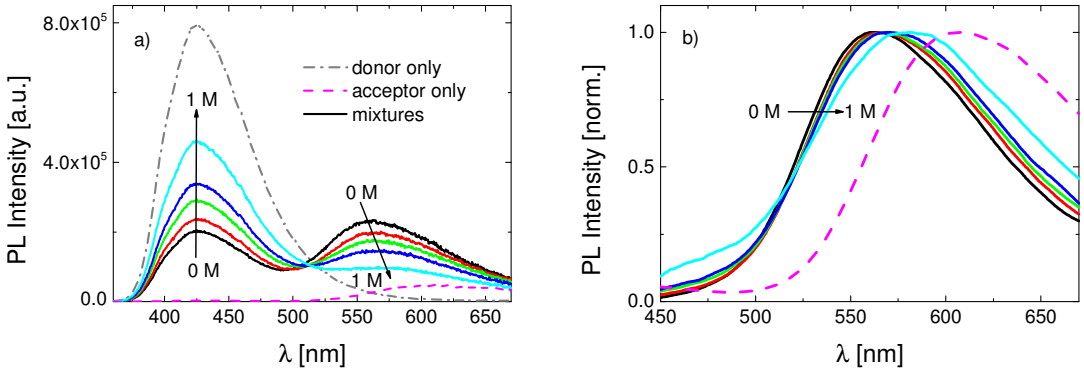

Figure 3-15: **a)** PL spectra of an aqueous solution of CLP (0.66 mM), P3TMAHT (0.08 mM), and of their mixtures containing increasing amounts of NaCl at 20 °C **b)** Normalized PL spectra of the acceptor (solid lines) obtained after subtracting the contribution of CLP emission from the mixture spectra shown in a). Also shown is the pure acceptor spectrum (dashed line). The directions of the arrows indicate the increasing concentration of NaCl [0.00, 0.15, 0.30, 0.55 and 1.00 M].

The presence of NaCl influences the shape of the PL spectrum significantly: the emission of CLP is recovered, while that of P3TMAHT weakens. Replacing the Na^+ cation of the added salt by Li^+ or by Cs^+ affects the emission similarly (Figure 3-S6). Note that these monovalent chlorides change neither the shape nor the intensity of the PL spectra of the pure polymers (Figure 3-S7). Therefore, the evolution of the emission properties is directly related to the mutual presence of the two polymers. Apparently, the number of donors and acceptors residing in close proximity to each other decreases as more salt is present in the mixture. Apart from quantifying the FRET efficiency, the emission profile of the mixtures gives hints on the overall interaction capacity. This point is stressed in Figure 3-15b. We know that λ^{PL}_{max} of the acceptor is blue-shifted in the presence of CLP (compare the solid lines with the dashed one). As more NaCl is present in the mixture, the magnitude of this shift decreases, indicating that not only the spatial distance of coumarins to thiophenes, but also the extent of overall inter-polymer interactions is reduced.

From the PL spectra of these mixtures bearing varying amounts of salts, one can see that the efficiency of FRET depends strongly on the salt concentration not only at 20 °C, but also above the C_p. Figure 3-16a demonstrates the continuous decrease in FRET efficiency with the increase in salt concentration, both at 20 and at 50 °C, with absolute values regulated by the temperature. As for each salt concentration energy transfer is still significantly more efficient at 20 °C than at 50 °C, this system is double stimuli-responsive. The temperature-regulated FRET on-off switch is most effective in the presence of solution ions at 0.15 M.*

* This can be interesting for biological applications since the ion concentration corresponds to physiological conditions.

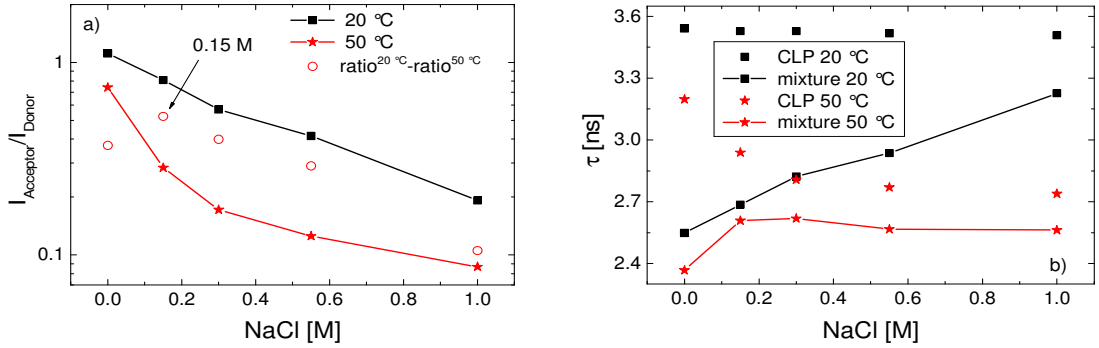

Figure 3-16: **a)** FRET efficiency expressed as $I_{Acceptor}/I_{Donor}$ at 20 °C and 50 °C as a function of the NaCl concentration. The hollow symbols quantify the change of the $I_{Acceptor}/I_{Donor}$ value when going from 20 to 50 °C. **b)** The amplitude-weighted fluorescence lifetime of CLP measured for pure solutions and the mixtures at 20 °C and 50 °C *vs.* NaCl concentration.

In agreement with the steady-state results, the CLP lifetime* is strongly quenched in mixtures at 20 °C, but increases proportionally to the salt concentration (Figure 3-16b). At 50 °C, the quenching efficiency, i.e. the reduction of donor lifetime, becomes very low for 0.15 M NaCl and remains constant for higher salt contents. Note that the phase transition of CLP both in ion-free and 1 M NaCl containing mixture has an only small effect on the FRET efficiency.

3.4.2 Solution Properties in Relation to Salt Concentration

Figure 3-16 demonstrated that an increase in either solution temperature or in salt concentration has, in principal, similar effects on the efficiency of energy transfer. In order to understand which molecular contacts, to what extent, are affected by a change in temperature and/or salt concentration, high-resolution ^{1}H NMR and Nuclear Overhauser Effect Spectroscopy (NOESY) experiments were performed.

*3.4.2.1 NMR studies**

NMR allows for determining proximities between different proton-bearing chemical groups up to ~5 Å.[183] Figure 3-17 summarizes the ^{1}H NMR spectra recorded at 13.4 °C for both of the polymers and for their mixture in D_2O, including the assignment of the ^{1}H signals to the respective chemical groups. The ^{1}H NMR spectrum of CLP shown in Figure 3-17d displays narrow resonances for chemical groups labeled with *c*-*h*, pointing to an open, flexible

* Somehow, temperature has a more prominent quenching effect on the donor lifetime in the presence of salts.

* The NMR experiments, the data analysis and interpretation were performed by *Michael R. Hansen* and *Manfred Wagner* in the *Max Planck Institute for Polymer Research* in Mainz.

structure. Earlier NMR studies of an analogous yet unlabeled copolymer noted that the backbone had considerably broadened and reduced signals in D_2O as compared to those observed in a good solvent ($CDCl_3$). On the other hand, the resonant peaks corresponding to EG-rich side chains remained sharp, i.e., the hydration of these macromolecules was not uniform with more water molecules surrounding the hydrophilic side chains and less water molecules around the backbone.[42,165] In contrast to CLP, P3TMAHT shows much broader ^{1}H signals (Figure 3-17c), e.g., the resonance of the thiophene proton (*7*) is of low intensity and spreads over ~1 ppm. These features are clear indications of an aggregated structure and in agreement with what has previously been suggested for this polymer.[119,169]

The mixture spectra is given in Figure 3-17b. Clearly, this spectrum shows much narrower ^{1}H signals from P3TMAHT than the one in Figure 3-17c, while signals from CLP have comparable ^{1}H line widths with those in Figure 3-17d. Moreover, the ^{1}H signals associated with thiophene protons (*7*) and the methyl groups (*1*) of P3TMAHT include shifts to higher frequencies in the mixtures. This demonstrates that P3TMAHT aggregates are partly dispersed in the presence of the CLP.

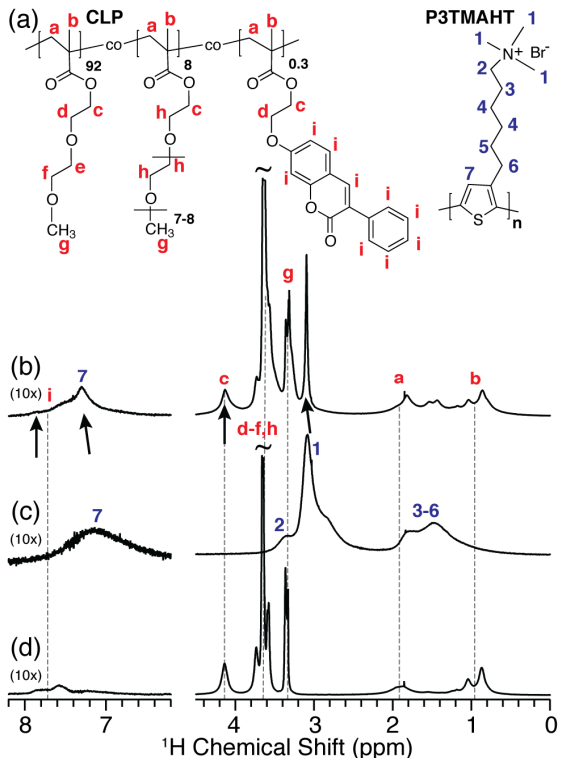

Figure 3-17: Liquid-state ^{1}H NMR spectra recorded at 13.4 °C in D_2O for **b)** the mixture of CLP (8.5 g L^{-1}, 44.9 mM in repeat units) and P3TMAHT (2.0 g L^{-1}, 6.6 mM in repeat units) and **c)** P3TMAHT (2.0 g L^{-1}) and **d)** CLP (8.5 g L^{-1}). All spectra were recorded at 850.27 MHz (20.0 T) for ^{1}H. The assignment scheme given in **a)** uses (red) letters and (blue) numbers for CLP and P3TMAHT, respectively. The arrows between b) and c) mark ^{1}H resonances in the mixture that can be assigned specifically to the individual components.

Based on the assignments of CLP and P3TMAHT, the ^{1}H signals of the first methylene group of the side chains (*c*) and of the coumarin (*i*) of CLP together with those from the methyl end groups of P3TMAHT (*1*) appear well-resolved with no signal overlap in the mixture of CLP and P3TMAHT. These signals can be used as observation points for Nuclear Overhauser Effect (NOE) as shown in Figure 3-18. For a mixing time of 200 ms, we record intra-correlations between the thiophene (*7*) and the side chain (*2*-*6*) of P3TMAHT, while CLP shows strong correlations between the methacrylate backbone (*a*-*b*) and the EG (*d*-*g*) side chains. A set of intermolecular ^{1}H-^{1}H NOE cross peaks is detected between the first methylene group of the glycol side chains (*c*) of CLP and the methyl end groups (*1*) of P3TMAHT as marked by the arrows in Figure 3-18. Also observed are correlations between the coumarin (*i*) of CLP and the methyl end groups (*1*) of P3TMAHT. Based on these results, it is reasonable to conclude that the average distance between these contact points of the polymers in D_2O at 13.4 °C is less than of 5 Å,[184] and this close proximity is responsible for the efficient FRET.

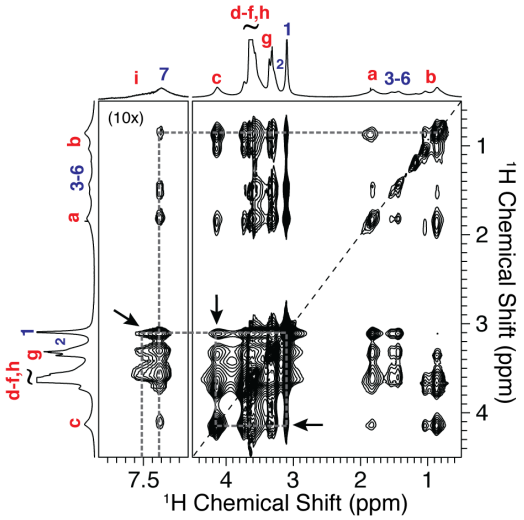

Figure 3-18: 2D ^{1}H-^{1}H NOESY spectrum for the mixture of CLP (8.5 g L^{-1}) and P3TMAHT (2.0 g L^{-1}) in D_2O at 13.4 °C with NOE mixing time of 200 ms. The spectrum was recorded at 850.27 MHz (20.0 T) for ^{1}H. The assignment follows that of Figure 3-17a. Arrows indicate specific NOE cross peaks between CLP and P3TMAHT. The intensity of the signals arising between 7 and 8 ppm are expanded by a factor of 10 for better visibility.

Since the maximum temperature that the NMR probe could handle was 60 °C and the transition detectable by NMR occurred at temperatures higher than that, we were not able to detect the phase transition of CLP in D_2O. However, as the phase transition temperature was significantly lower in the presence of NaCl, temperature variable ^{1}H NMR and 2D ^{1}H-^{1}H NOESY could be employed for the solutions containing 1 M NaCl. The results are as summarized in Figure 3-19. At 13.4 °C, the ^{1}H NMR spectrum of the mixture in 1 M NaCl

show similarities to the one recorded in de-ionized water in Figure 3-17b. However, the ^{1}H signals assigned to the thiophene protons (*7*) and those of the methyl end groups (*1*) of P3TMAHT have decreased intensities in 1M NaCl. This difference comes as a result of an increase in ^{1}H line width, indicating that P3TMAHT has a stronger tendency to aggregate in this mixture. Note that the spectrum of pure P3TMAHT in D_2O does not differ from that in 1 M NaCl (Figure 3-S8). The fact that CLP does not disperse the P3TMAHT aggregates as effectively as in de-ionized D_2O points to reduced inter-polymer interactions in the presence of NaCl.

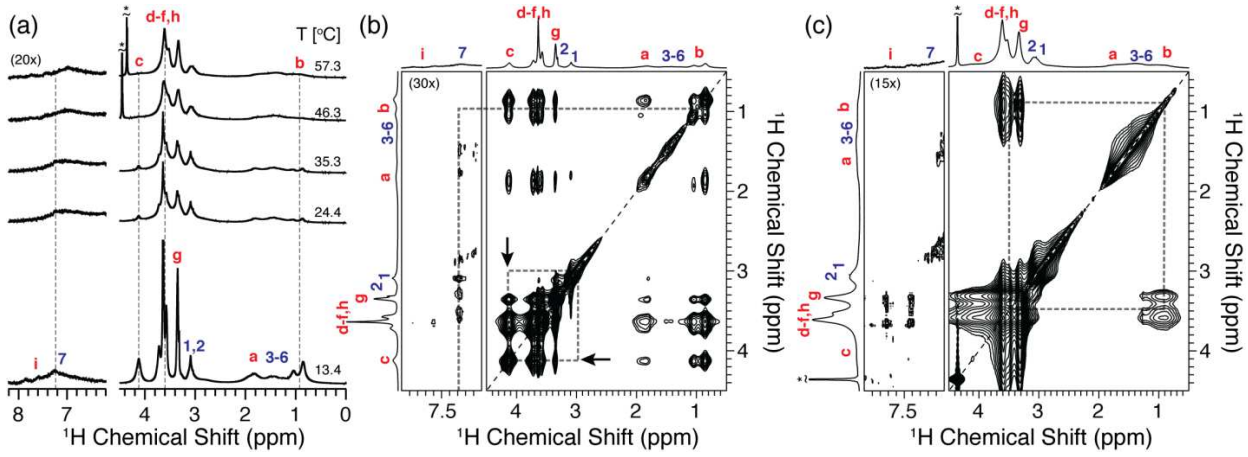

Figure 3-19: **a)** ^{1}H NMR spectra of the mixture of CLP (8.5 g L^{-1}) and P3TMAHT (2.0 g L^{-1}) in 1 M NaCl. 2D ^{1}H-^{1}H NOESY spectra for the same mixture obtained with a NOE mixing time of 200 ms at **b)** 13.4 °C and **c)** 57.3 °C. All spectra were recorded at 850.27 MHz (20.0 T) for ^{1}H and the assignment follows that of Figure 3-17a. The asterisks in a) and c) mark the position of the residual water signal. The intensity of the signals between 7 and 8 ppm is expanded according to the given factors for better visibility.

As the solution temperature is raised, the intensity of the signals in Figure 3-19a decreases gradually with an increase in the line width. This is most valid for the ^{1}H signals assigned to CLP, where the signal for the first methylene group of the glycol side chains (*c*) disappears completely above 46.3 °C. Moreover, the signals from the methacrylate backbone (*a* and *b*) are significantly broadened even at 24.4 °C. These observations suggest that the LCST transition of CLP occurs gradually at the molecular scale, first with stiffening of the methacrylate backbone followed by continuous dehydration of the whole chain. At elevated temperatures, this eventually leads to the restricted motions of the glycolic side chains.

The NOESY spectra recorded at 13.4 °C and 57.3 °C are illustrated in Figure 3-19b and c, respectively. At 13.4 °C, the 2D spectrum shows strong intramolecular ^{1}H-^{1}H cross peaks between each of the different chemical groups for CLP only, while those for P3TMAHT are of very low intensity when comparing to those in de-ionized D_2O (cf. Figure 3-18). These observations are valid also for the spectrum at 57.3 °C. Moreover, at both temperatures, the

strong intermolecular cross peaks present in D_2O between the first methylene group of the side chains of CLP (*c*) and the methyl end groups of P3TMAHT (*1*) are absent (marked by the arrows in Figure 3-19 b). There is also no evidence for the interactions of the latter with the coumarin of CLP (*i*). This proves that the presence of NaCl both below and above the C_p reduces the inter-polymer interactions; at least those below 5 Å.* When heated, the significantly broadened signals of the mixture are indicative of the presence of immobilized chains. Here, an important question to address is whether the salt-induced changes in the interaction capacity evident from NMR and photophysical studies are governed by the conformation/aggregation behavior of the chains, in particular of CLP. SLS measurements on these solutions at 20 °C and 50 °C can elucidate this point.

3.4.2.2 Static light scattering measurements†

Structural parameters deduced for solutions at 20 °C are summarized in Table 3-2.

Table 3-2: Structural data as deduced from the SLS measurements for aqueous CLP solutions (0.66 mM) and its mixture with P3TMAHT (0.08 mM) at 20 °C.

Polymer	R_g [nm]	$M_{w,app}$ [10^6 g mol^{-1}]	ρ [10^{-3} g cm^{-3}]	N_{agg}
CLP in 0 M NaCl	96	16	3.3	350
CLP in 0.3 M NaCl	102	24	4.2	530
CLP in 1 M NaCl	120	61	6.5	1300
Mixture in 0 M NaCl	101	13	2.3	
Mixture in 1 M NaCl	120	30	3.2	

All solutions of CLP exhibit much higher values for $M_{w,app}$ and R_g than compatible with the existence of single chains. This was observed also for solutions in PBS (cf. Table 3-1). Correlated with the presence of NaCl ions denser, heavier, and larger associates are formed, evidencing the salting-out event. A similar trend is observed also for the mixtures: the R_g, $M_{w,app}$, and ρ increase with the salt concentration, however, $M_{w,app}$ and ρ values remain lower compared to those of the pure CLP. P3TMAHT becomes only slightly more aggregated in the presence of 1 M NaCl (Figure 3-S9), which might be attributed to a screening of electrostatic repulsions.

* It seems to be that the short range interactions (active <5 Å) which are strong in the absence of NaCl or before the phase transition are hindered when NaCl is added to the mixtures or when they are heated.

† Light scattering measurements were performed by *Leonardo Chiappisi* in the *Stranski-Laboratory for Physical and Theoretical Chemistry of Technische Universität Berlin*.

Table 3-3: Structural data for aqueous CLP solutions (0.66 mM) and its mixture with P3TMAHT (0.08 mM) at 50 °C.

Polymer	R_g [nm]	$M_{w,app}$ [10^6 g mol^{-1}]	ρ [10^{-3} g cm^{-3}]	N_{agg}
CLP in 0 M NaCl	64	350	243	7600
CLP in 0.3 M NaCl	139	840	58	18500
CLP in 1 M NaCl	138	830	58	18200
Mixture in 0 M NaCl	59	31	28	
Mixture in 1 M NaCl	134	420	32	

Table 3-3 summarizes the structural parameters analyzed for the solutions heated above their C_p. It is obvious from the dramatic increase of the $M_{w,app}$ and especially of the ρ that all solutions have experienced the LCST-type phase transition. Similar packing densities were reported by Trezebicka *et al*. for structurally analogous copolymers.[64] The remarkable feature here is the effect of NaCl on the structure of the aggregates: Concerning the pure CLP solutions, the chains in the presence of 1 M NaCl constitute large and heavy globules which are relatively loose compared with the small and dense aggregates formed in de-ionized water. Such an influence of salts on the polydispersity and the size of mesoglobules was noted by Ballauff and coworkers in their work concerning the EG containing dendronized polymers.[66] For pNIPAm solutions, Pelton *et al*. also observed that a high concentration of NaCl led to larger pNIPAm particles or equivalently a lower concentration of mesoglobules.[60*]

Going from the pure CLP solution to the mixtures, one can observe the same trend associated with the salt concentration but also that the aggregates are lighter and less dense. This is particularly valid in case of the salt-free system, where the globular density of CLP is reduced ca. 8 fold in the mixture (from 0.24 to 0.03 g cm^{-3}), i.e. the interchain aggregations of CLP are hindered.

3.4.3 Discussion

The efficient energy transfer, the spectral shift of the acceptor and strong intermolecular NOE cross-peaks indicate that the CLP and the P3TMAHT chains are interacting. As the two polymers are mixed, they form interconnected networks, within which few contact points (including the coumarin and P3TMAHT side chains, cf. NOE spectra) enable free movements of chain segments. Also, within this architecture, the thermoresponsive chains seem to act as a surfactant and interrupt the aggregation of the polycation.

[*] In both studies, the observed influence of solution ionic strength on the size of aggregates was associated with the traces of ions accumulating on the surface of the particles.

When the ion-free mixture is heated above its C_p, the chains form compact aggregates, however, compared with pure CLP globules, these are much lighter (ca. 10 times) and relatively water-draining. In contrast to what was concluded for the mixture in PBS (cf. Section 3.3), there are indications of inter-polymer interactions even above the C_p. FRET efficiency remains relatively high, almost comparable to its value measured at room temperature. Also, the polyelectrolyte-induced C_p shift is most prominent in the absence of salts. These findings point to the fact that the interactions established between the two polymers before the phase transition are rather stable so that CLP chains have weak tendency to aggregate. In addition to unspecific hydrophobic interactions, an *electrostatic* attraction between the P3TMAHT cation and the ether oxygens of the OEG moieties might contribute to such stability of inter-polymer complexes. Winnik *et al*. reported slightly negative Zeta Potential values (indicative of a charged surface) for mesoglobules of the naphthalene and/or pyrene functionalized "non-ionic" pNIPAm.[61] Such ions accumulating on somewhat analogous CLP associates might lead to a complexation similar to the one between specific metal cations and crown ether containing polymers.[185] Regardless of the origin, in the absence of salt, inherently strong inter-polymer interactions seem to keep the chains in close proximity.

The mixtures containing NaCl differ largely when compared to the de-ionized case. With the increase in NaCl concentration, the shift in λ^{PL}_{max} of the acceptor is less prominent and the energy transfer efficiency is gradually reduced. The effect of P3TMAHT on the turbidity profile of CLP is also weakened. NMR spectra suggest that no intermolecular interactions take place below 5 Å and a larger fraction of P3TMAHT chains aggregate in these mixtures. The pronounced effects of NaCl on the interactions between the two macromolecules might be related to two factors. First is the salting out of CLP, apparent from the formation of denser and larger associates of CLP. This might limit the accessibility of coumarins to thiophenes. Second factor is the screening of electrostatic interactions which account for the stability of the complexes in de-ionized water. Nevertheless, the CLP associates are loose enough to allow access of the coumarins. This leads to the much less substantial but still measurable FRET.

As for the mixture in PBS, drastic changes in aggregation properties are recorded when the mixtures including salts are heated above the C_p. Firstly, transfer efficiency is dramatically reduced. Second of all, LLS measurements show only a mono-modal distribution of aggregates, with no evidence of a second species that can be attributed to single P3TMAHT chains/aggregates. Therefore, the change in the mixture spectrum is attributed to the formation of almost pure domains of dehydrated CLP chains. However, the slight blue-shift in

λ^{PL}_{max} of the acceptor and the measured energy transfer suggest that the interactions of the CLP with the polycation are not completely hindered even in such dense domains. It is likely that as the temperature is increased, the gradual collapse of CLP forces the P3TMAHT out of the vicinity of coumarins, mostly towards the exterior of these inter-polymer complexes. This could lead to P3TMAHT forming a shell around collapsed CLP chains. Such an internal structure might be favorable as it would firstly keep the ionic water soluble groups in contact with water, therefore stabilizing the inter-polymeric globules, and secondly because of the protection of hydrophobic segments. The result is large and stable but not very dense inter-polymer aggregates with a segregated morphology. At this point, it is useful to summarize these findings in a structural picture as shown in Scheme 3-2.

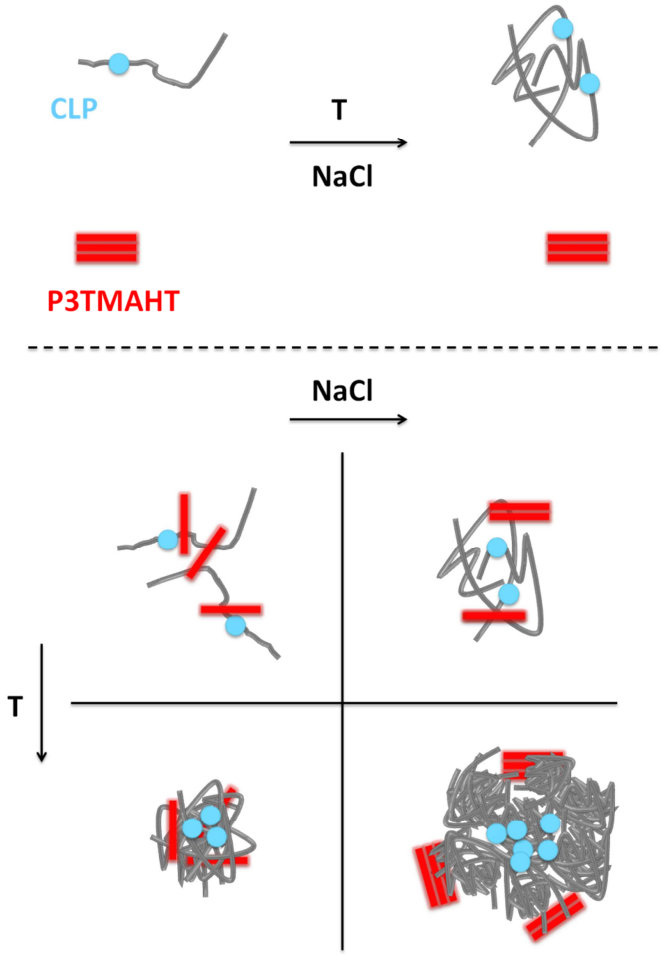

Scheme 3-2: Proposed model for the structural changes in the pure compounds (top) and the mixtures (bottom) upon addition of NaCl, or upon increasing the temperature above the C_p.

In this simplified scheme, an increase in NaCl concentration or in solution temperature promotes dehydration and associations of CLP. P3TMAHT is rather insensitive to both parameters. NaCl is not only changing the conformation of CLP but also the interaction

strength between the two polymers.* Therefore, for a given molecular composition, it is the solution ionic strength which determines whether the FRET efficiency can be modulated with temperature or not. For the mixtures, the structural impact of heating in the presence of ions is more drastic than changing the ionic strength of the isothermal solution: intermolecular aggregates of locally segregated components are formed.

3.4.4 Conclusions

I showed via several methods that the coumarin labeled p(MEO_2MA-*co*-OEGMA), CLP, chains are in an open conformation in the ion-free mixture, enabling several contacts with the cationic polythiophene, P3TMAHT. Within this mobile network, self-aggregated P3TMAHT chains are rather dispersed and there are inter-polymeric contact points with less than of 5 Å distance. As NaCl is included in these mixtures, the electrostatic interactions of CLP with the polycation are screened in parallel to the partial dehydration of CLP. This is reflected as a reduction of the efficiency of FRET and of the extent of inter-polymer interactions. Upon the LCST-transition of CLP, the two polymers aggregate in a rather packed complex, where each component forms relatively pure domains. Such architecture restricts chain movements and limits the availability of the coumarins to P3TMAHT chains. However, this observation is only valid in the presence of salts and is dependent on it. In the absence of salts, the interactions are strong enough to keep the two polymers in contact against the temperature triggered-aggregations of CLP chains. This means that to obtain a change in fluorescence color with temperature, the solution has to bear a certain amount of ions (less than 1 M). Overall, the structure of this macromolecular assembly is very sensitive to changes in temperature and solution ionic strength and the system is able to report such changes with a change in its emission color. Notably, the assembly accomplishes most efficient temperature sensing at physiological salt concentration, which might be useful for biochemical sensing purposes.

* In the absence of NaCl, the structure of pure CLP mesoglobules is clearly different than that in the presence of NaCl, the reasons of which are yet unclear.

3.5 Supplementary Information

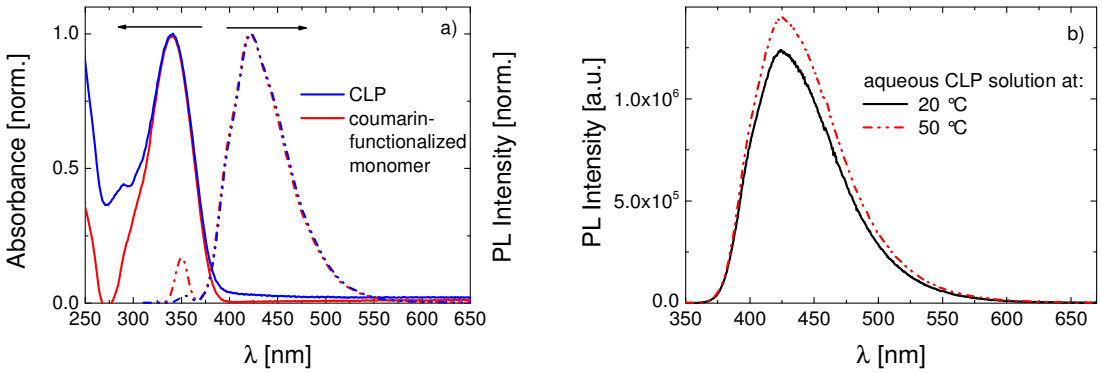

Figure 3-S1: **a)** The normalized absorbance and fluorescence spectra of the coumarin-functionalized monomer and the CLP in $CHCl_3$, **b)** the PL spectra of CLP at 20 °C and 50 °C (well below and above the C_p, respectively).

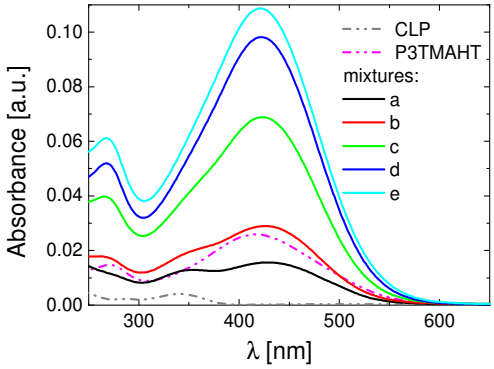

Figure 3-S2: Absorbance spectra of mixtures of the donor CLP (0.6 mM) and the acceptor P3TMAHT at increasing concentrations: a) 0.04 mM b) 0.08 mM c) 0.18 mM d) 0.26 mM e) 0.30 mM

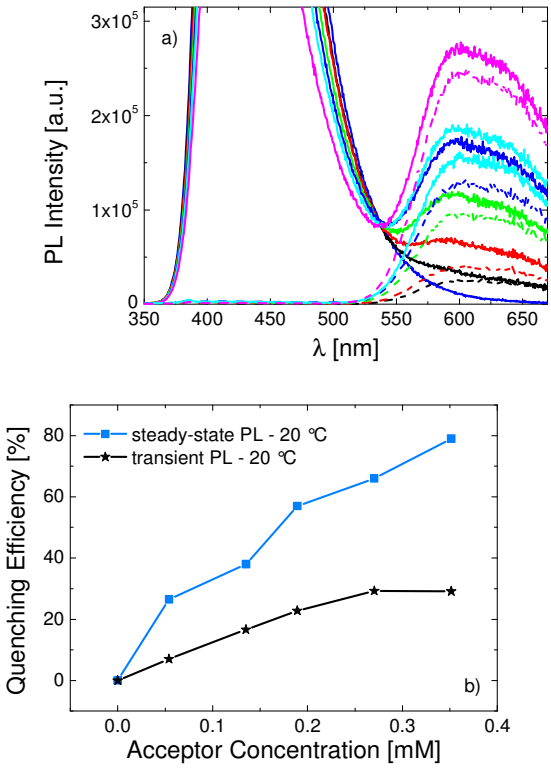

Figure 3-S3: **a)** Steady-state PL spectra of mixtures of CLP with increasing amount of zwitterionic polythiophene at 20 °C. The dashed lines which are correspondingly colored are the emission from the thiophene at each concentration measured under identical conditions. **b)** Efficiency for quenching of CLP's PL at 20 °C as a function of the anionic polythiophene concentration, as calculated from the transient fluorescence decay data and steady-state emission spectra by use of *Eq.* 2-7. The concentration of each polymer and experiment conditions are the same as for the CLP and P3TMAHT experiments.

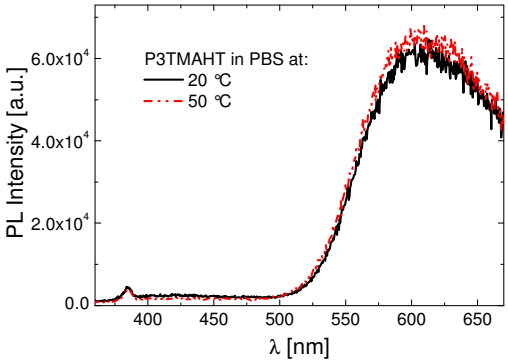

Figure 3-S4: Emission spectra of the acceptor P3TMAHT (0.09 mM) in PBS at 20 °C and 50 °C excited at 340 nm.

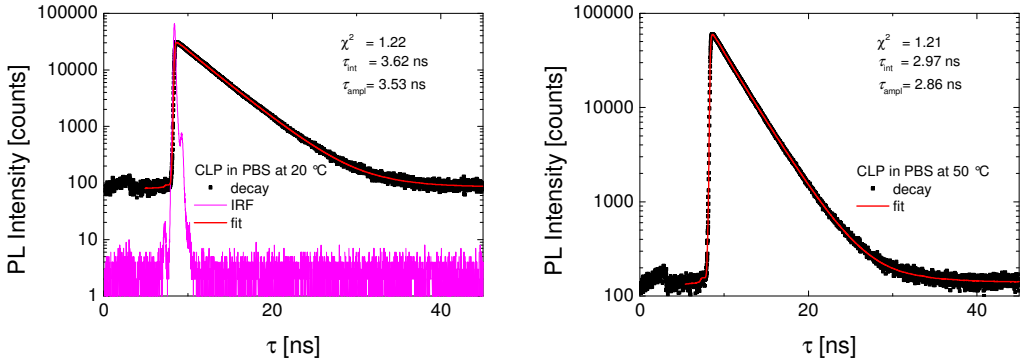

Figure 3-S5: Fluorescence decay curves of CLP solution in PBS (0.09 mM) with IRF function and the biexponential fits employed. The solution at 20 (left) and 50 °C (right) was excited at 360 nm and the emission was collected at 425 nm. Also given are the corresponding lifetimes and the quality of the fits described by χ^2.

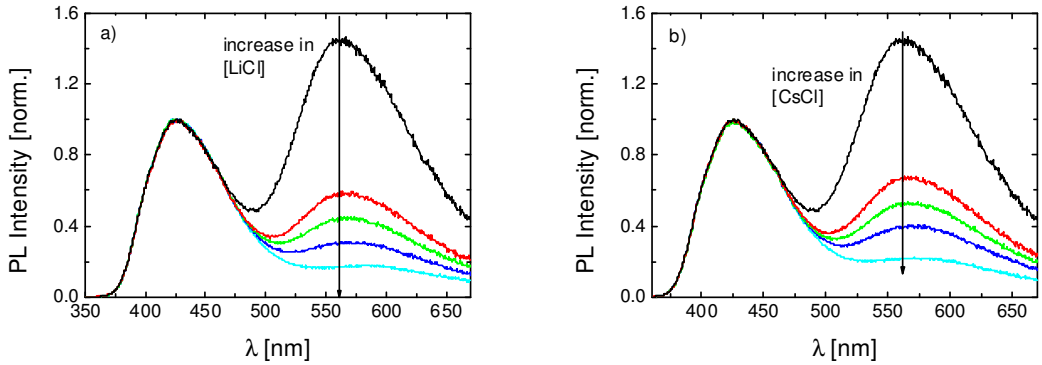

Figure 3-S6: PL spectra of the mixtures (CLP and P3TMAHT, 0.66 mM and 0.08 mM, respectively), normalized to CLP emission maximum. The direction of the arrow shows the concomitant decrease in P3TMAHT emission and the increase in the concentration of LiCl **a)** and CsCl **b)**. Solutions were excited at 340 nm and spectra were recorded at 20 °C.

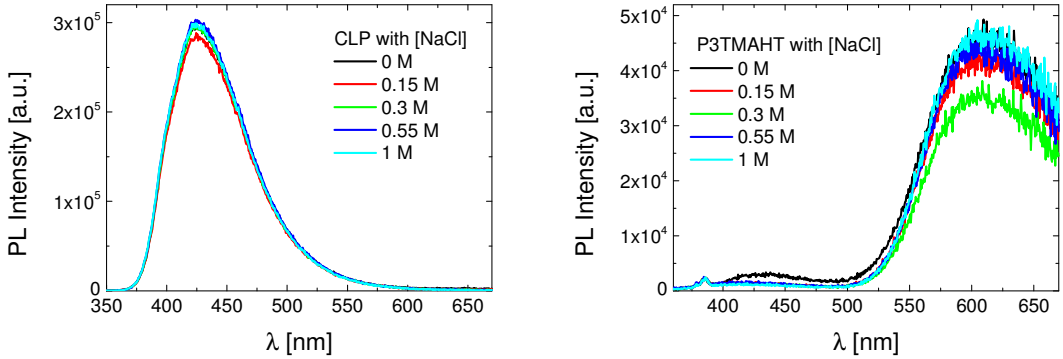

Figure 3-S7: Effect of NaCl on emission of CLP (left) and of P3TMAHT (right). The solutions were excited at 340 nm and the spectra were recorded at 20 °C.

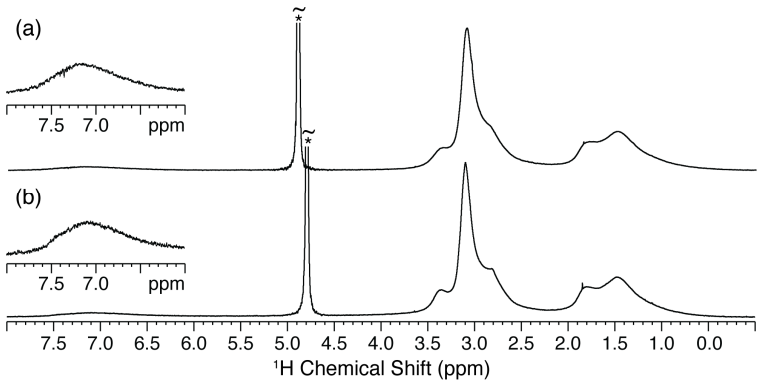

Figure 3-S8: ^{1}H NMR spectra recorded at 13.4 °C for P3TMAHT (2.0 g L^{-1}) in **a)** D_2O and **b)** 1M NaCl. Both spectra were recorded at 850.27 MHz (20.0 T) for ^{1}H. The expansion to the left illustrate the region of the thiophene protons while the asterisks mark the position of the residual water signal.

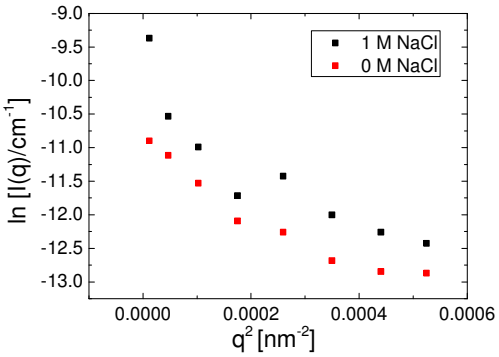

Figure 3-S9: The angular dependence of the intensity of scattered light from P3TMAHT aqueous solution with or without NaCl.

4 The Role of Chemical Structure of Dye-Labeled LCST-type Polymers on their Temperature-Regulated Fluorescence Response*

4.1 Background

This chapter presents how the chemical structure of LCST-type polymers affects their ability to act as aqueous molecular probes, e.g., fluorescent thermometers. The polymers are based on different thermoresponsive units, either on acrylamides or on OEG bearing (meth)acrylates. Although the fundamental mechanisms and grounds of the responsive behavior are comparable for most thermoresponsive polymers, properties such the extent of chain contraction and aggregation, or the structure of mesoglobules may differ significantly depending on the polymer structure.[1,42,48,49,64,69] Considering the application of these materials for optical sensing purposes, a thorough understanding of the solubility behavior is crucial. However, for the particular case of sensing through a fluorescence response, such aspects have not been stressed in detail.

To that aim, I implemented the sensing approach relying on the sensitivity of *solvatochromic* dyes (cf. Scheme 1-2b). This sensing concept has been exemplified by different polarity-sensitive fluorophores covalently attached to thermoresponsive polymers, as in the form of hydro/micro/nano-gels,[35,98,186] of linear chains in aqueous solution,[38,44,100,187,188] or of micelles.[20,142] For molecular probes based on the combination of a solvatochromic dye and thermoresponsive polymer to function, the solubility transition of the polymer must evoke drastic changes in the dye's micro-environment. Ideally, transformation of the water-exposed surrounding of the fluorophore at lower temperatures to a polymer-rich one after the phase transition results in a marked shift of its λ^{PL}_{max}. For some solvatochromic fluorophores,

* This chapter includes content from: S. Inal *et al.*, "Structure-related Differences in the Temperature-Regulated Fluorescence Response of LCST-type Polymers" *Journal of Materials Chemistry C* **2013**, *1*, 6603.

changes in the emission intensity and the fluorescence lifetime accompany the spectral shift.[103,107]

In the following, I will demonstrate the temperature-dependent properties of such a solvatochromic dye, i.e. a naphthalimide derivative, randomly incorporated into three different types of responsive polymers. The outcome of the PL studies suggests that the micro-environment provided to the dye, both before and after the phase transition, differs substantially with respect to the chemical structure of the host polymer. Correlated to laser light scattering studies, these findings are ascribed to the different degrees of pre-aggregation of the chains at low temperatures and to the extent of dehydration that the phase transition evokes.

4.2 Materials*

The copolymers of this work were prepared by standard statistical free radical copolymerization of a methacrylate monomer bearing the 4-dimethylamino-1,8-naphthalimide (4-DMN) dye with NIPAm, 2-(2'-methoxyethoxy)ethyl acrylate (MEO_2A), or an appropriate mixture of MEO_2MA and OEGMA. The resulting polymers are named as labeled pNIPAm (**P1**), pMEO_2A (**P2**), and p(MEO_2MA-*co*-OEGMA) (**P3**), respectively. The chemical structures of all three thermoresponsive polymers with their corresponding co-monomers are shown in Scheme 4-1.

* The thermoresponsive polymers and SEC analysis were provided by *Jonas D. Kölsch* from the *University of Potsdam*.

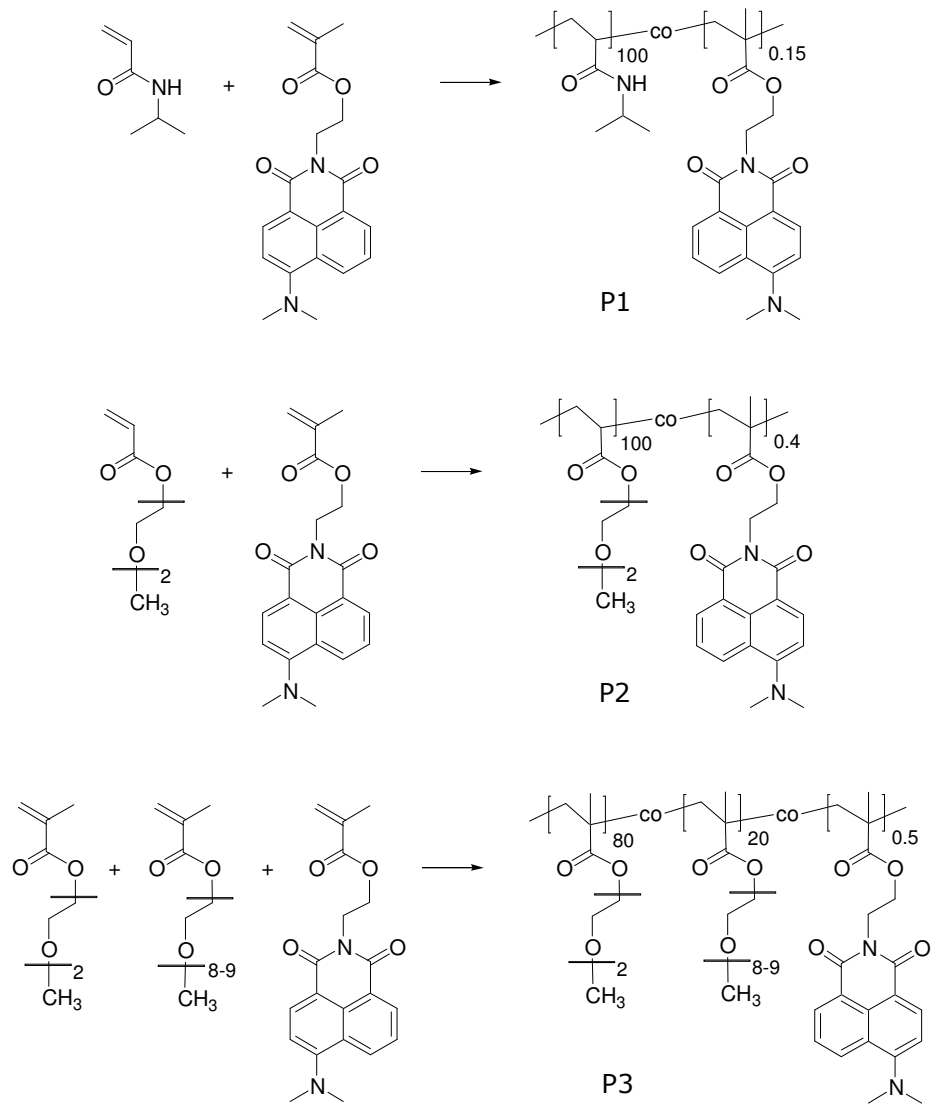

Scheme 4-1: Chemical structure of the thermoresponsive copolymers labeled with 4-DMN functionalized monomer. From top to bottom: labeled pNIPAm (**P1**), labeled $pMEO_2A$ (**P2**), and labeled $p(MEO_2MA$-*co*-OEGMA) (**P3**)

The temperature dependence of the optical transmittance recorded for the aqueous solutions of the polymers at 0.1 g L^{-1} is shown in Figure 4-1. All within a comparable range, the increase of C_p is in the order **P1 < P2 < P3**. Although the acrylate backbone of **P2** is more hydrophilic than the methacrylate one of **P3** and additional α-methyl groups might prevent water from forming hydrogen bonds due to steric effects,[189] the onset temperature is obviously more strongly affected by the length of the pendant OEG chains.[52]

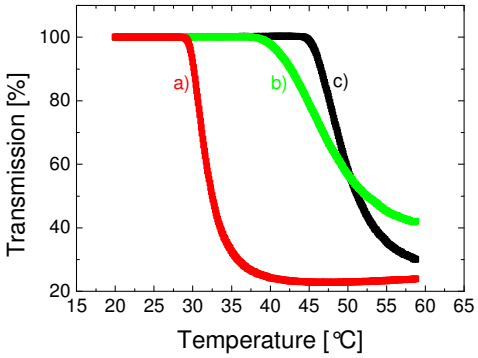

Figure 4-1: Turbidity profiles of the labeled **a) P1**, **b) P2**, and **c) P3**. All solutions are 0.1 g L^{-1} in PBS.

The dye content in all polymers corresponds to roughly one chromophore per polymer chain.* A summary of structural characterization and thermosensitive properties is given in Table 4-1.

Table 4-1: The analytical data of the copolymers (M_w^{app} and DP correspond to mass average molar mass and degree of polymerization, respectively).

Polymer	M_n^{app} [a] [kg/mol]	M_w^{app}/M_n^{app} [a]	DP [b]	dye content [c] [% mol]	NC [d]	C_p [e] [°C]	T (50%) [f] [°C]
P1	30	2.4	265	0.15	0.4	30	34
P2	21	1.9	120	0.4	0.5	38	52
P3	59	4.3	240	0.5	1.2	44	51

[a] determined by SEC in DMF, using PS standards,

[b] nominal number average of monomer repeat units per chain,

[c] calculated from the UV-VIS spectra of the monomer and the copolymer solutions in $CHCl_3$ according to *Beer-Lambert`s law* (molar extinction coefficient (ε): 13000 L mol^{-1} cm^{-1}),

[d] average number of chromophores per chain,

[e] deduced from Figure 4-1,

[f] temperature at which the transmission is reduced by 50%, deduced from Figure 4-1.

The data in Table 4-1 point to dissimilarities between the molecular weight, the PDI (M_w^{app}/M_n^{app}) or the DP of the polymers. While these differences certainly affect some thermodynamic properties such as the LCST, as fluorescence properties (particularly those recorded above the C_p), are more of a microscopic property, I expect that the differences at this range do not complicate the comparisons.

* Such low amounts of the fluorophore were chosen to ensure that the optical properties of the isolated fluorophore are conserved upon incorporation into the polymer, and that possible effects on the solubility and phase transition properties are minimized.

4.3 Photophysical Characterization of the Materials

4.3.1 Fluorescent Monomer *vs.* Polymer

In order to define the (polarity of the) environment of the dye within the polymeric structures, it is useful first to probe the photophysical properties of the 4-DMN functionalized monomer in different solvents. The absorption spectrum of the monomer is dominated by a broad and intense band with its maximum appearing between 391 and 440 nm. Analogously, emission spectra exhibit a broad shape in all solvents other than hexane. A change of the solvent from hexane to dimethylsulfoxide results in bathochromic shifts of the absorption and of the emission maximum ($\Delta\lambda^{abs}_{max}$ = 46 nm and $\Delta\lambda^{PL}_{max}$ = 86 nm, Figure 4-2), accompanied by a significant reduction of the fluorescence quantum yield (from 61 to 1.9%, Table 4-S1).

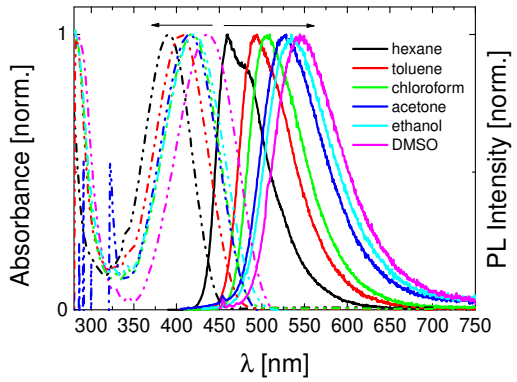

Figure 4-2: The normalized absorbance (dashed-dotted lines) and the PL (solid lines) spectra of the 4-DMN functionalized monomer in selected solvents.

The magnitude of these changes is characteristic for a pronounced ICT from the electron-rich amino group (methyl-substitution increasing the inductive effect) to the electron-poor imide moiety upon excitation.[190-196] An additional red-shift in λ^{PL}_{max} and a further drop in quantum yield are measured in protic solvents, e.g. in ethanol or water. This is indicative of the sensitivity of optical spectra to specific solvent effects such as hydrogen-bonding which is responsible for an increased non-radiative decay rate (for the relationship of quantum yield with hydrogen- bonding ability of the corresponding solvent, see Figure 4-S1a).[107,190,193,196,197] Hydrogen bonds are established, for instance, between the solvent molecules and carbonyl oxygen or/and the imide nitrogen of 4-DMN. For this dye, such interactions have a big impact on the photophysical properties as is evident from the nonlinear relationship of the orientation polarizability with the Stokes shift (Figure 4-S1b). Due to this strong environmental sensitivity, besides several reports regarding their use in chemo-sensors for detection of metal

ions,[198-200] these fluorophores were also exploited as a tool for monitoring protein-protein interactions,[105,194] or as a potential sensor for DNA.[201-203*]

Table 4-2 gives a summary of the basic photophysical characteristics of the copolymers.

Table 4-2: Summary of the photophysical properties of the copolymers (λ^{abs}_{max}: wavelength of maximum absorbance, λ^{PL}_{max}, φ: fluorescence quantum yield)

Polymer	λ^{abs}_{max} [a] [nm]	λ^{PL}_{max} [a] [nm]	φ [a] [%]	λ^{PL}_{max} [b] [nm]	λ^{abs}_{max} [c] [nm]	λ^{PL}_{max} [c] [nm]	φ [c] [%]
P1	448	544	1.6	530	422	513	63
P2	439	542	1.5	537	418	514	62
P3	434	535	24	535	418	512	62

[a] 0.5 g L^{-1} solution in PBS at 20 °C,
[b] 0.5 g L^{-1} solution in PBS at 50 °C,
[c] in $CHCl_3$.

For all polymers in PBS, the λ^{PL}_{max} is shifted to shorter wavelengths compared to the value recorded for the aqueous monomer solution (560 nm, cf. Table 4-S1). This might indicate that the dye attached to the polymers is inherently located in a less polar environment than water.[204] To verify this, I compared the optical properties of aqueous polymer solutions with those of the monomer solution in diethylene glycol dimethyl ether and N-methylformamide. These solvents mimic the side chains of the respective polymers, poly(meth)acrylates and pNIPAm, respectively. The **P1** solution in PBS has a very low quantum yield (φ = 1.6%), comparable to that of the monomer dissolved in N-methylformamide. Interestingly, aqueous **P3** exhibits a yield of 24%, which is even higher than that of the monomer in diethylene glycol dimethyl ether (φ = 12%). This implies that 4-DMN attached to **P3** interacts only weakly with water molecules. Also, the dipoles of the organic micro-environment consisting of the **P3** backbone and the side chains somehow do not affect the 4-DMN dipole moment in the excited state in the same way that diethylene glycol dimethyl ether does. On the other hand, the quantum efficiency of all the polymer solutions in $CHCl_3$, is rather high (up to 63%). It is only slightly lower than the efficiency of the monomer in the same solvent (70%, cf. Table 4-S1). This shows that as long as the chains are well-dissolved and expanded in a nonpolar solvent, side chains (even quite polar ones such as the OEG) do not affect the emission properties of the solvatochromic dye. In such cases, it is the surrounding solvent which governs the properties of the local micro-environment of the dye. In this context, the fact that the aqueous solution of **P2** has a quantum

* In addition to their ICT character, the 4-amino-1,8-naphthalimide derivatives exhibit outstanding properties, e.g., non-ionic character, high extinction coefficient and quantum yield, durability towards quenching by oxygen or photooxidation, and low tendency to self aggregate. Also, their relatively small size facilitates the incorporation into polymeric structures and promotes their use for such fluorometric sensing purposes.

yield (φ = 1.5%) significantly lower than that of the monomer in diethylene glycol dimethyl ether manifests the impact of the length of OEG side chains and the backbone flexibility on the extent of exposure of the fluorophores to water. It is, therefore, the physical state of the chains with their capacity of water uptake that determines the polarity of the local environment of the dye, and this physical state depends largely on the chemical structure of the copolymer.

4.3.2 Fluorescence Response to Phase Transition

The steady-state and transient fluorescence properties of aqueous polymer solutions were studied as a function of temperature, including temperatures well below and above the C_p. The results for each polymer are summarized in the following sections. Note that the solutions become cloudy above the phase transition temperature, however, no macroscopic separation is observed during the course of the measurements due to the dilute solution conditions (0.1 g L^{-1}). To ensure that all measurements are performed on an equilibrated sample, PL measurements did not start earlier than 15 minutes after a new temperature was reached. Also, I did not observe any change in the shape of the emission spectra at 50 °C after keeping the solutions at this temperature over night.

4.3.2.1 NIPAm-based copolymer- P1

The steady-state PL spectra of aqueous **P1** solution recorded at various temperatures are demonstrated in Figure 4-3. A drastic increase of the intensity sets in as the temperature is raised above ca. 25 °C. Upon further heating, the PL intensity reaches up almost to 25 fold of its initial value. The increase in quantum efficiency along with a blue-shift of λ^{PL}_{max} from 544 nm to 530 nm is indicative of changes occurring in the dye micro-environment, most prominent in the linear range between 25 and 35 °C (Figure 4-3b). Accordingly, the (intensity-averaged) fluorescence lifetime of the dye gets longer with the increase in temperature (Figure 4-S2). The temperature onset of these changes coincides well with that observed in the absorbance spectrum of the solution (Figure 4-S3). Also, temperature has no such effect on the aqueous monomer solution (Figure 4-S4). These findings indicate that the changes in fluorescence properties of **P1** are to be attributed to the polymer phase transition; to the nonpolar polymer-rich environment of the dye in NIPAm globules (see Scheme 1-2b for the sensing mechanism). Upon further heating (T>40 °C), the enhancement is overcompensated by temperature-activated non-radiative decay channels[*], which results in the

[*] With an increase in temperature, the processes (collisions with solvent molecules, vibrational and rotational motions) which result in an increase in the non-radiative decay constant are promoted. This leads to a decrease in the fluorescence intensity and its lifetime.

decrease of the PL intensity. Overall, it is the change of the chain conformation and aggregation properties that leads to the drastic changes observed in the photophysical properties. Since the coil-globule transition is reversible, the working principle of this pNIPAm-based temperature sensor can be repeated. The reversible fluorescence on/off response renders the polymer useful for sensing applications.

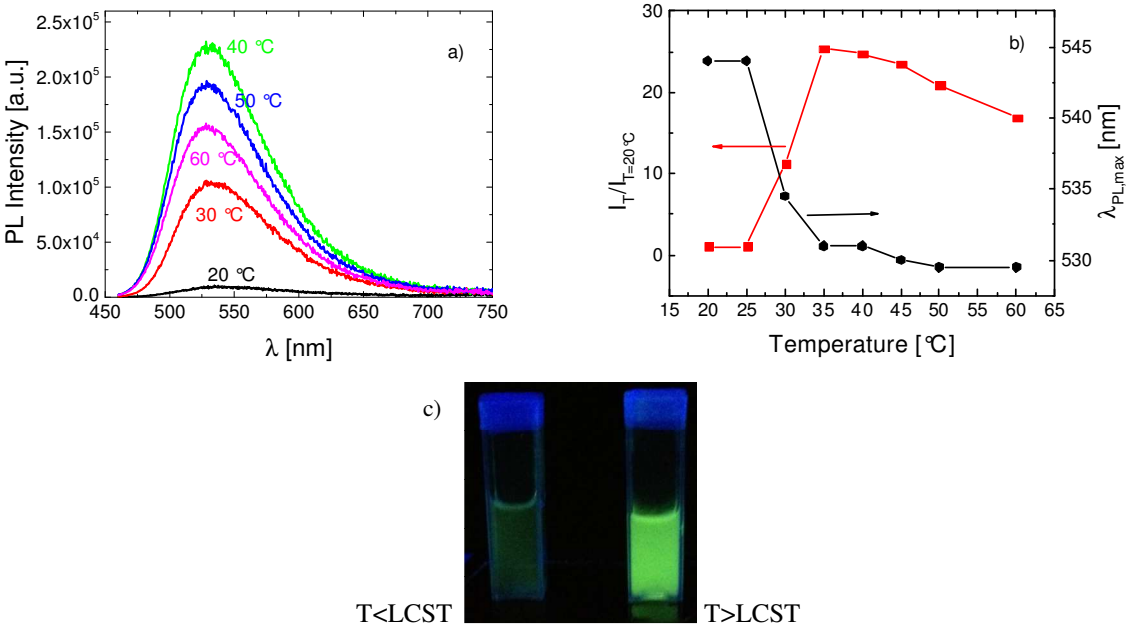

Figure 4-3: **a)** The evolution of the fluorescence spectrum of **P1** in PBS (0.1 g L^{-1}) with temperature, recorded at an excitation wavelength of 450 nm **b)** The correlation between λ^{PL}_{max}, the relative emission intensity ($I_T/I_{T=20\,°C}$), and the temperature of the solution. Data are taken from the spectra in a). The photographs in **c)** were taken under UV illumination at 365 nm.

4.3.2.2 OEG-based copolymers- P2 and P3

The temperature-dependent fluorescence properties of **P2** bearing only the short OEG side chains are shown in Figure 4-4. As for **P1**, heating of the solution of this polymer in PBS above its C_p leads to a sudden increase in the intensity of emission. This is accompanied with a blue-shift of λ^{PL}_{max}. However, these changes are rather weak: the quantum efficiency increases only by a factor of 2, while λ^{PL}_{max} shifts only by ca. 5 nm.

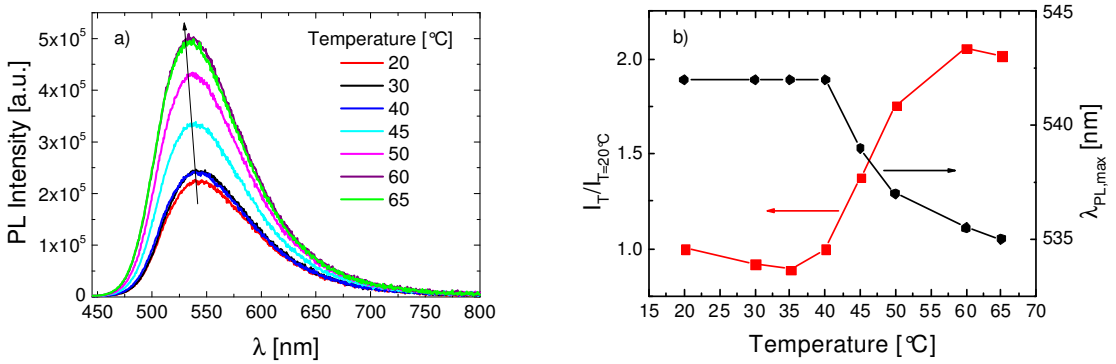

Figure 4-4: **a)** The effect of temperature on the fluorescence characteristics of **P2** in PBS (0.1 g L^{-1}). Excitation wavelength was 435 nm. **b)** The correlation between λ^{PL}_{max}, the relative emission intensity ($I_T/I_{T=20\,°C}$), and the temperature of the solution. Data are taken from the spectra in a).

For the same dye now attached to the methacrylate backbone bearing both short and long OEG side chains, neither the emission intensity nor the spectral shape is significantly affected by the temperature rise (Figure 4-5). In agreement with the decrease in the steady-state intensity, the fluorescence lifetime is slightly shortened as the temperature increases (Figure 4-S5). However, this decrease does not follow a specific pattern and is therefore attributed to non-radiative processes becoming more efficient at elevated temperatures.[49,106] Note that, this random decrease of PL intensity with increasing temperature is observed also at a higher polymer concentration (0.5 g L^{-1}). In contrast to the case of **P1** and **P2**, the dye in **P3** does not sense a change in its micro-environment with increasing the temperature, i.e., the probe environment is not perturbed by the chain collapse and their subsequent aggregation.

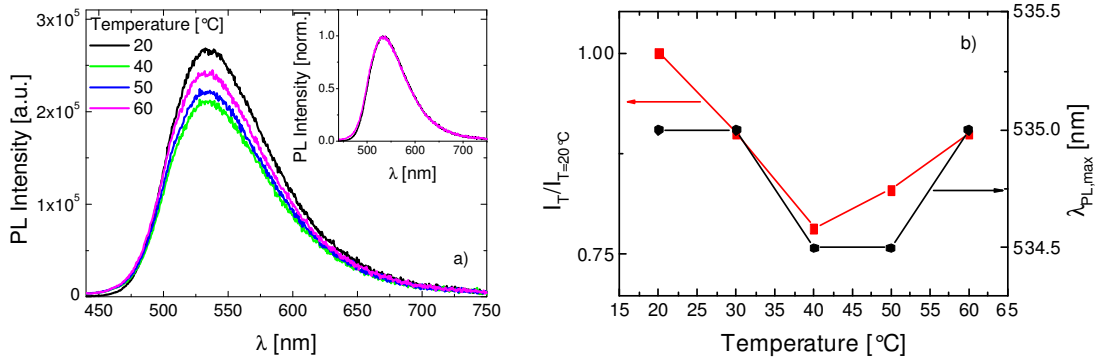

Figure 4-5: **a)** The fluorescence spectra of **P3** in PBS (0.1 g L^{-1}) at various temperatures. Excitation was at 430 nm. The inset depicts the emission spectra at 20 and 60 °C normalized to their maximum emission intensity. **b)** The correlation between λ^{PL}_{max}, the relative emission intensity ($I_T/I_{T=20\,°C}$), and the temperature of the solution. Data are taken from the spectra in a).

These results are quite surprising as the LCST transition of **P3** must, in principle, lead to the formation of a more hydrophobic micro-environment. For another polarity sensitive dye

(7-nitro-2,1,3-benzoxadiazole) labeled onto a similar thermoresponsive chain, i.e. p($MEO_2MA_{0.94}$-*co*-$OEGMA_{0.06}$), a ca. 30% decrease of PL intensity was reported upon heating the polymer solution to temperatures above the C_p.[146] The study noted this contrasting behavior of the OEGMA-based polymer in comparison with the previously published work on the same dye within a NIPAm network.[187] The authors stated that the PL response of the polymer to temperature seemed to be determined by two competitive factors: the intrinsic decrease of quantum yield at elevated temperatures and the emission enhancement due to the overall decrease in polarity. Although the effect of the polymer structure on determining the governing role of either factor was not stressed, the significant effect of the polymer matrix on the quantum yield was emphasized.[146] Apparently, the aqueous solubility and phase transition phenomena of these polymers differ substantially. I, therefore, anticipated that SLS studies could provide additional insight on the association/aggregation behavior of the chains below and above their C_p, which could then assist to explain the observed fluorescence characteristics.

4.4 Aqueous Solubility and Aggregation*

Table 4-3 summarizes the structural information obtained for the polymers in PBS at three different temperatures. The measurements at 15 °C are informative about the structures present well below the C_p of all polymers, while 30 °C corresponds to the onset of the decrease of **P1** transmission, and 50 °C corresponds to the temperature at which the transmission from OEG-bearing polymer solutions are reduced by roughly 50%. Note that the heating rate and the equilibrium times at each temperature are comparable to those of the photophysical studies discussed above.

Table 4-3: SLS data for polymer solutions in PBS (0.1 g L^{-1}) at various temperatures (T)

Polymer	T [°C]	R_g [nm]	$M_{w,app}$ [10^6 g mol^{-1}]	ρ [10^{-3} g cm^{-3}]	N_{agg}
P1	15	<25	0.18	2.1 [a]	2
P1	30	120	1040	110	14500
P1	50	127	2920	262	40600
P2	15	<25	0.04	0.5 [a]	1
P2	30	<25	0.06	0.7 [a]	2
P2	50	130	1040	86	26000
P3	15	54	2.9	3.4	11
P3	30	54	3.2	3.7	13
P3	50	134	670	51	2600

[a] the calculated value of ρ for R_g = 25 nm.

* Light scattering measurements were performed by *Leonardo Chiappisi* in the *Stranski-Laboratory for Physical and Theoretical Chemistry of Technische Universität Berlin*.

As reported in Table 4-3, **P1** and **P2** solutions at 15 °C contain well-hydrated assemblies composed of only a few chains. For these solutions, the scattered light intensity was independent of the scattering angle in the examined q range, which agrees with the presence of short flexible chains (R_g<25 nm) that do not form larger assemblies. In contrast to **P1** and **P2**, **P3** solution contains loose aggregates consisting of ca. 11 chains with an R_g of 54 nm already before its phase transition. The apparent chain density of these water-draining structures is similar to that reported in Chapter 3 for the solutions of the analogue coumarin labeled copolymer CLP in PBS.

The phase transition of the **P1** solution is manifested via a drastic increase of all structural parameters upon raising the temperature from 15 to 30 °C. Heating the solution further to 50 °C leads to bigger, denser and heavier aggregates. For the solutions of OEG-based copolymers at 30 °C which is below their C_p, we observe a slight increase in the number of associating chains. This is in contrast to what is usually reported for acrylamide polymers,[47] and might be an evidence that intermolecular aggregation is the dominant process of the phase transition of OEG-based polymers.[42] Upon raising the temperature of these solutions up to 50 °C, the scattering data signal the solubility transition that the polymers have undergone: the intensity of the scattered light increases largely, and so do R_g, $M_{w,app}$, and N_{agg}.

Although these solutions all become turbid, comparing the values of $M_{w,app}$, ρ, and N_{agg} of **P1** at 30 °C with those of **P2** and particularly of **P3** at 50 °C reveals a particular trend: at a very early stage of its transition (30 °C), pNIPAm forms much denser aggregates compared to the OEG-based copolymers at 50 °C, an "elevated" temperature corresponding to a later phase of their solubility transition. It appears as that pNIPAm chains dehydrate to a much larger extent given that the experimental conditions are the same for all polymers. Also, the change in the chain packing density is much more drastic for the **P1** solution compared to **P3**. In this respect, **P2** aggregates also differ from **P3**, i.e., the number of **P2** chains accumulating in one aggregate is 10 fold higher than that of **P3** at 50 °C.

4.5 Discussion

At 15 °C, well below the phase transition temperature of **P1** (0.1 g L^{-1} in PBS), the fluorophore emits weakly with a considerably red-shifted λ^{PL}_{max}. As SLS gives no evidence for inter-associations, we can conclude that the aqueous **P1** solution comprises well-hydrated chains on which 4-DMN fluorophores reside fully exposed to water. As the solution temperature increases above the C_p, the emission intensity increases dramatically. The emission maximum gradually shifts to the shorter wavelengths with further heating. The fact that the emission above the C_p is even more intense than that of the monomer dissolved in the

NIPAm-like solvent points to a rigid micro-environment. Here the polar polymer units cannot reorient anymore and the naphthalimide units are shielded from water. These contribute to the high quantum yield that the dye attains upon the phase transition of **P1**. It is therefore reasonable to define the environment of the fluorophore as rather rigid and occupied mostly by collapsed **P1** chains.

Before the phase transition sets in, no evidence for pre-association is found for **P2** chains. The solution at 15 °C displays a red-shifted λ^{PL}_{max} and a quantum yield much smaller than that of the monomer in its structurally similar solvent. Similar to the **P1** case, these facts evidence the presence of swollen chains and a water-exposed environment of the dye. However, upon the solubility transition, the photophysical properties of the dye do not change as strong as when it is attached to **P1**, meaning that its micro-environment becomes only slightly less polar than that provided by swollen chains. The fluorophore-water contacts are retained even after the dehydration of the polymer (note the low polymeric density of the **P2** globules in contrast to that of the **P1**).

One of the several parameters leading to the observed differences in the photophysical response of **P2** (and of **P3**) in comparison to **P1** is that the aggregates of pNIPAm are stabilized by strong intramolecular and intermolecular N–H···O=C hydrogen bonds, whereas no hydrogen donator site exists in OEG-based polymers.[42,165] Concerning a comparative investigation on thermoresponsive polymers, Zhou *et al*. concluded that the individual single chain globules of a poly (N,N-diethylacrylamide) are less compact compared to those formed by pNIPAm due to the lack of interchain hydrogen-bonding.[79] Moreover, from temperature-variable ^{1}H NMR and IR studies of an analogous, yet unlabeled, p($MEO_2MA_{0.95}$-*co*-$OEGMA_{0.05}$), Wu *et al.* reported the presence of soluble and mobile side chains after the phase transition.[42] This points out to an only weak dehydration of the OEG chains. This finding is in accordance with earlier reports showing that longer OEG units preserve their mobility upon heating the solution above its LCST.[82,161] In fact, the NMR studies of the CLP of the Chapter 3 showed the gradual nature of the transition and that OEG side chains exhibit relatively mobile signals even at elevated temperatures. From the aspect of sensing capability, Hoogenboom *et al.* demonstrated the influence of the hydrophilicity of the polymer on the efficiency of fluorescent thermometers based on a MEO_2MA-type copolymer bearing a polarity-sensitive dye.[44] When the fluorescent copolymer included longer OEG chains, the sensing capability was lost. The authors proposed that the hydrophilic copolymer remains well-hydrated even in the collapsed state. Consequently, I reason that in addition to the lack of intra hydrogen-bonding, hydrophilic OEG side chains of MEO_2A and MEO_2MA copolymers hinder an effective dehydration process.

Similar to **P2**, **P3** does not respond to the phase transition with characteristic fluorescence changes, however, the situation is still quite different. Firstly, well below its C_p, the solution contains associates.[*] The rather high quantum yield indicates that the fluorophores must be somewhat protected from the hydrogen-bonding interactions with water molecules and from other possible quenching mechanisms. Such a unique surrounding of the probe is presumably related to the more rigid methacrylate backbone and, despite their low amount in the composition, to the pre-aggregation that OEGMA chains are held responsible for. The outcome is a relatively emissive solution already before the phase transition takes place. In addition to the argument above based on the incomplete dehydration of OEG side chains, the complete loss of the sensing capability in **P3** can as well be reasoned by the limited flexibility of the polymer backbone. Recall that the aggregates of **P3** contain 10 times fewer chains compared with those of the **P2**. The α-methyl groups can cause restrictions on the free rotation of chains resulting in less flexible conformations. This may prevent the chains from forming dense aggregates.

The above findings show that fluorescence response of the naphthalimide dye to the polymer phase transition differs largely with regard to the chemical structure of the polymer matrix. To determine whether this behavior is a characteristic of the fluorophore or specific to the polymer itself, I will demonstrate the temperature-dependent fluorescence properties of copolymers which were synthesized analogously to **P1** and **P3**, but bear a different type of solvatochromic dye. Figure 4-6 shows the steady-state emission properties of the very same *coumarin* dye as in the CLP (cf. Chapter 3) but now also as a part of a NIPAm-based copolymer (denoted as p(NIPAm-*co*-coumarin)) at various temperatures. For the molecular data regarding these copolymers, see Table 4-S2.

[*] The pre-association of OEGMA-based fluorescent copolymers might be related to the amphiphilic nature of their structure, the competition of some groups for dissolution and some others for contraction. Also these polymers are formed of three monomeric units, which might lead to less homogenous structures.

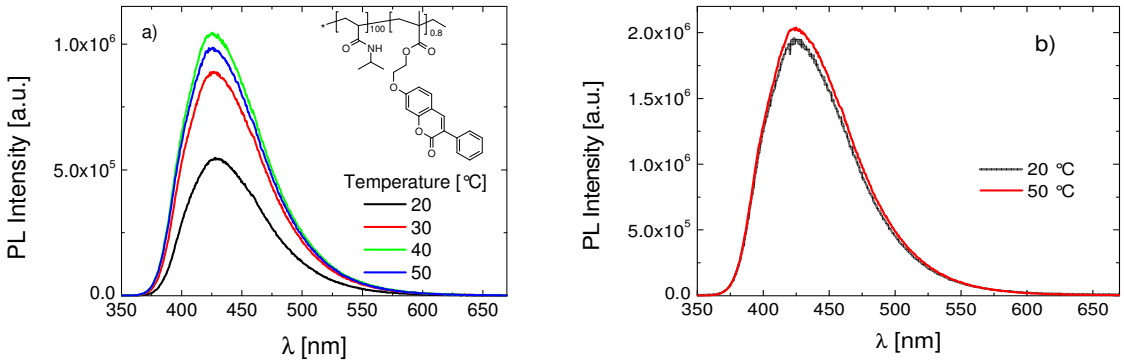

Figure 4-6: The variable-temperature emission spectra of the aqueous solution (0.12 g L^{-1}) of **a)** p(NIPAm-*co*-coumarin) **b)** CLP. Also shown in a) is the chemical structure of p(NIPAm-*co*-coumarin). The excitation wavelength is 340 nm. Note that 50 °C is well above the C_p of the polymers (Table 4-S2).

Evident from the enhanced emission of the polymer at temperatures above the C_p, the p(NIPAm-*co*-coumarin) follows the trend of **P1**. On the contrary, the dye attached to the methacrylate backbone bearing OEGMA chains, i.e. CLP, is rather insensitive to changes in temperature, just like **P3**.

4.6 Conclusions

In this chapter, I demonstrated three different fluorescent materials from acrylamide- and OEG-based thermoresponsive polymers for temperature sensing purpose and investigated their sensing performance in conjunction with their aqueous solubility behavior. Based on the correlation of fluorescence properties with light scattering results, it is concluded that the aggregation properties of polymer chains govern the contribution from the polarities of the main/side chains and the degree of water exposure, both affecting the photophysical properties of the solvatochromic dye. Therefore, the emission properties of the dye are found to be strongly peculiar to the exact chemical structure of the macromolecule that it is attached to. For instance, while the ICT-type naphthalimide emits very weakly when incorporated into pNIPAm or into the polyacrylate bearing only short OEG side chains, it becomes strongly emissive when attached to the polymethacrylate consisting longer OEG side chains. Moreover, compared with the other two polymers, the pNIPAm experiences a much more drastic change in chain packing density at a very early stage of its phase transition and signals this by a large increase in its fluorescence intensity. Therefore, only the labeled pNIPAm features the envisaged sensor´s function, while the emission properties of OEG-bearing copolymers exhibit either weak or negligible changes in response to the phase transition. Copolymers analogous with the thermoresponsive units but differing in the type of the reporter dye follow this very same trend of the temperature response. This ensures the governing role of the chemical structure of the host polymer rather than that of the

fluorophore. The contrasting behavior of OEG-based chains (in terms of the solubility-insolubility behavior) is attributed to the lack of internal hydrogen-bonding capability and their inefficient dehydration. Nevertheless, the OEGMA-based ternary copolymer is a special case, as it provides a particularly different environment to the fluorophore. Such surrounding allows a high quantum yield below the C_p, which also hardly changes as the chains collapse and aggregate. In addition to the effect of longer side chains, such behavior is associated with the backbone rigidity. These findings might have fundamental importance for the practical use of these polymers. For instance, for applications relying on drastic conformational changes such as in vivo monitoring of the trigger of the transition, NIPAm-based scaffolds feature ideal hydration and collapse properties. On the other hand, OEGMA-based polymeric structures should be used if the application necessitates environmental stability, e.g., for a molecules carried within.

4.7 Supplementary Information

Table 4-S1: The photophysical characterization of 4-DMN labeled monomer dissolved in various solvents (δ_t: Hansen solubility parameter of solvents at 25 °C, δ_d, δ_p, and δ_h: the dispersive, polar and the hydrogen-bonding term of δ_t, respectively, $\lambda^{abs}{}_{max}$, $\lambda^{PL}{}_{max}$, φ, and τ: fluorescence lifetime)

Solvent	δ_t [a]	δ_d	δ_p	δ_h	$\lambda^{abs}{}_{max}$ [nm]	$\lambda^{PL}{}_{max}$ [nm]	φ [%]	τ [ns]
Hexane	14.9	14.9	0.0	0.0	391	459.5	61.0	6.9
Tetrachlorocarbon	17.8	17.8	0.0	0.6	400	476.5	70.0	7.0
Diethylene glycol dimethyl ether	18.0 [b]	15.7 [b]	6.1 [b]	6.5 [b]	415	522.0	12.0	2.4
Toluene	18.2	18.0	1.4	2.0	406	492.5	65.0	7.7
Chloroform	19.0	17.8	3.1	5.7	418	506.5	70.0	9.0
Acetone	20.1	15.5	10.4	7.0	415	526.0	3.6	3.0
Acetic Acid	21.3	14.5	8.0	13.5	424	539.0	2.6	3.2
Acetonitrile	24.6	15.3	18.0	6.1	419	532.0	4.0	2.8
Dimethylformamide	25.0	14.3	11.9	16.6	423	532.5	1.5	7.8
Dimethylsulfoxide	26.6	18.4	16.4	10.2	437	546.0	1.9	7.4
Ethanol	26.6	15.8	8.8	19.4	420	536.5	1.9	4.2
N-Methylformamide	30.1 [b]	17.4 [b]	18.8 [b]	15.9 [b]	423	538.0	1.7	5.9
Water	47.9	15.5	16.0	42.4	440	560.0	0.2	2.8

[a] in units of [$mPa^{0.5}$] from J. E. Mark, ed., *Physical Properties of Polymers Handbook*, American Institute of Physics, Woodbury, N.Y., 1996,
[b] from C. M. Hansen, *Hansen Solubility Parameters: A User's Handbook, Second Edition*, CRC Press, Boca Raton, FL, 2007.

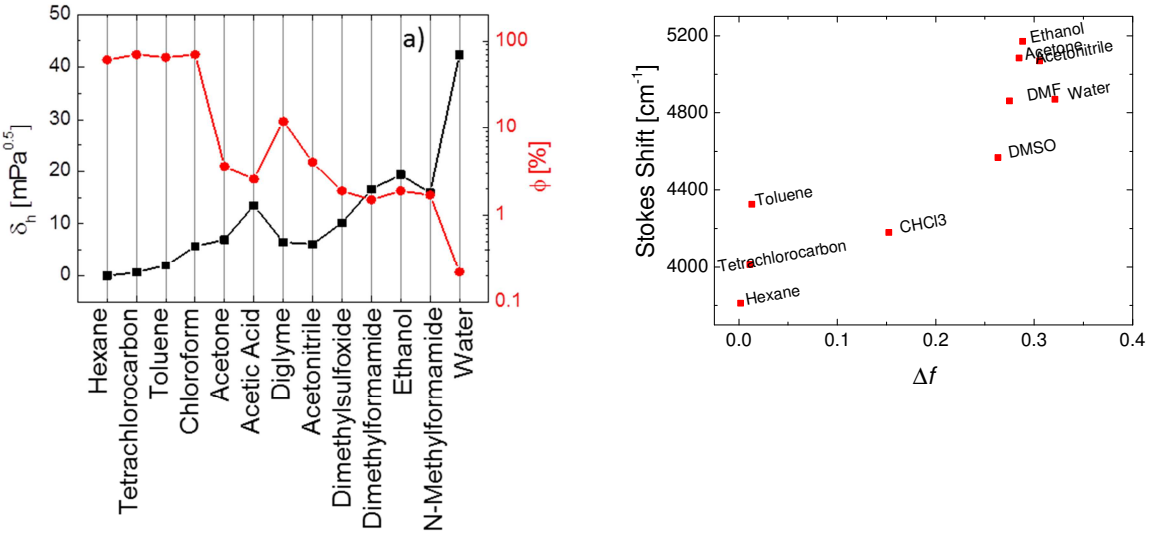

Figure 4-S1: **a**) The relationship between the quantum yield (φ) of the monomer in various solvents and the corresponding hydrogen-bonding parameter (δ_h). All values are taken from Table 4-S1. **b)** *Lippert-Magna* plot (Δf vs. $\Delta\bar{\nu}$) for the 4-DMN labeled monomer. Stokes Shift ($\Delta\bar{\nu}$) of the fluorophore in each solvent was calculated from the values reported in Table 4-S1 and Δf was determined according to *Eq.* 2-13.

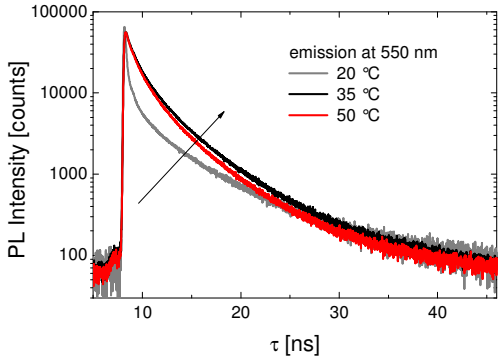

Figure 4-S2: Time-resolved PL traces of an aqueous solution of **P1** at 20, 35, and 50 °C. The excitation and the emission were at 470 and 550 nm, respectively.

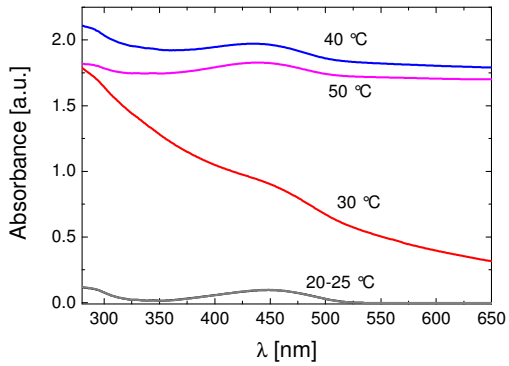

Figure 4-S3: Absorbance spectra of aqueous solution (0.5 g L^{-1}) of **P1** at various temperatures.

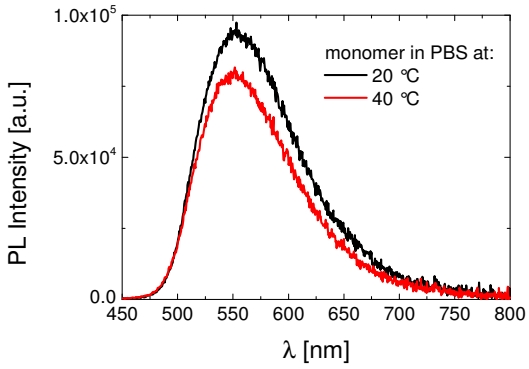

Figure 4-S4: Emission spectra of the 4-DMN labeled monomer in PBS at 20 and 40 °C.

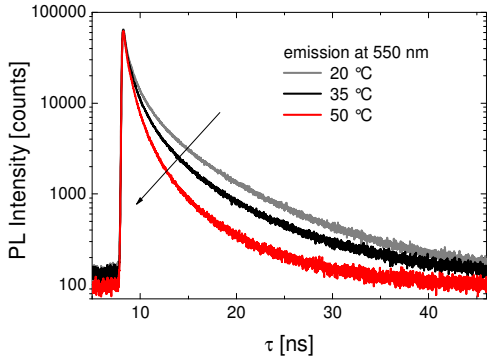

Figure 4-S5: Time-resolved PL traces of aqueous solution of **P3** at 20, 35, and 50 °C. The sample was excited at 470 nm and the emission was detected at 550 nm.

Table 4-S2: Molecular characterization and thermosensitive properties of the coumarin-labeled copolymers

Polymer	M_n^{app} [a] [kg/mol]	M_w^{app}/M_n^{app} [a]	DP [b]	dye content [c] [% mol]	NC [d]	C_p [e] [°C]	T (50%) [f] [°C]
p(NIPAm-*co*-coumarin)	24	2.7	210	0.8	1.6	28	30
CLP	21	3	100	0.3	0.3	29	31

[a] determined by SEC in DMF, using PS standards,

[b] nominal number average of monomer repeat units per chain,

[c] calculated from the UV-VIS spectra of the monomer and the copolymer solutions in $CHCl_3$ according to *Beer-Lambert`s law* (ε: 20000 L mol^{-1} cm^{-1}),

[d] average number of chromophores per chain,

[e] onset of the decrease of transmission in PBS solution (2 g L^{-1}),

[f] temperature at which the transmission is reduced by 50% in PBS solution (2 g L^{-1}).

5 Fluorescent Thermoresponsive Polymer as a Ratiometric Probe for Temperature and a Specific Protein*

5.1 Background

This chapter presents a fluorescent thermoresponsive copolymer which can report changes in solution temperature as well as in analyte concentration through a remarkable fluorescence output. Fluorometric sensing of multiple stimuli by platforms integrating thermoresponsive polymers is not a new concept. [23,26] Incorporation of solvatochromic, pH-, UV- or ion-reactive dyes into thermo or pH-responsive polymeric species enables fluorescent probes that can respond to a variety of inputs.[24,27,28,35,146,205] For example, NIPAm-based micro-gels attained dual sensitivity as fluorophores sensitive both to Cu^{+2} and to solvent polarity were integrated into the structure.[34] Similarly, copolymer consisting of NIPAm, a polarity sensitive dye, and an ion-sensitive monomer enabled multiple detections of pH, temperature, and specific ions with a fluorescence output.[38] Thermoresponsive block copolymers with the two blocks labeled with two types of FRET dyes possessing different pH-switchable emission characteristics allowed thermo- and pH-modulation of the emission of unimers in a ratiometric manner.[27]

For this work, a fluorescent dual-sensitive material was designed, combining the response of a solvatochromic dye´s fluorescence to thermally-induced polymer phase transition with its sensitivity to a specific biological macromolecule, an antibody. That means, instead of utilizing an additional moiety for molecular recognition, the fluorophore itself acts as the receptor and senses changes in the antibody concentration. Provided that the operation temperature is not higher than the LCST, the recognition event proceeds via binding of the antibody to the dye moieties of the NIPAm-based copolymer. As complexes are formed

* Published in part: S. Inal *et al.*, "A Water Soluble Fluorescent Polymer as a Dual Color Sensor for Temperature and a Specific Protein" *Journal of Materials Chemistry B* **2013** DOI: 10.1039/c3tb21245a

between the labeled chains and the antibody, the LCST shifts to higher temperatures[*]. On the other hand, the stability of the copolymer/antibody complexes exhibited a significant temperature dependence as the increase in temperature and the associated solubility transition weakened their association. The subsequent release of the antibody from the polymer sites is exploited for a proof of concept *competitive binding* assay[†], the mechanism of which is facilely monitored from the temperature *vs*. transmission curves.

The remainder of the chapter focuses on the photophysical response of the same dye attached to the polymethacrylate backbone bearing OEG side chains. Similar to the naphthalimide case reported in the previous chapter, the fluorescence properties are insensitive to the phase transition of the polymer, but also to the binding of the antibody. Although the latter is expected to cause a strong perturbation on the micro-environment of the dye, it, surprisingly, does not induce a distinct fluorescence read-out. As reasons for this contrasting behaviour are discussed, I will emphasize the importance of structural considerations for the design of such molecular sensors.

5.2 Materials[‡]

In analogy to those of Chapter 4, the materials of this work are based on either NIPAm or on a mixture of MEO_2MA and OEGMA monomers. The fluorescent structures are prepared via free radical copolymerization of the corresponding thermoresponsive monomers with the methacrylate monomer labeled with the solvatochromic fluorophore 7-(diethylamino)-coumarin-3-carboxylic acid (DEAC). Scheme 5-1 shows the chemical structures of the monomers and of the resulting copolymers.

[*] The opposite shift in LCST upon such recognition event is exemplified in Scheme 1-3.

[†] This is an assay that is typically used to monitor the concentration of a free analyte. Ideally, it works as the following: The solution comprises a ligand and a compound which is bound to the ligand. One or both of these components are fluorescently labeled, giving a specific fluorescence output before the analyte is introduced into the solution. Upon addition of the analyte, which should exhibit an intrinsically high efficiency of binding to the ligand, the bound compound is released from the ligand and the analyte binds instead. This arrangement modifies the initial fluorescence characteristics. Finally, the extent of the PL changes is correlated with the concentration of the bound analyte.

[‡] The polymers and the SEC analysis were provided by *Jonas D. Kölsch* from the *University of Potsdam.*

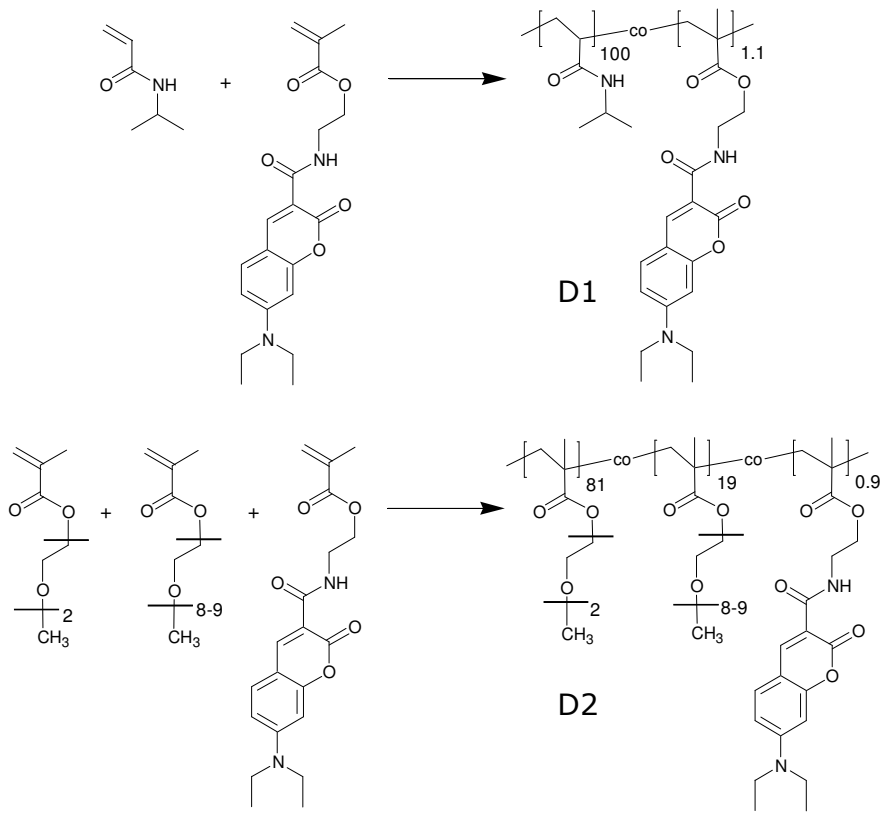

Scheme 5-1: The chemical structure of the DEAC-functionalized monomer and of the thermoresponsive copolymers: labeled pNIPAm (**D1**), and labeled p(MEO_2MA-*co*-OEGMA) (**D2**)

The analytical data of these copolymers are summarized in Table 5-1. The presence of the dye in the copolymer structure was quantified via UV-VIS spectroscopy. As expected, the incorporation of the hydrophobic dye shifted the C_p of the original polymers to lower temperatures. The fact that the average number of fluorophores per polymer chain is greater than one might result in photophysical characteristics different than those of the isolated monomer.

Table 5-1: The analytical data of the copolymers.

Polymer	M_n^{app} [a] [kg/mol]	M_w^{app}/M_n^{app} [a]	DP [b]	dye content [c] [% mol]	NC [d]	C_p [e] [°C]	T (50%) [f] [°C]
D1	23	1.9	196	1.1	2.2	20	23
D2	44	2.5	177	0.9	1.6	41	44

[a] determined by SEC in DMF, using PS standards;

[b] nominal number average of monomer repeat units per chain;

[c] calculated from the UV-VIS spectra of the monomer and the copolymer solutions in $CHCl_3$ according to *Beer-Lambert`s law* (ε: 35000 L mol^{-1} cm^{-1});

[d] average number of fluorophores per chain;

[e] onset of the decrease of transmission in PBS solution (2 g L^{-1});

[f] temperature at which the transmission is reduced by 50% in PBS solution (2 g L^{-1}).

As their photophysical properties depend strongly on polarity, viscosity, and pH of the micro-environment, as well as on hydrogen-bonding interactions, 7-aminocoumarins have received considerable interest for chemo-sensing applications.[206,207] Due to the push-pull character of the conjugated system, the excited state forms an ICT state upon electronic excitation. For some derivatives of 7-aminocoumarins, depending on the strength of the electron donating and accepting capability of the related moieties,[208] the amino group was reported to undergo an internal rotation upon photoexcitation. This results in full charge separation through a perpendicularly orientated donor orbital with respect to that of the acceptor, generating a TICT state.[106] A complete list of photophysical findings of the DEAC-functionalized monomer dissolved in a variety of solvents can be found in Table 5-S1. These findings evidence the formation of an ICT state. For instance, when the monomer is dissolved in solvents of high polarity, the λ^{PL}_{max} shifts bathochromically accompanied with a decrease in quantum yield and fluorescence lifetime.[103] These effects are more pronounced in protic solvents. Also, the quantum yield is enhanced in solvents of high viscosity, ascribed to inhibition of the TICT state. However, the magnitude of the solvent-mediated shifts is not as drastic as that reported for 4-DMN, i.e., the naphthalimide labeled monomer of Chapter **4**. A change of the solvent from toluene to dimethylsulfoxide results in 35 nm red-shift of $\Delta\lambda^{PL}_{max}$, which was 53 nm for the naphthalimide derivative.

5.3 Photophysical Properties of the NIPAm-based Copolymer

5.3.1 Response to Temperature

Marked changes in the PL spectrum emerge as the aqueous solution temperature of **D1** is raised above 20 °C. As documented in Figure 5-1, the formerly, two weakly emitting bands evolve into a single emission component at higher temperatures, i.e., T >20 °C. While the red-emitting band dwindles, the intensity of the higher energy emission increases by about 6 fold, with its maximum shifting slightly to shorter wavelengths. The quantum yield of the dye attains a value even higher than that measured in the structurally similar solvent, i.e., N-methylformamide (9%, cf. Table 5-S1). These findings point to a rigid environment provided to the fluorophores above the C_p. Such environment seems to limit encounters of the dye with water and to enhance such between polymer segments. Accordingly, absorbance and time-resolved PL spectra exhibit distinct changes with increasing the solution temperature, e.g., an abrupt increase in scattering intensity and a longer lifetime extracted for the emission at 475 nm (Figure 5-S1, and 5-S2). Note that the emission spectrum of the aqueous monomer solution has no such response to temperature in the examined range (Figure 5-S3). Therefore,

the temperature-triggered changes in the emission profile of **D1** are attributed to the LCST-type chain collapse and aggregation.

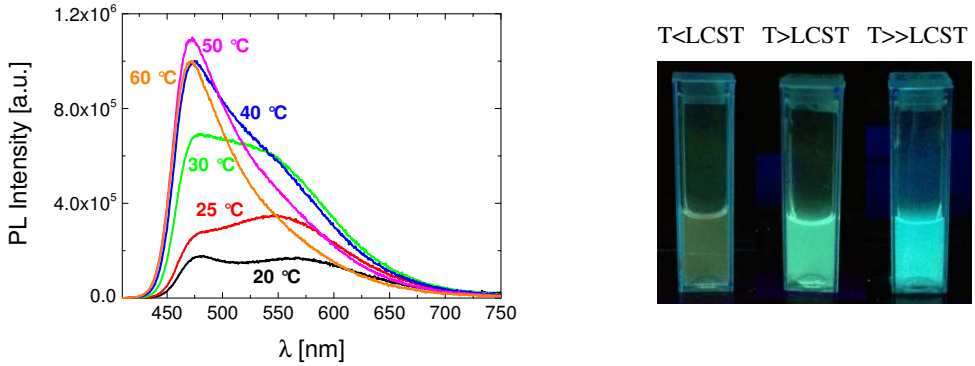

Figure 5-1: The evolution of the PL spectra of **D1** in PBS (0.15 g L^{-1}) with temperature. The PL spectra were recorded at an excitation wavelength of 400 nm while the photographs were taken under UV illumination at 365 nm.

Comparing the low temperature-emission spectra of the aqueous monomer with that of the **D1** solution in PBS, we can see that they are clearly different. In contrast to **D1** spectrum composed of two bands, the monomer comprises only the peak centered at about 475 nm. For the polymer, the species responsible for the emission at longer wavelengths exhibit also a ground-state absorption* (Figure 5-S1). With its relatively long emission lifetime (>10 ns), this feature disappears not only above the C_p and but also in very dilute solutions of the polymer, i.e., $<10^{-4}$ g L^{-1} (Figure 5-S4). These findings evidence the presence of DEAC aggregates, promoted presumably by interchain associations of the labeled chains. Although it is favored that the photophysical properties of the label are preserved upon incorporation into the polymer structure, the possibility to modulate the relative emission intensity of the two emitting species, i.e. the single dye and its aggregates, by a stimulus, such as the temperature here, makes this polymer quite advantageous to construct a ratiometric fluorescent sensor.

5.3.2 Response to the Antibody

Apart from the distinguished fluorescence response to variations in solution temperature, **D1** also reports the presence of a monoclonal antibody through its optical spectra. The anti-DEAC antibody introduced to the aqueous **D1** solution induces remarkable changes in the PL characteristics (Figure 5-2).

* Also, the excitation spectra detected for emission at 480 nm and at 560 nm do not resemble each other.

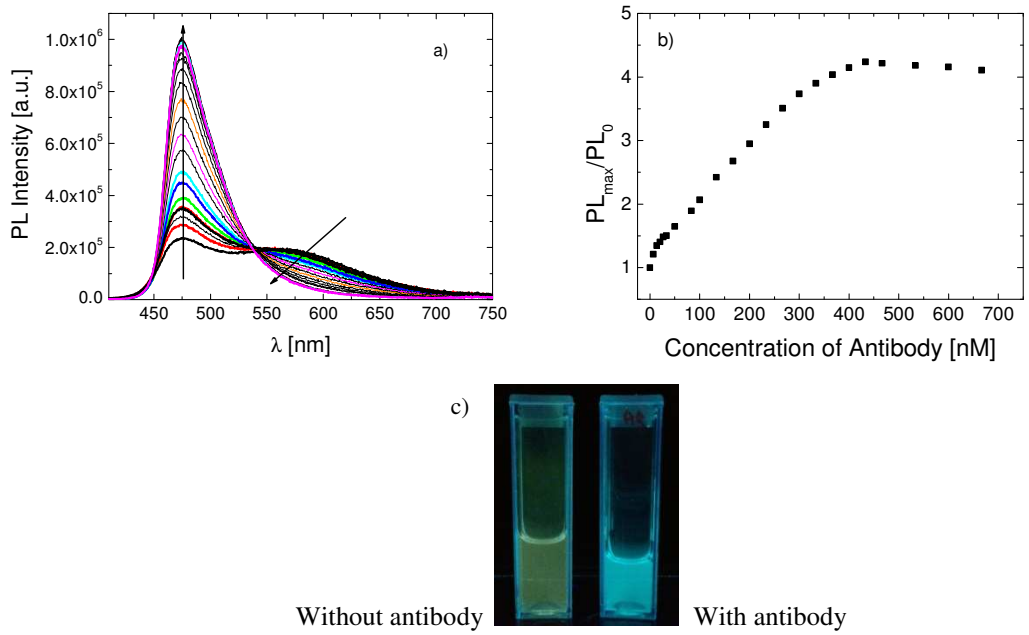

Figure 5-2: **a)** Fluorescence spectra of **D1** solution in PBS (0.005 g L^{-1}) at 15 °C containing varying amounts of the antibody [from 6.7 nM to 660 nM]. The direction of the arrows shows the increase in antibody concentration. The excitation wavelength was 400 nm. **b)** The relative change of the maximum emission intensity as a function of antibody concentration. Data are taken from Figure 5-2a. The photographs in **c)** were taken under illumination at 365 nm.

Despite the similarity to those triggered by increasing temperature, these changes are more drastic: while the aggregate band is suppressed, the emission from the isolated dye moieties at shorter wavelengths builds up. The slight blue-shift in λ^{PL}_{max} points to a more hydrophobic environment around the dye. As more protein was present in the solution, I measured also a longer lifetime of the emission at 475 nm (Figure 5-S5). For a polymer concentration of 0.005 g L^{-1}, the presence of the antibody in the solution at any concentration between about 6 to 300 nM invokes correspondingly different values of emission intensity, evident from the linear region of Figure 5-2b. Also, as scattering does not interfere, the antibody-induced changes in the absorbance spectrum are clearly visible, and qualitatively correlated with its concentration (Figure 5-3).

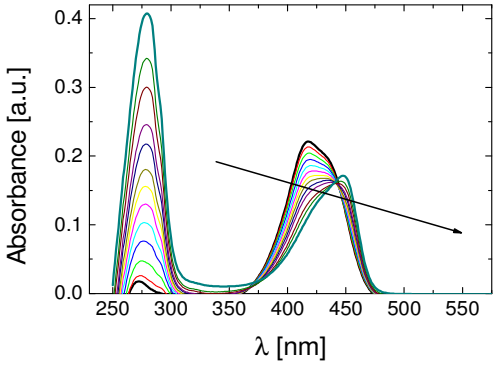

Figure 5-3: Absorbance spectra of **D1** solution in PBS (0.005 g L^{-1}) at 15 °C containing varying amounts of the antibody [from 6.7 nM to 660 nM]. The direction of the arrow shows the increase in antibody concentration.

In Figure 5-2 and 5-3, the almost complete disappearance of the spectroscopic features that are attributed to DEAC aggregates evidences their disruption. This might involve changes in chain conformation/association properties as a result of antibody binding. In parallel, the binding event shifts the C_p of **D1** to higher temperatures accompanied with lowered turbidity values (Figure 5-4a).

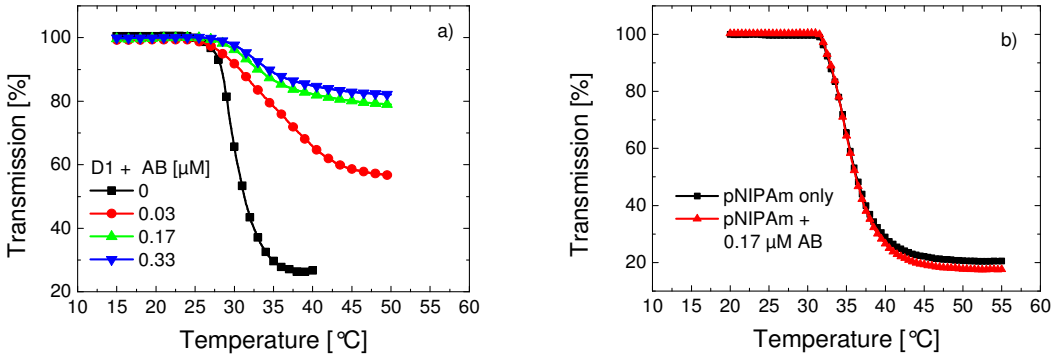

Figure 5-4: Temperature-transmission profiles of **a) D1** solution in PBS (0.1 g L^{-1}) containing varying amounts of the antibody (AB) (0, 0.03, 0.17, and 0.33 μM), and **b)** a solution of unlabeled pNIPAm in PBS (0.01 g L^{-1}) in the presence (red triangles) and absence of the antibody (0.17 μM) (black squares)

The hydrophilicity of the polymer chains is increased upon addition of the protein such that temperature induced-aggregations of labeled pNIPAm are hindered. The role of steric hindrance in retarding interchain aggregations should be noted as well. In general, the direction of the LCST shift depends on the type of the analyte, on the recognition unit, and on the nature of interactions between these groups and water. For instance, Rimmer *et al.* reported that binding of the recognition units of the highly branched pNIPAm to a gram negative bacterium decreased the LCST of the polymer by more than 20 °C.[94,209] Such a decrease was reported upon complexation of guest molecules with β-cyclodextrin moieties of

NIPAm chains.[210] Similarly, Gibson *et al*. showed the increased scattering intensity from pyridyl functionalized (MEO_2MA-*co*-OEGMA) solution in the presence of glutathiones.[50] On the other hand, the phase transition temperature of a biotinylated OEGMA-based copolymer shifted to higher temperatures upon specific binding of Avidin to the biotin moieties.[211] Likewise, the LCST of the p(NIPAm-*co*-crown ether) increased upon the formation of complexes between the crown moiety and its guest cation, as a result of the increased hydrophilicity.[212] It must be emphasized that pNIPAm synthesized analogously to **D1** but devoid of DEAC moieties does not exhibit changes in its turbidity profile in the presence of the antibody (Figure 5-4b). This ensures that the shift of the C_p is caused by the *specific binding* of the antibody to DEAC sites rather than a complexation with amphiphilic NIPAm units.* Therefore, it seems to be that when the antibody captures a dye attached to a chain (which is regarded as a constituent of an interchain associate), the pre-aggregated chains are separated. This, eventually, disrupts the dye aggregates. Within the binding pocket of the antibody the dye has a rather rigid, water-free, and nonpolar environment, enhancing its emission. Such increase in PL intensity was observed for DEAC dyes as they formed complexes with cyclodextrins.[109] The rigid hydrophobic environment within the dextrin nano-cavities was suggested to inhibit the formation of the TICT state.

5.3.2.1 Temperature control on the molecular recognition event

The antibody-sensing experiments above were performed at an isothermal temperature below the C_p of the polymer. However, when the antibody is introduced to aqueous **D1** solution at 40 °C (well above the C_p), neither the shape nor the intensity of the PL spectrum is affected. Furthermore, as this mixture is cooled down to 15 °C, the photophysical changes indicative of the binding event can once again be detected (Figure 5-5). For the evolution of other optical properties, i.e. the absorbance spectra and the decay traces, with the relevant heating and mixing steps, see Figure 5-S6.

* Interactions between responsive chains and other macromolecules are to be expected. For instance, in Chapter 3, I showed that the C_p shifts to higher temperatures as a result of direct interactions of the OEGMA-based copolymer (CLP) with the polycation P3TMAHT.

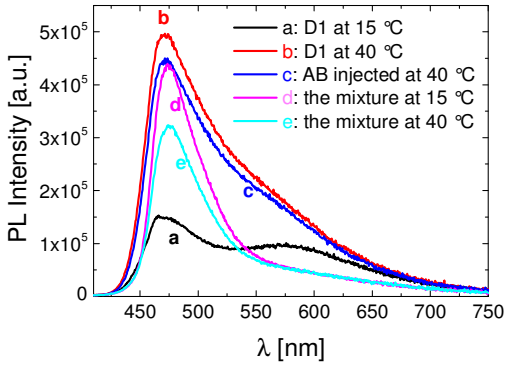

Figure 5-5: Steady-state emission spectra of **D1** solution in PBS (0.01 g L^{-1}) at 15 and 40 °C with and without the antibody (AB). a: **D1** at 15 °C, b: **D1** is heated to 40 °C, c: 0.17 µM of AB is injected into the polymer solution at 40 °C, d: the mixture is cooled down to 15 °C, e: the mixture is heated up to 40 °C.

Apparently, DEAC is accessible to the antibody only when **D1** chains are in a well-extended conformation. As the chains collapse and aggregate, the fluorophores are blocked. Regulating the access of a binding site attached to a thermoresponsive chain by the particular temperature sensitivity of the polymer has been reported before.[95,213,214] Exploiting the LCST-type solubility transition of pNIPAm chains, we can therefore switch the protein sensing on and off.

5.3.2.2 A Competitive binding event

The control of recognition event with temperature led to the question whether the intrinsic polymer response could further be exploited for the development of proof-of-concept assays. Figure 5-4 demonstrated that the temperature sensitivity of the polymer is retained; however its C_p shifts to higher temperature as the antibody complexes with the DEAC moieties. Figure 5-6 shows that after treatment with 20 fold excess of DEAC molecules (the fluorescent monomer), the mixture of **D1** (0.01 g L^{-1}) with 0.17 µM of antibody exhibits a "re-clouding". This ternary mixture was prepared by injecting the DEAC labeled monomer to the solution, comprising **D1** and the antibody, either at 15 °C followed by heating to 40 °C or directly at 40 °C (line *c* and *d*, respectively).* Scattering is identified by the appearance of an absorption tail which extends towards the IR region. Note that the addition of the fluorescent monomer to pure **D1** solution does not introduce such a scattering contribution (Figure 5-S7).

* It is crucial to ensure that the heating times and rates are identical in all experiments so that the effect of annealing on the size and intensity of the globules formed, therefore on the scattering intensity, is negligible.

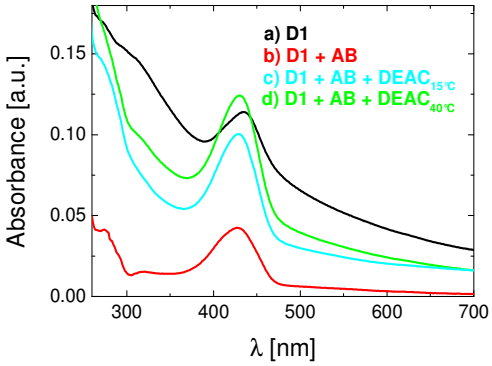

Figure 5-6: Absorbance spectra of aqueous solutions of **D1** (0.01 g L^{-1}) recorded at 40 °C: a) pure **D1** solution, b) the mixture of **D1** with antibody (0.17 µM), c) the ternary mixture of **D1** with antibody (0.17 µM) and with DEAC-labeled monomer (4 µM) added at 15 °C before heating, d) the ternary mixture of **D1** with the antibody and with the same amount of monomer added at 40 °C. Heating time after reaching the designated temperature, i.e., 40 °C was identical and lasted for 60 min.

The increase in turbidity (compared to the binary mixture of **D1** with the antibody) in the presence of the fluorescent monomer indicates that a fraction of the antibody is released from the DEAC sites of the polymer. Apparently, the detached antibody now forms complexes with the monomer available in the solution so that **D1** chains can more efficiently collapse and inter-aggregate. Here, an important point is whether this *competitive binding*, i.e. binding of the antibody to the low molar mass monomer rather than to the polymer moieties, occurs already at 15 °C or whether the process necessitates elevated temperatures. One way to address this is to examine the effect of monomer addition at 15 and at 40 °C on the fluorescence spectrum of the binary mixture at the respective temperature. As pointed out above (cf. Figure 5-5, line *a*), the emission spectrum of the **D1** solution recorded at temperatures below its C_p included an aggregate-assigned band at ca. 575 nm. While this feature was still visible at 40 °C (cf. Figure 5-5, line *b*), it became fully suppressed upon addition of a sufficient amount of the antibody at 15 °C (cf. Figure 5-5, line *d*). In Figure 5-7, one can see that the aggregate emission reappears as the monomer is injected into the mixture at 40 °C, while no such effect is present for the low temperature spectrum of the ternary mixture prepared at 15 °C. The aggregate emission generated at 40 °C is indicative of an increase in the number of DEAC aggregates, i.e., the antibody-free sites.

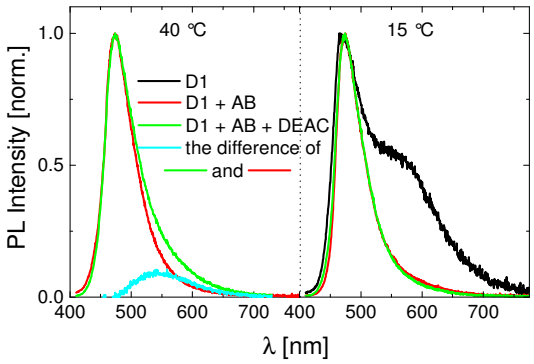

Figure 5-7: Normalized steady-state PL spectra of various solutions at 40 °C (left panel) and at 15 °C (right panel). The mixture of **D1** with 0.17 μM of antibody (red line), ternary mixture including DEAC (4 μM) (green line), the contribution of the free DEAC calculated by subtracting the spectrum of the binary mixture from that of the ternary (cyan line). Black line is the spectrum of **D1** at 15°C.

This shows that below the C_p the antibody is not released from the polymer and that the antibody detachment requires higher temperatures. The driving force of the observed detachment at 40 °C is yet not clear, but it might be related to a temperature-activated process, e.g., increased mobility/diffusion of the sensing components or the dehydration of the chains. There have been examples in which the latter was assigned as the trigger of similar kind of dissociation mechanisms. For example, Stayton and co-workers reported that the biotin bound-streptavidin functionalized-NIPAm chains released a significant amount of the biotin upon heating the mixture above its LCST.[214,215] Yamaguchi *et al.* observed an autonomous complexation and decomplexation behavior of a guest molecule with the β-cyclodextrin groups attached to NIPAm chains through remarkable changes in the turbidity profile.[210] At elevated temperatures, the guest molecule was released due to steric hindrance around the complex (from the crowding of collapsed neighboring NIPAM chains).[210] Here, regardless of the trigger of the mechanism, the released antibody at 40 °C cannot re-bind to the DEAC of **D1** because chain collapse and aggregation partly block the accessibility of the dye on polymer chains. Instead, the antibody remains stably bound to low molar mass dye present excessively in the solution. The relatively firm nature of the new antibody-DEAC complexes is evidenced by the temperature-transmission profile of the ternary mixture (line *d* of Figure 5-6) that was cooled down to room temperature and reheated, shown in the following Figure 5-8.

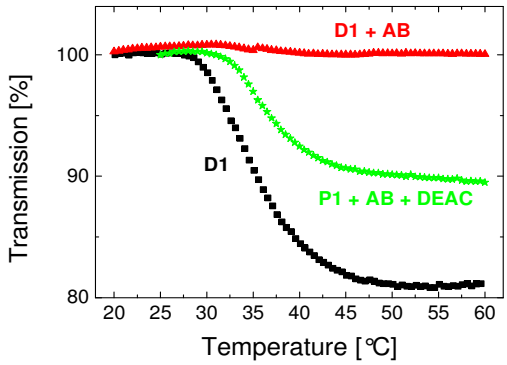

Figure 5-8: Temperature-transmission profile of the aqueous solution of **D1** (0.01 g L-1, black squares), containing 0.17 µM of antibody (red triangles), and containing both the antibody (0.17 µM) and the monomer (4 µM) (green stars). The profiles were recorded for the same solutions labeled as a,b, and d of Figure 5-6.

The ternary mixture displays a situation that is intermediate between the presence of only pure **D1** (no interference to interchain aggregations) and the case where **D1** solution is saturated with the antibody (strong suppression of interchain aggregations). I, therefore, suggest that the competitive binding mechanism is activated only above the C_p and that this proof of concept experiment might pave the way for assays utilizing thermoresponsive polymers. Scheme 5-2 depicts the proposed mechanism of sensing with **D1**.

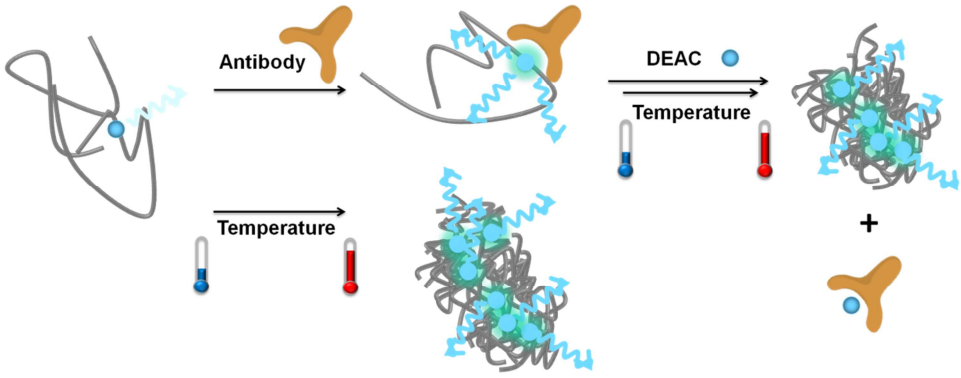

Scheme 5-2: Dual responsiveness of **D1** to the presence of antibody and to increasing the solution temperature above the C_p. In the absence of antibody and/or at low temperatures, the emission from the DEAC is weak. Upon formation of globules at elevated temperatures and/or binding of the antibody at low temperatures, the emission becomes intense. When heated, antibody attached to **D1** chains is released out to the solution where it forms new complexes with the DEAC-labeled monomer. This promotes inter-aggregation of **D1** chains.

5.4 Photophysical Properties of the OEGMA-based Copolymer

Besides elucidating the NIPAm-based copolymer, I also examined the effect of temperature and the presence of antibody on photophysical properties of the OEGMA-based copolymer **D2**. The investigations on this structure are important as the findings will further

evaluate the universality of the phenomenon revealed in the previous Chapter. Moreover, it is interesting to see whether the fluorescence response to the antibody binding is also specific to the host polymer. In accordance with the previous findings, no change in the emission properties of **D2** could be associated with its phase transition. Figure 5-9 demonstrates the temperature-independent shape of the PL spectrum. As the fluorescence intensity decreases gradually with the increase in temperature, the average fluorescence lifetime also shortens (Figure 5-S8). The fluorescence reduction is not correlated to the onset of polymer phase transition and is thus attributed to the temperature-facilitated deactivation of PL.

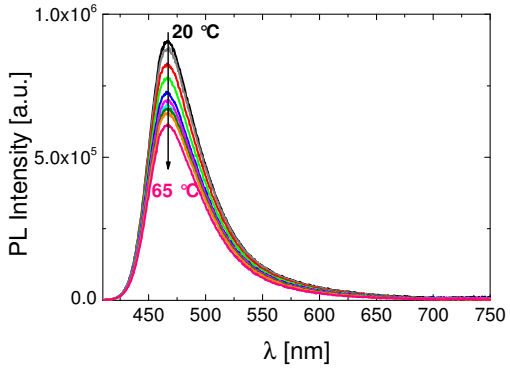

Figure 5-9: The effect of temperature on the fluorescence characteristics of **D2** in PBS (0.15 g L^{-1}). Excitation wavelength was 400 nm. The direction of the arrow shows the increase in solution temperature from 20 to 65 °C.

Although **D2** exhibits a LCST-type transition (see the following Figure 5-10a for its turbidity profile), along with the decrease in PL intensity, the constant λ^{PL}_{max} suggests that the dye's environment is not affected by the polymer phase transition. Apparently, when bound to a polymethacrylate backbone, the rather hydrophobic micro-environment of the fluorophore is preserved due to a particular arrangement of neighbouring molecules. Therefore, although **D2** is relatively emissive in aqueous solutions (φ: 25%), it does not feature the temperature sensing ability of **D1**.[*]

I, lastly, addressed the effect of antibody binding on the optical spectra of **D2**. First of all, it was found via ELISA tests that the antibody binds to the DEAC moieties of **D2** (Figure 5-S9), however, at a reduced extent than to those of **D1**. Second of all, upon binding, the C_p shifts to slightly higher temperatures (Figure 5-10a). Compared to **D1** at the same conditions, (cf. Figure 5-4a) this elevation is very weak.[†] Moreover, as opposed to **D1**, binding of the antibody to the DEAC results in a bathochromic shift of the emission maximum by ca. 8 nm

[*] For further discussion on this topic, see Chapter 4.5.

[†] It is likely that only a small fraction of the antibody present in the solution participates in the binding event.

(Figure 5-10b). This shift is accompanied with a slight reduction of the maximum PL intensity (Figure 5-S10). The shape of the absorbance spectrum exhibits no significant change, as well. According to preliminary results, increasing the antibody concentration does not change the trend of this fluorescence response.

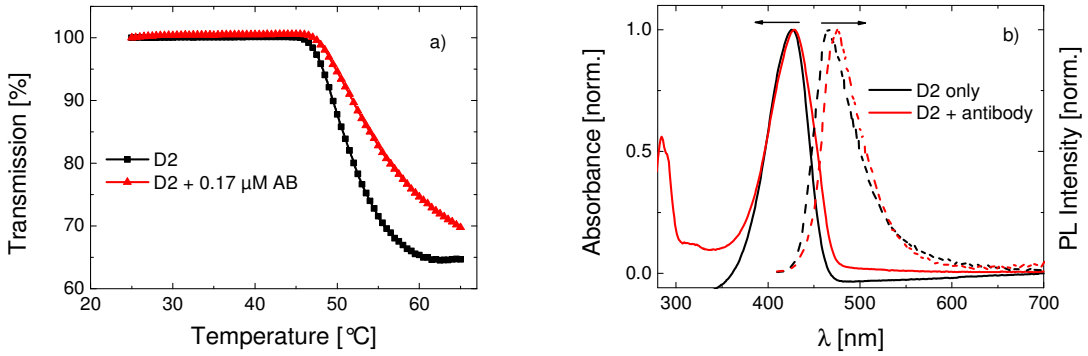

Figure 5-10: **a)** The temperature-transmission profile of **D2** solution in PBS (black squares-0.1 g L^{-1}) with the antibody (AB) (0.17 µM) (red triangles) **b)** Normalized absorbance (solid lines) and PL (dashed lines) spectra of the aqueous solution of **D2** (0.05 g L^{-1}) in the presence and absence of 0.17 µM of antibody at 20 °C.

With respect to PL spectra, similar observations were reported for a chromophore-modified cyclodextrin upon its interaction with guest molecules.[216] Bound to the guest, the chromophore inherently located in the interior of the hydrophobic cavity of dextrin was excluded into the more polar, aqueous solution. On the basis of this interpretation, I can only speculate the following: As it is suggested by the slight shift of LCST, the associates* of **D2** chains providing a hydrophobic environment to the dye are dispersed upon antibody binding. Although the dyes which are complexing with the antibody might have now less segmental mobility, i.e. an inhibited TICT state, this new environment might be less hydrophobic than that provided by the polymer chains, leading to the slight red-shift in emission spectrum. On the other hand, the antibody complexion with a certain fraction of the dyes might enhance the water exposure of some others as a result of the expansion of the chains.

5.5 Conclusions

In this chapter, I presented the photophysical characterization of two thermoresponsive fluorescent copolymers bearing covalently attached TICT-type DEAC dye, promising for optical sensing applications. When the dye is incorporated into a NIPAm-based polymer, the emission in aqueous media is very weak at low temperatures or in the absence of antibody. Upon heating the solution above its C_p or in the presence of the antibody, the emission

* This aggregation is not experimentally proven; however, according to the experience with analogous OEGMA-based fluorescent copolymers, interchain associations are fairly possible for **D2**.

intensity increases dramatically accompanied with a change in spectral shape. Therefore, the labeled NIPAm serves as a ratiometric fluorescent probe for temperature and for a specific protein. The recognition event proceeds through binding of the antibody to the dye moieties of the copolymer and can be controlled by tuning the chain conformation with temperature: Above the C_p, biological sensing is suppressed. The intrinsic LCST response is further exploited for the development of a proof-of-concept competitive binding event: Heating of the polymer-antibody mixture above its C_p releases a fraction of the bound antibody from the polymer sites out to the solution. As the low molar mass fluorescent monomer is injected into this mixture, the released antibody competitively binds to the monomer. This, in return, allows more effective temperature-induced aggregations of NIPAm chains. Since the fluorophores of the polymer are buried inside the globules, the new antibody-monomer complexes remain rather stable. As a result of that, the competitive binding mechanism is monitored from the turbidity profile of the mixtures, observed as a drop of C_p. On the contrary, in aqueous solutions of the OEGMA-based copolymer, DEAC mostly preserves its fluorescence properties upon the LCST-type phase transition, but also when it binds to the anti-DEAC antibody. In agreement with the conclusions of Chapter 4, these findings suggest the universality of the phenomenon about the OEGMA-based fluorescent copolymers.

5.6 Supplementary Information

Table 5-S1: The photophysical characterization of the fluorescent monomer dissolved in various solvents

Solvent	δ_t [a]	δ_d	δ_p	δ_h	λ^{abs}_{max} [nm]	λ^{PL}_{max} [nm]	φ [%]	τ [ns]
Diethylene glycol dimethyl ether	18.0 [b]	15.7 [b]	6.1 [b]	6.5 [b]	413	455	75.0	2.3
Toluene	18.2	18.0	1.4	2.0	413	436	71.0	2.5
Chloroform	19.0	17.8	3.1	5.7	420	449	76.0	2.8
Cylco-Hexanone	19.6	17.8	6.3	5.1	417	458	62.0	1.7
Acetone	20.1	15.5	10.4	7.0	414	460	18.2	0.6
Acetonitrile	24.6	15.3	18.0	6.1	415	463	8.1	0.2
Dimethylformamide	25.0	14.3	11.9	16.6	419	466	8.8	0.3
Dimethylsulfoxide	26.6	18.4	16.4	10.2	422	471	9.4	0.3
Ethanol	26.6	15.8	8.8	19.4	419	465	6.6	0.2
Triethyleneglycol	27.5 [b]	16.0 [b]	12.5 [b]	18.6 [b]	424	470	27.0	0.9
N-Methylformamide	30.1 [b]	17.4 [b]	18.8 [b]	15.9 [b]	420	468	9.0	0.4
Water	47.9	15.5	16.0	42.4	423	473	4.5	1.0

[a] in units of [$mPa^{0.5}$] from J. E. Mark, ed., *Physical Properties of Polymers Handbook*, American Institute of Physics, Woodbury, N.Y., 1996;
[b] from C. M. Hansen, *Hansen Solubility Parameters: A User's Handbook, Second Edition*, CRC Press, Boca Raton, FL, 2007.

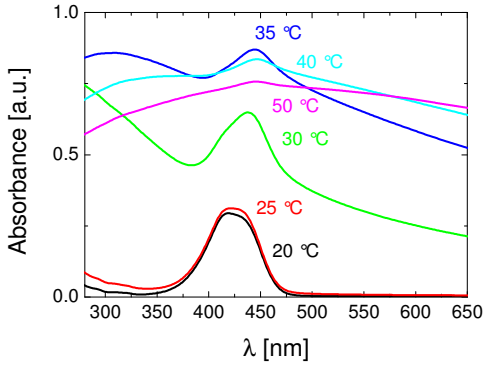

Figure 5-S1: Absorbance spectra of aqueous **D1** solution (0.5 g L^{-1}) at various temperatures.

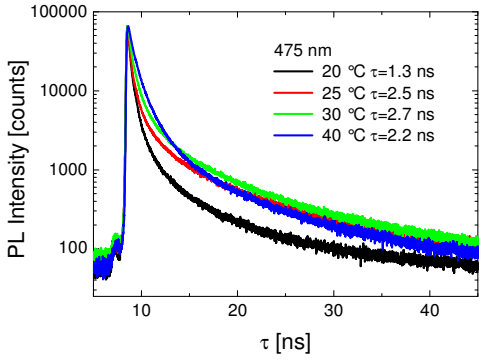

Figure 5-S2: Time-resolved PL traces of aqueous **D1** solution at 20, 25, 30 and 40 °C, with intensity averaged lifetimes (τ_{int}). The sample was excited at 405 nm and the emission was detected at 475 nm.

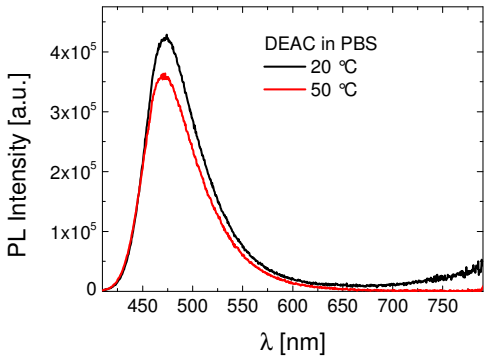

Figure 5-S3: Emission spectra of the DEAC-functionalized in PBS at 20 and 50 °C. Excitation wavelength was 400 nm.

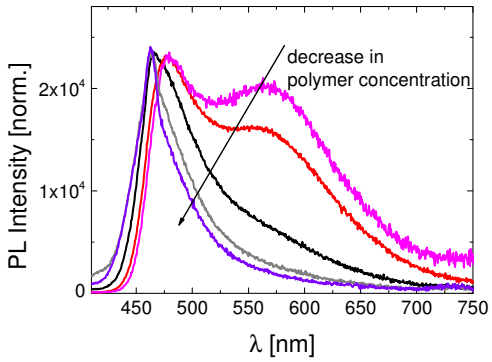

Figure 5-S4: The normalized PL spectra of aqueous solutions of **D1** at various concentrations at 20 °C. The direction of the arrow shows the decrease in polymer concentration from 0.1 to 0.0001 g L^{-1}.

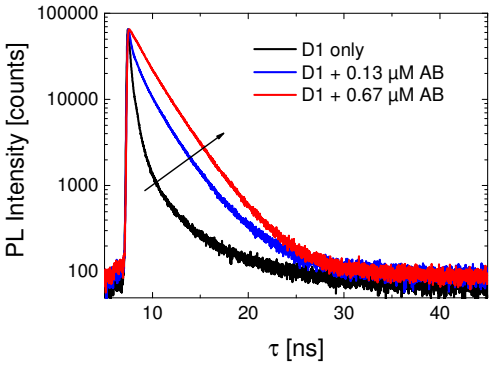

Figure 5-S5: Time-resolved PL traces of an aqueous solution of **D1** (0.005 g L^{-1}) with and without antibody (AB). The solution at 15 °C was excited at 405 nm and its emission was detected at 475 nm.

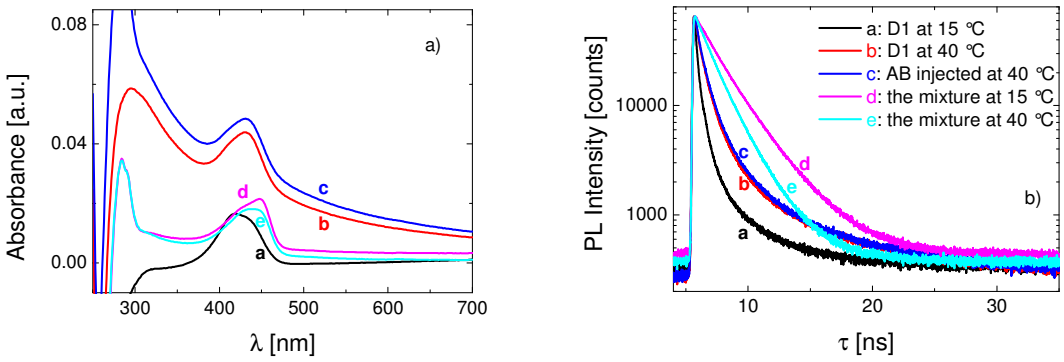

Figure 5-S6: Absorbance spectra **a)** and the time-resolved fluorescence decay curves **b)** of **D1** solution in PBS (0.01 g L^{-1}) at 15 and 40 °C with and without the antibody. The letters rank the steps of the heating and mixing protocol: a) **D1** at 15 °C, b) **D1** is heated to 40 °C, c) 0.17 μM of antibody (AB) is injected into the **D1** solution at 40 °C, d) this mixture is cooled down to 15 °C, e) the mixture is heated up to 40 °C.

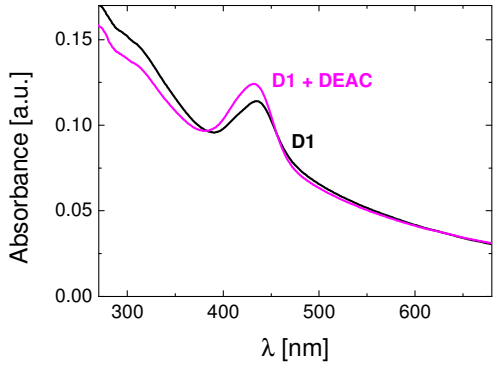

Figure 5-S7: Absorbance spectra of solutions of **D1** in PBS (0.01 g L^{-1}) recorded at 40 °C: pure **D1** solution (black line) and its mixture with DEAC (4 μM) (magenta line). Heating time after reaching the designated temperature, i.e., 40 °C was identical and lasted for 60 min.

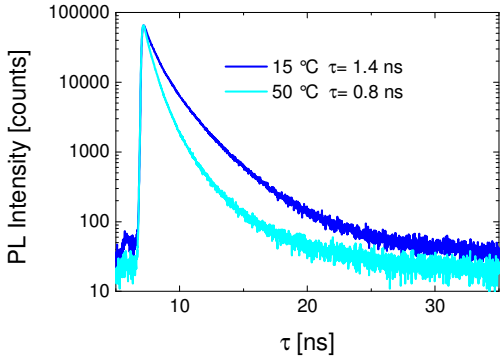

Figure 5-S8: Time-resolved PL traces of an aqueous **D2** solution at 15 and 50 °C with intensity-averaged lifetimes (τ_{int}). The excitation and the emission wavelength is 405 and 475 nm, respectively.

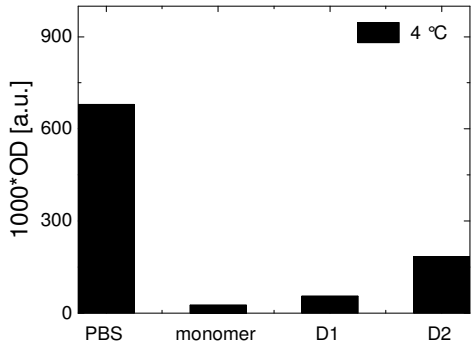

Figure 5-S9: ELISA tests showing the antibody binding efficiency of the monomer and the polymers at 4 °C. When DEAC is bound to a polymer backbone, its availability to the antibody drops, in the order of **D1>D2**

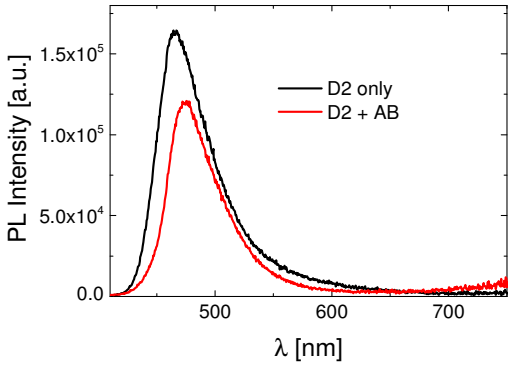

Figure 5-S10: PL spectra of the aqueous solution of **D2** (0.01 g L^{-1}) in the presence and absence of 0.17 µM of antibody (AB) at 20 °C. The excitation wavelength was 400 nm.

6 Summary and Outlook

This work deals with the development and evaluation of sensing schemes based on dye-labeled thermoresponsive copolymers. The concepts employed hereby rely on the ability of certain dyes to change their fluorescence properties in response to changes of the micro-environment, with the underlying photophysical effects being FRET or solvatochromism. I recorded remarkable changes in the fluorescence spectra of the copolymer solutions not only in response different stimuli applied, such as changes in the solution temperature and ionic strength, but also as a consequence of inter-polymer association/disassociation or biochemical binding. The extent of the spectral changes provided direct information on the quantity of the trigger. All of the designed sensing strategies worked in aqueous media, at low polymer concentrations and neutral pH. In certain conditions, the stimuli-induced change in fluorescence could be monitored simply by visual inspection, as a distinguished change of the fluorescence color. However, understanding the fluorescence response of these polymers was not straightforward. Instead, it required a comprehensive study on the aqueous solubility behavior of the chains, which this thesis has concentrated on.

The chemical structure of the host responsive polymer determines the performance of the optical sensing mechanism. When the stimulus leads to a collapse and aggregation of polymer chains, the degree of the changes in fluorescence properties defines the *sensitivity* of the system. The solvatochromic approach relied on the sensitivity of the photophysical properties of solvatochromic dyes towards the hydration state of polymer chains. The sensitivity is thus higher if the change invoked in the dye micro-environment is larger. In principle, since all thermoresponsive polymer solutions become comparably turbid upon heating, sensitive probes for temperature based on solvatochromic dyes can be readily constructed, regardless of the chemical structure of the host polymer. In this work, this was proven to be incorrect. In fact, *the ability of the fluorescent polymer to respond to temperature with a fluorescence output depended largely on the exact chemical structure of the macromolecule.* In Chapter **4**, I demonstrated this phenomenon by evaluating the properties of three different types of thermoresponsive polymers, i.e., a polyacrylamide (pNIPAm), a polyacrylate bearing short OEG chains (pMEO_2A) and a polymethacrylate bearing both short and long OEG chains (p(MEO_2MA-*co*-OEGMA)), all labeled with the same naphthalimide

moiety. Interestingly, only the labeled NIPAm exhibited a strong change in fluorescence properties, i.e., a ca. 25 fold increase of the PL intensity in response to a 10 °C increase in temperature. The sensing ability was completely lost with the labeled p(MEO_2MA-*co*-OEGMA) while only a negligible (ca. 2 times) increase of the PL intensity was measured for the labeled pMEO_2A.

Changing the type of the solvatochromic dye does not change the sensitivity of the probes. The same trend, i.e. polyacrylamide´s exhibiting distinguished fluorescence response and polymethacrylate´s insensitivity to temperature, was valid for the polymers analogous with the polymeric structure but differing with the type of the solvatochromic probe. This was shown in Chapter **4** for the copolymers labeled with a coumarin dye. The universality of the phenomenon was furthermore evidenced by the DEAC-labeled copolymers (labeled pNIPAm and p(MEO_2MA-*co*-OEGMA)) of Chapter **5**. This ensures *the governing role of the chemical structure of the host polymer* rather than that of the fluorophore on sensing efficiency.

The differences in the sensing performance are directly correlated with the aqueous solubility behavior of the polymers. The diverse fluorescence response of each polymer was strongly associated with how they dissolved in water. Through laser light scattering studies, in Chapter **4**, I found *different degrees of pre-aggregation of the chains at low temperatures* and *a variation in the extent of dehydration* for each polymer. For instance, the labeled pNIPAm and pMEO_2A were very similar in their hydration behavior below the cloud point C_p. Both polymers existed as single swollen chains and the presence of water around the dye was also evidenced from particular spectral features. On the other hand, the labeled p(MEO_2MA-*co*-OEGMA) formed loose aggregates in water. The "pre-aggregation" of these chains led to a more hydrophobic environment already before the phase transition sets in, causing an enhanced quantum yield of the dye. Therefore, it was the aggregation properties of the chains which determined the emission characteristics of the dye, i.e., the extent of water exposure or the contribution of the polarities of the other chains. Although the turbidity profiles of the polymers were quite similar, their temperature-induced aggregation behavior differed as well. In the early stages of its transition, the globules of pNIPAm chains became much larger and denser than those of the poly(meth)acrylates. Such a high magnitude of change in chain packing density, i.e. a more efficient dehydration and aggregation, enabled the remarkable fluorescence response of the dye within pNIPAm. On the other hand, the case of the p(MEO_2MA-*co*-OEGMA) was quite special: dye environment, which was already relatively water-free before, did not change after the transition.

Sensing of multiple stimuli is possible without complex chemical structures. Although sensing of multiple stimuli by fluorescent responsive polymers has been an

explored topic, I showed new approaches how to achieve this without the need of highly complex polymer architectures. Chapter **3** demonstrated a novel route for physical and chemical sensing: the combination of a coumarin-labeled p(MEO_2MA-*co*-OEGMA) as the donor with a thiophene-based polyelectrolyte (P3TMAHT) serving as the acceptor. As these polymers were mixed in water, I recorded strong energy transfer from the coumarin donor to the polycation below the C_p, as a result of unspecific hydrophobic interactions between the two macromolecules. Interestingly, as these interactions were relatively weak*, they were strongly altered by changes both in temperature and in salt concentration.* For example, an increase in solution temperature or ionic strength reduced the FRET efficiency significantly. This response was fully reversible and could directly be detected by naked eye owing to a distinct change in the fluorescence color.

Dual sensing of temperature and a specific protein was possible by using the aqueous solution of only one polymer. This NIPAm-based system shown in Chapter **5** was a binary copolymer of NIPAm with the solvatochromic DEAC dye. I demonstrated that the solubility of the copolymer was responsive to both temperature and an anti-DEAC antibody. To both stimuli, the polymer responded with characteristic changes in its fluorescence profile, however, what was exploited in the antibody sensing was the specific sensitivity of the dye´s fluorescence towards antibody binding. This made the copolymer special as *the reporter dye acted also as the recognition unit*. Moreover, as with the OEGMA-based polymer-P3TMAHT system, the read-out was a ratiometric change in intensity. The separation of the dye aggregates upon phase transition or antibody binding led to a change in emission color, while the increased hydrophobicity of the dye micro-environment resulted in an increase in overall fluorescence intensity. The linearity of the spectral changes in the examined concentration range of the protein is quite promising for diagnostics purposes and might pave the way for alternative strategies of the detection and quantification of multiple stimuli.

In dual-responsive systems, one parameter dictates whether the system can respond to the second stimulus. For the mixture of the coumarin-labeled p(MEO_2MA-*co*-OEGMA) with P3TMAHT to respond to temperature with a fluorescence output, the solution had to bear a certain amount of ions (alkali chlorides). *In the absence or in access of salts the temperature sensitivity was lost.* Through a combination of NMR, fluorescence, and light scattering studies, we found that in the presence of salts the polymers form large and phase-segregated aggregates above the C_p. Such internal structure led to an increase in donor-acceptor distance and thus to a very low FRET efficiency. On the other hand, in the absence of salts, inter-polymer interactions were inherently stronger below the C_p, and they were maintained even upon the phase transition. This led to efficient FRET over the entire

temperature range. Notably, most efficient temperature sensing was at physiological salt concentration, which might be useful for biochemical sensing purposes.

For the DEAC-labeled pNIPAm, the antibody sensing could be (de)activated by changing the operation temperature. When the solution temperature was raised above the C_p, the addition of the antibody did not affect the fluorescence properties, i.e., binding of the antibody was hindered. Above the C_p the hydrophobic DEAC fluorophores attached to pNIPAm chains were rather buried inside the globules, which rendered them inaccessible for the antibody.

The temperature sensitivity of the chains can be utilized for various purposes such as to initiate a separate binding event. In fact, besides controlling the recognition event, the temperature sensitivity allowed monitoring complex phenomena such as a competitive binding event. We found that heating of the preformed complexes of the DEAC-labeled pNIPAm with the antibody released a fraction of the bound antibody. If the fluorescent monomers were present in the same solution as well, the released antibody formed complexes with this lower-molar mass monomer instead. Interestingly, for this competitive binding event to take place, the solution temperature should be above the C_p. Only when the chains collapsed/aggregated and "hided" their fluorophores, the antibody could not bind back but rather remained attached to the monomer. This led to stable monomer-antibody complexes, the presence of which could be easily monitored from the turbidity profile. This is an intriguing example showing that the temperature sensitivity of the chains can be utilized other than sensing changes in solution temperature.

For further improvement of sensing strategies, the structure-functionality relationships concerning the hydration of chains and the features of phase transition such as its sharpness are of great importance. Considering the current polymers that I studied, sensing (relying on the solvatochromism of covalently attached dyes) was efficient only with pNIPAm. Nevertheless, given their superior bio-compatibility and anti-toxicity in comparison with the polyacrylamides, the use of OEGMA-based polymers as components of biological-sensing platforms is intrinsically more advantageous. However, to be able to render them applicable for such sensing platforms, some questions need to be answered. We believe that there is a particular arrangement of neighboring molecules in p(MEO_2MA-*co*-OEGMA)s, which, on the one hand, shields the dye from water below the C_p but also prevents large changes in the dye's micro-environment upon the phase transition. Is this governed by the backbone methyl groups or by the longer OEG chains? Or is an inefficient dehydration of OEG-based chains a reason for the reduced compactness of poly(meth)acrylate mesoglobules?

A systematic study on analogous polymers is required to elucidate which structural component should be eliminated or/and added in order to improve the sensing performance. For instance, PL and light scattering studies on a series of fluorescent p(MEO_2MA-*co*-OEGMA)s comprising the OEGMA monomer at various lengths or fluorescent p(MEO_2MA-*co*-OEGMA)s bearing the two macromonomers at different ratios can reveal the role of OEGMA groups in the pre-aggregation and in the solubility-insolubility transitions. Alternatively, a spacer unit as long as the OEGMA can be used to link the dye to the polymer in order to address the shielding effect. In fact, if we can obtain an OEG-based copolymer whose quantum yield is sufficiently low below the phase transition temperature, a change in dye micro-environment upon the LCST-transition is more likely-even though the dehydration of EG units is suggested to be less efficient than that of the pNIPAm. Consequently by adjusting the chemical structure and molecular architecture of the polymer, pEG-based probes can be as promising as NIPAm-based ones.

Although the solvatochromic approach for sensing was not efficient with the studies OEGMA-based structures, such copolymers were efficient FRET donors. In particular, the stability of the (relatively high) quantum yield in water against changes in temperature or ionic strength makes this polymer quite promising for imaging applications. Consequently, as we know more about how responsive polymers behave under different environmental conditions and the role of structural factors on the response mechanism; developing better sensing strategies based on these polymers should get far from being a real challenge.

7 Experimental Methods

7.1 Sample Preparation

In Chapter 3, solutions of CLP in PBS (pH 7.4, Sigma Aldrich) were prepared from a stock solution (2 g L^{-1}) which was kept overnight at 5 °C for complete dissolution. Solutions of P3TMAHT in PBS were also prepared from a stock solution (2 g L^{-1}) stirred at room temperature several hours. Mixtures of the two polymers were obtained by first diluting the thermoresponsive polymer to a fixed concentration (0.12 g L^{-1}, 0.6 mM in repeat units) and then adding aliquot amounts of the P3TMAHT stock solution to yield concentrations of the polyelectrolyte in the final mixture between 0.04 and 0.30 mM (based on repeat units) unless otherwise stated. The aqueous solutions were allowed to equilibrate at least 2 h at room temperature prior to the spectroscopic measurements. In all experiments, the total polymer concentration was kept below 0.2 g L^{-1} to reduce inner filter effects in fluorescence measurements. Solutions for spectroscopy and scattering measurements were prepared either with de-ionized water (Millipore, Milli-Q) or with D_2O (99.9% isotopic purity, Eurisotop (Gif-sur-Yvette, France)). In order to change the ionic strength of the solutions, predetermined volumes of aqueous salt solutions of, e.g., LiCl, NaCl or CsCl were used.

In Chapter 4 and 5, all solutions were prepared in PBS and kept overnight at 5 °C for complete dissolution. All experiments were performed within a few days after the preparation of the solutions. Solutions for scattering measurements were filtered through 250 nm cellulose filters. Specific conditions for measurements and the concentration of solutions are stated in detail in the text of the corresponding part.

7.2 Experimental Methods

7.2.1 UV-VIS Spectroscopy

Turbidity measurements were performed on a Varian Cary 500 UV-VIS photometer.[*] Transmittance of polymer solutions at 700 nm was monitored as a function of temperature

[*] Turbidity measurements were performed in the *Fraunhofer Institute for Applied Polymer Research* in *Golm*.

(with heating/cooling cycle at the rate of 0.1 °C min^{-1}, cell path length of 12 mm). Cloud points of the solutions in this work refer to the onset of the transmission loss. Absorption spectra of solutions were measured with a Varian Cary 5000 spectrometer. The samples were measured in quartz cells of 1 mm path length for the experiments reported in Chapter 3. For other measurements, PMMA or quartz cells of 10 mm path length were also used. As for the fluorescence measurements, a cuvette holder equipped with a Peltier element was used to perform the temperature-dependent measurements. In temperature-dependent measurements, each spectrum was acquired after reaching equilibrium, i.e., assuring that both the intensity and the shape of the spectrum were stable 15 minutes after reaching the desired temperature. UV-VIS spectra were used to estimate the dye content of the thermoresponsive polymers as in the following. Solutions of the dye-labeled monomer in $CHCl_3$ (a good solvent for NIPAm and acrylates) at (at least) five different concentrations were prepared and their absorbance spectra were recorded. The molar extinction (absorption) coefficient (ε) of the label was then obtained according to *Beer-Lambert´s law*:

$$A = -\log T = -\log \frac{I}{I_0} = \varepsilon c l \qquad \textbf{Equation 7-1}$$

where A is the absorbance of the sample and T is its transmission expressed as the ratio of the intensity of the transmitted light (I) to that of the incident light entering the cuvette (I_0). The law relates the reduction of I_0 to the concentration of the absorbers (c), to the length of the path, i.e. the thickness of the cuvette (l), and to ε, as it travels across the solution.[217] Based on this relationship, ε is extracted from the slope of the concentration of the dye solution *vs*. the maximum absorbance values curve. The absorbance of a dilute solution of the investigated polymer in $CHCl_3$ was then used to calculate the amount of the label.

7.2.2 Fluorescence Spectroscopy

Steady-state fluorescence spectra were measured with a HORIBA Jobin Yvon Fluorolog-3. The emission was always detected at the front face. In Chapter 3, the samples were measured in quartz cells of 1 mm path length; while in all other experiments PMMA or quartz cells of 10 mm path length were also used. Inner filter effects were negligible due to the short path length of the cuvettes (1 mm), crucial for the calculation of FRET efficiencies.

Time-resolved fluorescence measurements were performed by using a single photon counting (TCSPC) set-up with a Becker&Hickl PML-spectrometer (modified Oriel MS-125). TCSPC works like a stopwatch and measures the time difference between excitation and emission signals. This information is used to determine the lifetime of fluorescence, i.e., the

time that the molecule spends in the excited state before returning to the ground state. The electronics detect the arrival time of less than one photon per laser pulse. The recorded photons then build up a histogram of a photon distribution as a function of the fluorescence decay time and the detection wavelength. The detector of the set-up comprised a Becker&Hickl PML-16-C-1 (modified Hamamatsu) multi-alkaline photomultiplier. The 360 nm excitation at a repetition rate of 2.5 MHz was supplied from a Ti:sapphire laser source. A PicoQuant GmbH PDL 800-B laser driver was used in combination with two picosecond diode laser heads at 405 and at 470 nm, both operated at a repetition rate of 20 MHz. Upon each measurement cycle, instrument response function (IRF) was recorded at the excitation wavelength by using a scattering solution. IRF depends on the shape of the excitation pulse and on how this pulse is detected by the instrument. Thereby, the width of IRF represents the temporal resolution of the set-up, which was ca. 100 ps in our case. Raw data were fit with the data analysis software of PicoQuant GmbH (Germany). The decay times were extracted by means of a reconvolution fit based on an exponential decay model. During the analysis, the curves were generated from the best fit model parameters (lifetimes and pre-exponential factors) through the non-linear least squares fitting procedure. They were then convoluted with the IRF function. The resulting model function was finally compared with the measured curve to determine the quality of the fit. Until the best match was obtained, the values selected for fitting parameters were varied.

Considering that N number of molecules populates the excited state, these return to the ground state according to:

$$\frac{dN(t)}{dt} = (k_{\mathrm{r}} + k_{\mathrm{nr}})N(t) \qquad \textbf{\textit{Equation 7-2}}$$

where k_{r} is the emissive and k_{nr} is the radiationless rate of the decay. Since the number of excited molecules is proportional to the fluorescence intensity and the inverse of the lifetime (τ) is the sum of the decay rates depopulating the excited state, the time-dependent fluorescence intensity $I_{\mathrm{PL}}(t)$ is given by

$$I_{\mathrm{PL}}(t) = \sum_{i=1}^{i=n} a_{\mathrm{i}} e^{-t/\tau_{\mathrm{i}}} \qquad \textbf{\textit{Equation 7-3}}$$

where τ_{i} is the lifetime and a_{i} is the amplitude of the i^{th} emission component. The quality of the fit is quantified by χ^2 values, which were lower than ca. 2 for the fits performed in this work.

Typically, the variety of emissive species in the sample correlates with the complexity of the decay curve. In such cases, it is useful to define a lifetime averaged with respect to the intensity or the amplitude of the components. The intensity-weighted fluorescence lifetime τ_{int} was calculated as

$$\tau_{\mathrm{int}} = \frac{\sum_{i=1}^{i=n} a_{\mathrm{i}} {\tau_{\mathrm{i}}}^2}{\sum_{i=1}^{i=n} a_{\mathrm{i}} \tau_{\mathrm{i}}} \qquad \textit{Equation 7-4}$$

The amplitude-weighted fluorescence lifetime (τ_{ampl}) was estimated using:

$$\tau_{\mathrm{ampl}} = \frac{\sum_{i=1}^{i=n} a_{\mathrm{i}} \tau_{\mathrm{i}}}{\sum_{i=1}^{i=n} a_{\mathrm{i}}} \qquad \textit{Equation 7-5}$$

For the calculation of FRET efficiencies, the values of τ_{ampl} was used since these are proportional to the steady-state PL intensity.[103] All other average lifetimes reported were intensity weighted averages unless stated otherwise.

Quantum yields of the solutions were measured with a Hamamatsu C9920 set-up. This device includes an integrating sphere combined with a photonic multi-channel analyzer. As for the absorbance measurements, the solutions were in the dilute regime. The efficiencies were estimated by averaging twenty consecutive scans in order to improve the signal-to-noise ratio.

7.2.3 NMR Spectroscopy*

^{1}H NMR experiments were performed on a Bruker Avance III 850 NMR spectrometer employing a 5.0 mm TXI NMR probe equipped with a z-gradient. The CLP/ P3TMAHT samples in D_2O and 1 M NaCl were prepared using 99.9% D_2O with 8.5 g L^{-1} CLP and 2.0 g L^{-1} P3TMAHT, and filled into the NMR tube to a total volume of ~0.6 mL. At this concentration range, all solutions were clear at 13 °C, i.e., we did not observe any precipitation by visual inspection. The temperature was kept constant at an effective temperature of 13.4 °C for the experiments in D_2O, while the temperature was varied in 10 °C steps between 13.4 and 57.3 °C for those in 1 M NaCl. The sample temperature was determined via the ^{1}H chemical shift difference between CH_3 and OH signals in neat methanol,[218] and regulated via the Bruker temperature control unit. All experiments were recorded using a relaxation delay of 5 s and a ^{1}H π/2-pulse length of 9.60 µs. The standard ^{1}H

* NMR experiments and the related data analysis shown in Chapter 3.4.2.1 were performed by *Michael R. Hansen* and *Manfred Wagner* in the *Max Planck Institute for Polymer Research* in Mainz.

NMR experiments used 8 scans, a spectral width of 9375.0 Hz (11.03 ppm), and an acquisition time of 7 s.

To probe the inter/intra-molecular interactions within distances of 3-5 Å, the NOE effect was employed. This technique detects the transfer of magnetization between spins, which are close in space and not necessarily bound with a chemical bond, during a given mixing time. The obtained correlation spectrum appears as a contour plot that has diagonal peaks and correlation peaks. The latter corresponds to the chemical shifts of different spins that are sharing a mutual relaxation. The position of each peak is specified by two chemical shift coordinates. For this work, the 2D ^{1}H-^{1}H NOESY experiments were recorded using the standard three-pulse NOESY pulse sequence with gradient coherence pathway selection.[219] These experiments employed a NOE mixing time of 200 ms with each 16 scans for 256 t_1 increments, an acquisition time of 1 s, and a spectral width of 8503.4 Hz (10.00 ppm) in both dimensions. All standard ^{1}H NMR and 2D ^{1}H-^{1}H NOESY spectra were processed identically. The ^{1}H chemical shift referencing of the solutions in D_2O was performed via the residual ^{1}H signal of D_2O, using the reported temperature-dependence for HDO.[220] For the solutions in 1 M NaCl, the ^{1}H chemical shift of the first methylene group of the side chains for CLP was used as an internal ^{1}H chemical shift reference, since the residual ^{1}H signal of D_2O was perturbed by the presence of Na^+ and Cl^- ions,[221] i.e., we neglected viscosity changes of the solvent and assumed that the ^{1}H chemical shift of the first methylene group for the side chains for CLP was constant in the measured temperature range.

7.2.4 Laser Light Scattering*

Dynamic light scattering (DLS) and static light scattering (SLS) experiments were performed on the same ALV/CGS-3 instrument. The instrument was equipped with a He-Ne laser operating at a wavelength of 632.8 nm. The intensity-time autocorrelation functions $g^{(2)}(\tau)$ were recorded using an ALV 5000/E multiple-τ digital correlator. In the most fundamental level, these functions describe the rate of change in scattering intensity by comparing the intensity at an initial time t, $I(t)$, to the intensity at a later time τ, $I(t+\tau)$, and thereby providing a quantitative measurement for how fast the particles move in solution.

Since particles in a solution are in constant Brownian motion, the distance between scattering centers change with time and the intensity of the light that is scattered from them fluctuates. By measuring the degree of similarity between two scattering intensity signals over after the delay time τ, the device collects the reduction of their correlation with time, i.e., the

* Light scattering measurements were performed by *Leonardo Chiappisi* in the *Stranski-Laboratory for Physical and Theoretical Chemistry of Technische Universität Berlin*.

time it takes for the correlation between the two signals to disappear. The correlation function is expressed as an integral over the product of these intensities. For mono-disperse particles, the baseline subtracted and normalized intensity-time autocorrelation function is an exponential decay in the following form:[222]

$$g^{(2)}(\tau) = exp(-2\Gamma\tau) = \exp(-2Dq^2\tau) \qquad \textbf{\textit{Equation 7-6}}$$

where Γ is the rate of the decay, D is the translational diffusion coefficient of the particles and q is the magnitude of the scattering vector ($q = 4\pi n \sin(\theta/2)/\lambda$, with n: the refractive index of the solution, θ: the scattering angle, and λ: incident wavelength of the light). The slope of the logarithm of this correlation function *vs.* τ will correspond to $-2Dq^2$. Once the D is known, hydrodynamic radius R_h can be calculated according to *Stokes-Einstein* equation ($R_h = k_B T/6\pi\eta D$, η: viscosity of the solution). For a narrow distribution of sizes, the function can be expressed also in terms of cumulants. To obtain the rate of decay, analysis of the correlation function is generally performed by fitting a polynomial of up to the third order.[61] Only if the particles move by diffusion, Γ plotted as a function of q^2 will be a straight line with a slope equal to the diffusion coefficient.[222] In this work, the recorded curves were only qualitatively analyzed. As the measured decay function is the intensity-weighted sum of the decay of the individual particles, it contains information about the sizes and their distribution. For instance, as large particles diffuse slower, their correlation reduces to zero at longer times.

During the DLS measurements, the time averaged intensity of the scattered light was recorded simultaneously. The scattering intensities were collected at various scattering angles in the range of 30° to 135° (15° steps). All measurements were performed in a thermostated toluene bath (± 0.1 °C) for aqueous polymer solutions at varying temperatures. The angular dependence of the scattering intensity was analyzed to yield information about the particle size and weight. The scattering intensity was normalized using the scattering of toluene at 25 °C as a reference, having a Rayleigh ratio* of 1.34 10^{-5} cm^{-1} at 632.8 nm.[223] In the low q limit ($0.005 < q < 0.025$ nm^{-1}), given that the interactions between particles in solution are negligible, the particle form factor† corresponds to the scattering intensity measured as a function of q, $I(q)$.[224] Therefore the scattering intensity is a direct measure of the particle size. For such a case, the radius of gyration R_g and the scattering intensity (I) for $q \rightarrow 0$ are obtained by means of the Guinier approximation:

* This is defined as the ratio of the scattering intensity measured at a certain distance from the scattering center to the intensity of incident light.

† This factor is expressed as $P(\theta) \approx 1 - \left(R_g{}^2 q^2/3\right)$.

$$I(q) \approx I(0)exp\left(R_g{}^2 q^2/3\right) \qquad \textbf{Equation 7-7}$$

Accordingly, a semi-log plot of $I(q)$ *vs.* q^2 provides the R_g as the slope. Given that $I(q) = I(0)$, the apparent weight-averaged molecular weight ($M_{w,app}$) is determined as:

$$M_{w,app} = \frac{I(0)}{K_L c} \qquad \textbf{Equation 7-8}$$

where c is the concentration of the polymer solution. Here, the optical constant K_L is given as $K_L = 4\pi^2 n^2 (dn/dc)^2/(N_A \lambda^4)$ with $(dn/dc)^*$ and N_A being the refractive index increment and the Avogadro constant, respectively. When the scattering intensity $I(q)$ is independent of the scattering vector, R_g was regarded to be smaller than 25 nm (given that λ = 632 nm). The *dn/dc* of the CLP and the P3TMAHT in aqueous solution were estimated to be 0.15 $cm^3\ g^{-1}$ and 0.3 $cm^3\ g^{-1}$, respectively.[160,225,226] For aqueous solutions of **P1** and **P2** or **P3**, *dn/dc* was taken as 0.167 and 0.15 $cm^3\ g^{-1}$, respectively.[61,227]

The apparent chain density (ρ) defined as the polymer concentration within the spherical volume occupied by its chains was calculated according to:[61]

$$\rho = 3M_{w,app}/4\pi N_A R^3 \qquad \textbf{Equation 7-9}$$

where R is the effective radius of the aggregates considered and given as $R = \sqrt{5/3}\, R_g$.

The average number of chains accumulated in an aggregate, i.e. aggregation number, was then calculated as:

$$N_{agg} = M_{w,app}/M_w{}^{app} \qquad \textbf{Equation 7-10}$$

* This is the change in refractive index as a function of the change in concentration, measured typically by use of a differential refractometer.

8 Bibliography

[1] Aseyev, V.; Tenhu, H.; Winnik, F. M. *Advences in Polymer Science* **2011**, *242*, 29.
[2] Roy, D.; Cambre, J. N.; Sumerlin, B. S. *Progress in Polymer Science* **2010**, *35*, 278.
[3] Roy, D.; Brooks, W. L. A.; Sumerlin, B. S. *Chemical Society Reviews* **2013**, *42*, 7214.
[4] Kumar, A.; Srivastava, A.; Galaev, I. Y.; Mattiasson, B. *Progress in Polymer Science* **2007**, *32*, 1205.
[5] Galaev, I. Y.; Mattiasson, B. *Trends in Biotechnology* **1999**, *17*, 335.
[6] Alarcon, C. d. l. H.; Pennadam, S.; Alexander, C. *Chemical Society Reviews* **2005**, *34*, 276.
[7] Gibson, M. I.; O'Reilly, R. K. *Chemical Society Reviews* **2013**, *42,* 7204.
[8] Aguilar M. R., E. C., Gallardo A., Varquez B., Roman J. S. In *Topics in tissue engineering* Ashammakhi N., R. R., Chiellini E., Ed. 2007; Vol. 3, p 1.
[9] Gil, E. S.; Hudson, S. M. *Progress in Polymer Science* **2004**, *29*, 1173.
[10] Ward, M. A.; Georgiou, T. K. *Polymers* **2011**, *3*, 1215.
[11] Donini, C.; Robinson, D. N.; Colombo, P.; Giordano, F.; Peppas, N. A. *International Journal of Pharmaceutics* **2002**, *245*, 83.
[12] Kumar, A.; Galaev, I. Y.; Mattiasson, B. *Biotechnology and Bioengineering* **1998**, *59*, 695.
[13] Xing, S.; Guan, Y.; Zhang, Y. *Macromolecules* **2011**, *44*, 4479.
[14] Lendlein, A.; Jiang, H.; Junger, O.; Langer, R. *Nature* **2005**, *434*, 879.
[15] Zrínyi, M. *Colloid and Polymer Science* **2000**, *278*, 98.
[16] Filipcsei, G.; Fehér, J.; Zrínyi, M. *Journal of Molecular Structure* **2000**, *554*, 109.
[17] Miyata, T.; Uragami, T.; Nakamae, K. *Advanced Drug Delivery Reviews* **2002**, *54*, 79.
[18] Bajpai, A. K.; Bajpai, J.; Saini, R.; Gupta, R. *Polymer Reviews* **2011**, *51*, 53.
[19] Stuart, M. A. C.; Huck, W. T. S.; Genzer, J.; Muller, M.; Ober, C.; Stamm, M.; Sukhorukov, G. B.; Szleifer, I.; Tsukruk, V. V.; Urban, M.; Winnik, F.; Zauscher, S.; Luzinov, I.; Minko, S. *Nat Mater* **2010**, *9*, 101.
[20] Bhattarai, N.; Gunn, J.; Zhang, M. *Advanced Drug Delivery Reviews* **2010**, *62*, 83.
[21] Qiu, Y.; Park, K. *Advanced Drug Delivery Reviews* **2001**, *53*, 321.
[22] Lutolf, M. P.; Lauer-Fields, J. L.; Schmoekel, H. G.; Metters, A. T.; Weber, F. E.; Fields, G. B.; Hubbell, J. A. *Proceedings of the National Academy of Sciences* **2003**, *100*, 5413.
[23] Mizutani, A.; Nagase, K.; Kikuchi, A.; Kanazawa, H.; Akiyama, Y.; Kobayashi, J.; Annaka, M.; Okano, T. *Journal of Chromatography A* **2010**, *1217*, 522.
[24] Hu, J.; Liu, S. *Macromolecules* **2010**, *43*, 8315.
[25] Hendrickson, G. R.; Andrew Lyon, L. *Soft Matter* **2009**, *5*, 29.
[26] Basabe-Desmonts, L.; Reinhoudt, D. N.; Crego-Calama, M. *Chemical Society Reviews* **2007**, *36*, 993.

[27] Hu, J.; Zhang, X.; Wang, D.; Hu, X.; Liu, T.; Zhang, G.; Liu, S. *Journal of Materials Chemistry* **2011**, *21*, 19030.
[28] Pietsch, C.; Schubert, U. S.; Hoogenboom, R. *Chemical Communications* **2011**, *47*, 8750.
[29] Li, C.; Hu, J.; Liu, S. *Soft Matter* **2012**, *8*, 7096.
[30] Roth, P. J.; Haase, M.; Basche, T.; Theato, P.; Zentel, R. *Macromolecules* **2009**, *43*, 895.
[31] Pietsch, C.; Vollrath, A.; Hoogenboom, R.; Schubert, U. S. *Sensors* **2010**, *10*, 7979.
[32] Li, C.; Liu, S. *Chemical Communications* **2012**, *48*, 3262.
[33] Guo, Z.; Zhu, W.; Xiong, Y.; Tian, H. *Macromolecules* **2009**, *42*, 1448.
[34] Liu, T.; Hu, J.; Yin, J.; Zhang, Y.; Li, C.; Liu, S. *Chemistry of Materials* **2009**, *21*, 3439.
[35] Li, C.; Liu, S. *Journal of Materials Chemistry* **2010**, *20*, 10716.
[36] Hu, J.; Dai, L.; Liu, S. *Macromolecules* **2011**, *44*, 4699.
[37] Wu, W.; Zhou, T.; Shen, J.; Zhou, S. *Chemical Communications* **2009**, *0*, 4390.
[38] Onoda, M.; Uchiyama, S.; Ohwada, T. *Macromolecules* **2007**, *40*, 9651.
[39] Yin, J.; Li, C.; Wang, D.; Liu, S. *The Journal of Physical Chemistry B* **2010**, *114*, 12213.
[40] Wang, D.; Liu, T.; Yin, J.; Liu, S. *Macromolecules* **2011**, *44*, 2282.
[41] Zenkl, G.; Mayr, T.; Klimant, I. *Macromolecular Bioscience* **2008**, *8*, 146.
[42] Sun, S.; Wu, P. *Macromolecules* **2012**, *46*, 236.
[43] Akdemir, O.; Badi, N.; Pfeifer, S.; Zarafshani, Z.; Laschewsky, A.; Wischerhoff, E.; Lutz, J.-F. *ACS Symposium Series* **2009**, *1023*, 189.
[44] Pietsch, C.; Hoogenboom, R.; Schubert, U. S. *Angewandte Chemie International Edition* **2009**, *48*, 5653.
[45] Lutz, J.-F.; Akdemir, O.; Hoth, A. *Journal of the American Chemical Society* **2006**, *128*, 13046.
[46] Lutz, J.-F. *Journal of Polymer Science Part A: Polymer Chemistry* **2008**, *46*, 3459.
[47] Wu, C.; Wang, X. *Physical Review Letters* **1998**, *80*, 4092.
[48] Sun, S.; Wu, P. *The Journal of Physical Chemistry B* **2011**, *115*, 11609.
[49] Chee, C. K.; Rimmer, S.; Soutar, I.; Swanson, L. *Reactive and Functional Polymers* **2006**, *66*, 1.
[50] Summers, M. J.; Phillips, D. J.; Gibson, M. I. *Chemical Communications* **2013**, *49*, 4223.
[51] Phillips, D. J.; Gibson, M. I. *Biomacromolecules* **2012**, *13*, 3200.
[52] Weber, C.; Hoogenboom, R.; Schubert, U. S. *Progress in Polymer Science* **2012**, *37*, 686.
[53] Liu, R.; Fraylich, M.; Saunders, B. *Colloid & Polymer Science* **2009**, *287*, 627.
[54] Seuring, J.; Agarwal, S. *Macromolecular Rapid Communications* **2012**, *33*, 1898.
[55] Jones, R. A. L. *Soft Condensed Matter*; Oxford University Press: New York, 2002.
[56] Meeussen, F.; Nies, E.; Berghmans, H.; Verbrugghe, S.; Goethals, E.; Du Prez, F. *Polymer* **2000**, *41*, 8597.
[57] Heskins, M.; Guillet, J. E. *Journal of Macromolecular Science: Part A - Chemistry* **1968**, *2*, 1441.
[58] Seuring, J., Philipps-Universität Marburg, 2012.
[59] Somcynsky, T. *Polymer Engineering & Science* **1982**, *22*, 58.
[60] Pelton, R. *Journal of Colloid and Interface Science* **2010**, *348*, 673.

[61] Kujawa, P.; Aseyev, V.; Tenhu, H.; Winnik, F. M. *Macromolecules* **2006**, *39*, 7686.
[62] Aseyev, V.; Hietala, S.; Laukkanen, A.; Nuopponen, M.; Confortini, O.; Du Prez, F. E.; Tenhu, H. *Polymer* **2005**, *46*, 7118.
[63] Siu, M.; Liu, H. Y.; Zhu, X. X.; Wu, C. *Macromolecules* **2003**, *36*, 2103.
[64] Trzebicka, B.; Szweda, D.; Rangelov, S.; Kowalczuk, A.; Mendrek, B.; Utrata-Wesołek, A.; Dworak, A. *Journal of Polymer Science Part A: Polymer Chemistry* **2013**, *51*, 614.
[65] Dawson, K. A.; Gorelov, A. V.; Timoshenko, E. G.; Kuznetsov, Y. A.; Du Chesne, A. *Physica A: Statistical Mechanics and its Applications* **1997**, *244*, 68.
[66] Bolisetty, S.; Schneider, C.; Polzer, F.; Ballauff, M.; Li, W.; Zhang, A.; Schlüter, A. D. *Macromolecules* **2009**, *42*, 7122.
[67] Junk, M. J. N.; Li, W.; Schlüter, A. D.; Wegner, G.; Spiess, H. W.; Zhang, A.; Hinderberger, D. *Journal of the American Chemical Society* **2011**, *133*, 10832.
[68] Van Durme, K.; Van Assche, G.; Aseyev, V.; Raula, J.; Tenhu, H.; Van Mele, B. *Macromolecules* **2007**, *40*, 3765.
[69] Aseyev, V.; Tenhu, H.; Winnik, F. M. *Advances in Polymer Science* **2006**, *196*, 1.
[70] Chan, K.; Pelton, R.; Zhang, J. *Langmuir* **1999**, *15*, 4018.
[71] Balu, C.; Delsanti, M.; Guenoun, P.; Monti, F.; Cloitre, M. *Langmuir* **2007**, *23*, 2404.
[72] Wu, C.; Li, W.; Zhu, X. X. *Macromolecules* **2004**, *37*, 4989.
[73] Van Durme, K.; Van Assche, G.; Van Mele, B. *Macromolecules* **2004**, *37*, 9596.
[74] Skrabania, K.; Kristen, J.; Laschewsky, A.; Akdemir, Ö.; Hoth, A.; Lutz, J.-F. *Langmuir* **2006**, *23*, 84.
[75] Dimitrov, I.; Trzebicka, B.; Müller, A. H. E.; Dworak, A.; Tsvetanov, C. B. *Progress in Polymer Science* **2007**, *32*, 1275.
[76] Lahasky, S. H.; Hu, X.; Zhang, D. *ACS Macro Letters* **2012**, *1*, 580.
[77] Cheng, H.; Shen, L.; Wu, C. *Macromolecules* **2006**, *39*, 2325.
[78] Lu, Y.; Zhou, K.; Ding, Y.; Zhang, G.; Wu, C. *Physical Chemistry Chemical Physics* **2010**, *12*, 3188.
[79] Zhou, K.; Lu, Y.; Li, J.; Shen, L.; Zhang, G.; Xie, Z.; Wu, C. *Macromolecules* **2008**, *41*, 8927.
[80] Lutz, J.-F.; Hoth, A. *Macromolecules* **2006**, *39*, 893.
[81] Becer, C. R.; Hahn, S.; Fijten, M. W. M.; Thijs, H. M. L.; Hoogenboom, R.; Schubert, U. S. *Journal of Polymer Science Part A: Polymer Chemistry* **2008**, *46*, 7138.
[82] Han, S.; Hagiwara, M.; Ishizone, T. *Macromolecules* **2003**, *36*, 8312.
[83] Roth, P. J.; Jochum, F. D.; Forst, F. R.; Zentel, R.; Theato, P. *Macromolecules* **2010**, *43*, 4638.
[84] Deen, G. R. *Polymers* **2012**, *4*, 32.
[85] Xia, Y.; Yin, X.; Burke, N. A. D.; Stöver, H. D. H. *Macromolecules* **2005**, *38*, 5937.
[86] Qiu, X.-P.; Tanaka, F.; Winnik, F. M. *Macromolecules* **2007**, *40*, 7069.
[87] Tong, Z.; Zeng, F.; Zheng, X.; Sato, T. *Macromolecules* **1999**, *32*, 4488.
[88] Lutz, J.-F. *Advanced Materials* **2011**, *23*, 2237.
[89] Bebis, K.; Jones, M. W.; Haddleton, D. M.; Gibson, M. I. *Polymer Chemistry* **2011**, *2*, 975.
[90] Winnik, F. M. *Polymer* **1990**, *31*, 2125.
[91] Ringsdorf, H.; Simon, J.; Winnik, F. M. *Macromolecules* **1992**, *25*, 5353.
[92] Yip, J.; Duhamel, J.; Qiu, X. P.; Winnik, F. o. M. *Macromolecules* **2011**, *44*, 5363.
[93] Piçarra, S.; Gomes, P. T.; Martinho, J. M. G. *Macromolecules* **2000**, *33*, 3947.

[94] Sarker, P.; Shepherd, J.; Swindells, K.; Douglas, I.; MacNeil, S.; Swanson, L.; Rimmer, S. *Biomacromolecules* **2010**, *12*, 1.
[95] Pasparakis, G.; Vamvakaki, M.; Krasnogor, N.; Alexander, C. *Soft Matter* **2009**, *5*, 3839.
[96] Alexandridis, P.; Holzwarth, J. F. *Langmuir* **1997**, *13*, 6074.
[97] Uchiyama, S.; Kawai, N.; de Silva, A. P.; Iwai, K. *Journal of the American Chemical Society* **2004**, *126*, 3032.
[98] Gota, C.; Okabe, K.; Funatsu, T.; Harada, Y.; Uchiyama, S. *Journal of the American Chemical Society* **2009**, *131*, 2766.
[99] Shiraishi, Y.; Miyamoto, R.; Hirai, T. *Organic Letters* **2009**, *11*, 1571.
[100] Shiraishi, Y.; Miyamoto, R.; Zhang, X.; Hirai, T. *Organic Letters* **2007**, *9*, 3921.
[101] Akiyoshi, K.; Kang, E.-C.; Kurumada, S.; Sunamoto, J.; Principi, T.; Winnik, F. M. *Macromolecules* **2000**, *33*, 3244.
[102] Jares-Erijman, E. A.; Jovin, T. M. *Nat Biotech* **2003**, *21*, 1387.
[103] Lakowicz, J. R. *Principles of Fluorescence Spectroscopy*; 3rd ed.; Springer: New York, 2006.
[104] dos Remedios, C. G.; Moens, P. D. J. *Journal of Structural Biology* **1995**, *115*, 175.
[105] Loving, G. S.; Sainlos, M.; Imperiali, B. *Trends in Biotechnology* **2010**, *28*, 73.
[106] Valeur, B. In *Molecular Fluorescence*; Wiley-VCH Verlag GmbH: 2001, p 34.
[107] Marini, A.; Muñoz-Losa, A.; Biancardi, A.; Mennucci, B. *The Journal of Physical Chemistry B* **2010**, *114*, 17128.
[108] Nag, A.; Bhattacharyya, K. *Chemical Physics Letters* **1990**, *169*, 12.
[109] Tablet, C.; Matei, I.; Pincu, E.; Meltzer, V.; Hillebrand, M. *Journal of Molecular Liquids* **2012**, *168*, 47.
[110] Ramakrishna, G.; Ghosh, H. N. *The Journal of Physical Chemistry A* **2002**, *106*, 2545.
[111] Feng, F.; He, F.; An, L.; Wang, S.; Li, Y.; Zhu, D. *Advanced Materials* **2008**, *20*, 2959.
[112] Attar, H. A. A.; Monkman, A. P. *Advanced Functional Materials* **2008**, *18*, 2498.
[113] Herland, A.; Inganäs, O. *Macromolecular Rapid Communications* **2007**, *28*, 1703.
[114] Martinez-Tome, M. J.; Esquembre, R.; Mallavia, R.; Mateo, C. R. *Biomacromolecules* **2010**, *11*, 1494.
[115] Pu, K.-Y.; Shi, J.; Wang, L.; Cai, L.; Wang, G.; Liu, B. *Macromolecules* **2010**, *43*, 9690.
[116] Pu, K.-Y.; Liu, B. *Advanced Functional Materials* **2009**, *19*, 277.
[117] Ho, H.-A.; Najari, A.; Leclerc, M. *Accounts of Chemical Research* **2008**, *41*, 168.
[118] Qin, C.; Wong, W.-Y.; Wang, L. *Macromolecules* **2010**, *44*, 483.
[119] Knaapila, M.; Evans, R. C.; Garamus, V. M.; Almasy, L.; Szekely, N. K.; Gutacker, A.; Scherf, U.; Burrows, H. D. *Langmuir* **2010**, *26*, 15634.
[120] Inal, S.; Kölsch, J. D.; Chiappisi, L.; Kraft, M.; Gutacker, A.; Janietz, D.; Scherf, U.; Gradzielski, M.; Laschewsky, A.; Neher, D. *Macromolecular Chemistry and Physics* **2013**, *214*, 435.
[121] Pu, K.-Y.; Liu, B. *Advanced Functional Materials* **2011**, *21*, 3408.
[122] Duarte, A.; Pu, K.-Y.; Liu, B.; Bazan, G. C. *Chemistry of Materials* **2010**, *23*, 501.
[123] Thomas, S. W.; Joly, G. D.; Swager, T. M. *Chemical Reviews* **2007**, *107*, 1339.
[124] Jiang, H.; Taranekar, P.; Reynolds, J. R.; Schanze, K. S. *Angewandte Chemie International Edition* **2009**, *48*, 4300.
[125] Feng, X.; Liu, L.; Wang, S.; Zhu, D. *Chemical Society Reviews* **2010**, *39*, 2411.

[126] Fan, C.; Plaxco, K. W.; Heeger, A. J. *Journal of the American Chemical Society* **2002**, *124*, 5642.
[127] Chen, L.; McBranch, D. W.; Wang, H. L.; Helgeson, R.; Wudl, F.; Whitten, D. G. *Proceedings of the National Academy of Sciences of the United States of America* **1999**, *96*, 12287.
[128] Zhou, Q.; Swager, T. M. *Journal of the American Chemical Society* **1995**, *117*, 7017.
[129] Al Attar, H. A.; Monkman, A. P. *The Journal of Physical Chemistry B* **2007**, *111*, 12418.
[130] Davies, M. L.; Douglas, P.; Burrows, H. D.; da Graca Miguel, M.; Douglas, A. *The Journal of Physical Chemistry B* **2011**, *115*, 6885.
[131] Chen, L.; Xu, S.; McBranch, D.; Whitten, D. *Journal of the American Chemical Society* **2000**, *122*, 9302.
[132] Kaur, P.; Yue, H.; Wu, M.; Liu, M.; Treece, J.; Waldeck, D. H.; Xue, C.; Liu, H. *The Journal of Physical Chemistry B* **2007**, *111*, 8589.
[133] Wang, D.; Gong, X.; Heeger, P. S.; Rininsland, F.; Bazan, G. C.; Heeger, A. J. *Proceedings of the National Academy of Sciences* **2002**, *99*, 49.
[134] Nilsson, K. P. R.; Olle, I. *Nature Materials* **2003**, *2*, 419.
[135] Tang, Y.; Feng, F.; He, F.; Wang, S.; Li, Y.; Zhu, D. *Journal of the American Chemical Society* **2006**, *128*, 14972.
[136] An, L.; Tang, Y.; Feng, F.; He, F.; Wang, S. *Journal of Materials Chemistry* **2007**, *17*, 4147.
[137] Hong, J. W.; Hemme, W. L.; Keller, G. E.; Rinke, M. T.; Bazan, G. C. *Advanced Materials* **2006**, *18*, 878.
[138] Schild, H. G.; Tirrell, D. A. *Macromolecules* **1992**, *25*, 4553.
[139] Chee, C. K.; Rimmer, S.; Soutar, I.; Swanson, L. *Polymer* **1997**, *38*, 483.
[140] Chee, C. K.; Rimmer, S.; Soutar, I.; Swanson, L. *Polymer* **2001**, *42*, 5079.
[141] Chen, C.-Y.; Chen, C.-T. *Chemical Communications* **2011**, *47*, 994.
[142] Li, F.; Westphal, A. H.; Marcelis, A. T. M.; Sudholter, E. J. R.; Cohen Stuart, M. A.; Leermakers, F. A. M. *Soft Matter* **2011**, *7*, 11211.
[143] Hong, S. W.; Kim, K. H.; Huh, J.; Ahn, C.-H.; Jo, W. H. *Chemistry of Materials* **2005**, *17*, 6213.
[144] Gong, Y.; Gao, M.; Wang, D.; Möhwald, H. *Chemistry of Materials* **2005**, *17*, 2648.
[145] Gan, D.; Lyon, L. A. *Journal of the American Chemical Society* **2001**, *123*, 8203.
[146] Wan, X.; Liu, S. *Journal of Materials Chemistry* **2011**, *21*, 10321.
[147] Hong, S. W.; Kim, D. Y.; Lee, J. U.; Jo, W. H. *Macromolecules* **2009**, *42*, 2756.
[148] Willerich, I.; Gröhn, F. *Macromolecules* **2011**, *44*, 4452.
[149] Hofmann, C.; Schönhoff, M. *Colloid and Polymer Science* **2009**, *287*, 1369.
[150] Van Durme, K.; Rahier, H.; Van Mele, B. *Macromolecules* **2005**, *38*, 10155.
[151] Peng, S.; Wu, C. *Macromolecules* **2001**, *34*, 568.
[152] Leclerc, M. *Advanced Materials* **1999**, *11*, 1491.
[153] Monteserin, M.; Burrows, H. D.; Mallavia, R.; Di Paolo, R. E.; Macanita, A. L.; Tapia, M. J. *Langmuir* **2010**, *26*, 11705.
[154] Burrows, H. D.; Tapia, M. J.; Fonseca, S. M.; Pradhan, S.; Scherf, U.; Silva, C. L.; Pais, A. A. C. C.; Valente, A. J. M.; Schillen, K.; Alfredsson, V.; Carnerup, A. M.; Tomsic, M.; Jamnik, A. *Langmuir* **2009**, *25*, 5545.
[155] Burrows, H. D.; Lobo, V. M. M.; Pina, J.; Ramos, M. L.; Seixas de Melo, J.; Valente, A. J. M.; Tapia, M. J.; Pradhan, S.; Scherf, U.; Hintschich, S. I.; Rothe, C.; Monkman,

A. P. *Colloids and Surfaces A: Physicochemical and Engineering Aspects* **2005**, *270-271*, 61.
[156] Burrows, H. D.; Lobo, V. M. M.; Pina, J.; Ramos, M. L.; Seixas de Melo, J.; Valente, A. J. M.; Tapia, M. J.; Pradhan, S.; Scherf, U. *Macromolecules* **2004**, *37*, 7425.
[157] Sun, P.; Lu, X.; Fan, Q.; Zhang, Z.; Song, W.; Li, B.; Huang, L.; Peng, J.; Huang, W. *Macromolecules* **2011**, *44*, 8763.
[158] Kim, I.-B.; Dunkhorst, A.; Bunz, U. H. F. *Langmuir* **2005**, *21*, 7985.
[159] Mizusaki, M.; Kopek, N.; Morishima, Y.; Winnik, F. M. *Langmuir* **1999**, *15*, 8090.
[160] Zhou, J.; Ke, F.; Tong, Y.-Y.; Li, Z.-C.; Liang, D. *Soft Matter* **2011**, *7*, 9956.
[161] Ishizone, T.; Seki, A.; Hagiwara, M.; Han, S.; Yokoyama, H.; Oyane, A.; Deffieux, A.; Carlotti, S. *Macromolecules* **2008**, *41*, 2963.
[162] Kjoniksen, A.-L.; Nystroem, B.; Tenhu, H. *Colloids and Surfaces A: Physicochemical and Engineering Aspects* **2003**, *228*, 75.
[163] Zhou, X.; Ye, X.; Zhang, G. *The Journal of Physical Chemistry B* **2007**, *111*, 5111.
[164] Uchman, M.; Stepanek, M.; Prevost, S.; Angelov, B.; Bednar, J.; Appavou, M.-S.; Gradzielski, M.; Prochazka, K. *Macromolecules* **2012**.
[165] Lutz, J.-F.; Weichenhan, K.; Akdemir, O.; Hoth, A. *Macromolecules* **2007**, *40*, 2503.
[166] Kawaguchi, S.; Yekta, A.; Duhamel, J.; Winnik, M. A.; Ito, K. *The Journal of Physical Chemistry* **1994**, *98*, 7891.
[167] Li, X.; Ji, J.; Shen, J. *Macromolecular Rapid Communications* **2006**, *27*, 214.
[168] Yan, J.; Ji, W.; Chen, E.; Li, Z.; Liang, D. *Macromolecules* **2008**, *41*, 4908.
[169] Evans, R. C.; Knaapila, M.; Willis-Fox, N.; Kraft, M.; Terry, A.; Burrows, H. D.; Scherf, U. *Langmuir* **2012**, *28*, 12348.
[170] Zhang, Y.; Furyk, S.; Bergbreiter, D. E.; Cremer, P. S. *Journal of the American Chemical Society* **2005**, *127*, 14505.
[171] Zhang, Y.; Furyk, S.; Sagle, L. B.; Cho, Y.; Bergbreiter, D. E.; Cremer, P. S. *The Journal of Physical Chemistry C* **2007**, *111*, 8916.
[172] Baltes, T.; Garret-Flaudy, F.; Freitag, R. *Journal of Polymer Science Part A: Polymer Chemistry* **1999**, *37*, 2977.
[173] Freitag, R.; Garret-Flaudy, F. *Langmuir* **2002**, *18*, 3434.
[174] Shirin Fanaian, N. A.-M., Kaizheng Zhu, Anna-Lena Kjoniksen, Bo Nyström *Colloid and Polymer Science* **2012**, *290*, 1609.
[175] Thiyagarajan, P.; Chaiko, D. J.; Hjelm, R. P. *Macromolecules* **1995**, *28*, 7730.
[176] Ke, F.; Mo, X.; Yang, R.; Wang, Y.; Liang, D. *Macromolecules* **2009**, *42*, 5339.
[177] Florin, E.; Kjellander, R.; Eriksson, J. C. *Journal of the Chemical Society, Faraday Transactions 1: Physical Chemistry in Condensed Phases* **1984**, *80*, 2889.
[178] Einarson, M. B.; Berg, J. C. *Langmuir* **1992**, *8*, 2611.
[179] Ren, C.-l.; Tian, W.-D.; Szleifer, I.; Ma, Y.-Q. *Macromolecules* **2011**, *44*, 1719.
[180] Magnusson, J. P.; Khan, A.; Pasparakis, G.; Saeed, A. O.; Wang, W.; Alexander, C. *Journal of the American Chemical Society* **2008**, *130*, 10852.
[181] Weiss, J.; Li, A.; Wischerhoff, E.; Laschewsky, A. *Polymer Chemistry* **2012**, *3*, 352.
[182] Ananthapadmanabhan, K. P.; Goddard, E. D. *Langmuir* **1987**, *3*, 25.
[183] Wüthrich, K. *Science* **1989**, *243*, 45.
[184] Kumar, A.; Wagner, G.; Ernst, R. R.; Wuethrich, K. *Journal of the American Chemical Society* **1981**, *103*, 3654.
[185] Mi, P.; Chu, L.-Y.; Ju, X.-J.; Niu, C. H. *Macromolecular Rapid Communications* **2008**, *29*, 27.

[186] Iwai, K.; Matsumura, Y.; Uchiyama, S.; de Silva, A. P. *Journal of Materials Chemistry* **2005**, *15*, 2796.
[187] Uchiyama, S.; Matsumura, Y.; de Silva, A. P.; Iwai, K. *Analytical Chemistry* **2003**, *75*, 5926.
[188] Yin, L.; He, C.; Huang, C.; Zhu, W.; Wang, X.; Xu, Y.; Qian, X. *Chemical Communications* **2012**, *48*, 4486.
[189] Maeda, Y.; Yamauchi, H.; Kubota, T. *Langmuir* **2008**, *25*, 479.
[190] Dhar, S.; Singha Roy, S.; Rana, D. K.; Bhattacharya, S.; Bhattacharya, S.; Bhattacharya, S. C. *The Journal of Physical Chemistry A* **2011**, *115*, 2216.
[191] Dmitruk, S. L.; Druzhinin, S. I.; Minakova, R. A.; Bedrik, A. I.; Uzhinov, B. M. *Russ Chem Bull* **1997**, *46*, 2027.
[192] Pardo, A.; Martin, E.; Poyato, J. M. L.; Camacho, J. J.; Braña, M. F.; Castellano, J. M. *Journal of Photochemistry and Photobiology A: Chemistry* **1987**, *41*, 69.
[193] Saha, S.; Samanta, A. *The Journal of Physical Chemistry A* **2002**, *106*, 4763.
[194] Loving, G.; Imperiali, B. *Journal of the American Chemical Society* **2008**, *130*, 13630.
[195] Ramachandram, B.; Saroja, G.; Sankaran, B.; Samanta, A. *The Journal of Physical Chemistry B* **2000**, *104*, 11824.
[196] Yuan, D.; Brown, R. G. *The Journal of Physical Chemistry A* **1997**, *101*, 3461.
[197] Chipem, F. A. S.; Mishra, A.; Krishnamoorthy, G. *Physical Chemistry Chemical Physics* **2012**, *14*, 8775.
[198] Duke, R. M.; Veale, E. B.; Pfeffer, F. M.; Kruger, P. E.; Gunnlaugsson, T. *Chemical Society Reviews* **2010**, *39*, 3936.
[199] Grabchev, I.; Chovelon, J. M.; Qian, X. *Journal of Photochemistry and Photobiology A: Chemistry* **2003**, *158*, 37.
[200] Wang, H.; Wu, H.; Xue, L.; Shi, Y.; Li, X. *Organic & Biomolecular Chemistry* **2011**, *9*, 5436.
[201] Stevenson, K. A.; Yen, S. F.; Yang, N. C.; Boykin, D. W.; Wilson, W. D. *Journal of Medicinal Chemistry* **1984**, *27*, 1677.
[202] Veale, E. B.; Gunnlaugsson, T. *The Journal of Organic Chemistry* **2010**, *75*, 5513.
[203] Chen, Z.; Liang, X.; Zhang, H.; Xie, H.; Liu, J.; Xu, Y.; Zhu, W.; Wang, Y.; Wang, X.; Tan, S.; Kuang, D.; Qian, X. *Journal of Medicinal Chemistry* **2010**, *53*, 2589.
[204] Iwai, K.; Matsumoto, N.; Niki, M.; Yamamoto, M. *Molecular Crystals and Liquid Crystals Science and Technology. Section A. Molecular Crystals and Liquid Crystals* **1998**, *315*, 53.
[205] Wu, T.; Zou, G.; Hu, J.; Liu, S. *Chemistry of Materials* **2009**, *21*, 3788.
[206] Cigan, M.; Donovalova, J.; Szocs, V.; Gaspar, J.; Jakusova, K.; Gaplovsky, A. *The journal of physical chemistry. A* **2013**, *117*, 4870.
[207] Wagner, B. *Molecules* **2009**, *14*, 210.
[208] Raju B, B.; Varadarajan, T. S. *The Journal of Physical Chemistry* **1994**, *98*, 8903.
[209] Shepherd, J.; Sarker, P.; Swindells, K.; Douglas, I.; MacNeil, S.; Swanson, L.; Rimmer, S. *Journal of the American Chemical Society* **2010**, *132*, 1736.
[210] Ohashi, H.; Hiraoka, Y.; Yamaguchi, T. *Macromolecules* **2006**, *39*, 2614.
[211] Buller, J.; Laschewsky, A.; Lutz, J.-F.; Wischerhoff, E. *Polymer Chemistry* **2011**, *2*, 1486.
[212] Irie, M.; Misumi, Y.; Tanaka, T. *Polymer* **1993**, *34*, 4531.
[213] Pasparakis, G.; Cockayne, A.; Alexander, C. *Journal of the American Chemical Society* **2007**, *129*, 11014.

[214] Stayton, P. S.; Shimoboji, T.; Long, C.; Chilkoti, A.; Ghen, G.; Harris, J. M.; Hoffman, A. S. *Nature* **1995**, *378*, 472.
[215] Ding, Z.; Long, C. J.; Hayashi, Y.; Bulmus, E. V.; Hoffman, A. S.; Stayton, P. S. *Bioconjugate Chemistry* **1999**, *10*, 395.
[216] Zhong, C.; Mu, T.; Wang, L.; Fu, E.; Qin, J. *Chemical Communications* **2009**, *0*, 4091.
[217] Parson, W. W.; Schreck, S., Ed.; Springer: Heidelberg, 2007.
[218] Ammann, C.; Meier, P.; Merbach, A. *Journal of Magnetic Resonance (1969)* **1982**, *46*, 319.
[219] Wagner, R.; Berger, S. *Journal of Magnetic Resonance, Series A* **1996**, *123*, 119.
[220] Gottlieb, H. E.; Kotlyar, V.; Nudelman, A. *The Journal of Organic Chemistry* **1997**, *62*, 7512.
[221] Harings, J. A. W.; Deshmukh, Y. S.; Hansen, M. R.; Graf, R.; Rastogi, S. *Macromolecules* **2012**, *45*, 5789.
[222] Teraoka, I. In *Polymer Solutions*; John Wiley & Sons, Inc.: 2002, p 69.
[223] Itakura, M.; Shimada, K.; Matsuyama, S.; Saito, T.; Kinugasa, S. *Journal of Applied Polymer Science* **2006**, *99*, 1953.
[224] Sperling, L. H. *Introduction to Physical Polymer Science*; Wiley, 2005.
[225] Huang, Y.; Cheng, H.; Han, C. C. *Macromolecules* **2011**, *44*, 5020.
[226] Peng, Q.; Wyman, I. W.; Han, D.; Liu, G. *Canadian Journal of Chemistry* **2011**, *89*, 27.
[227] Yang, X.; Tong, Y.-Y.; Li, Z.-C.; Liang, D. *Soft Matter* **2011**, *7*, 978.
[228] Flory, P. J. *The Journal of Chemical Physics* **1942**, *10*, 51.
[229] Robeson, L. M. *Polymer Blends: A Comprehensive Review*; Hanser, 2007.

Appendix A: Flory-Huggins theory

To describe the mixing properties of polymer solutions, Flory and Huggins developed a theory on the basis of a rigid cubic lattice model. The theory includes the calculation of combinatorial entropy of mixing (the number of rearrangements during mixing) and of an interaction parameter expressing the enthalpy of mixing. As the theory is quite extended and is not within the scope of this thesis, here only the key equations useful for the understanding of how polymers dissolve in solution are shown. Each site of the lattice is occupied either by polymer or by solvent molecules (both occupy the same volume). The entropy of mixing per lattice site is calculated on the basis of the number of different ways of arranging these molecules. Given that φ_1 and φ_2 represent the volume fraction of the polymer and the solvent, respectively, the combinatorial entropy of mixing of the Flory-Huggins theory is simplified as:[222]

$$\Delta S_{\text{mix}} = -k_{\text{B}} n \left(\frac{\varphi_1}{r} \ln \varphi_1 + \varphi_2 \ln \varphi_2 \right) \qquad \textit{Equation A-1}$$

with n being the total number of lattice sites and r being the number of segments in one polymer chain, i.e., the degree of polymerization. Note that the first term is divided by the chain length. ΔS_{mix} is decreased by factor of $1/r$ due to connectivity of r segments into a single macromolecule.[59,228] For small molecules, the relatively higher value of the ΔS_{mix} compensates the enthalpic contribution and homogenous solutions can be obtained rather easily. Therefore, due to their macromolecular nature, polymers have a tendency to demix from their solutions.

The enthalpy of mixing is calculated considering the strength of interactions of unlike molecules in comparison with the interactions of the same type of molecules.[229] The enthalpy of mixing is defined as $\Delta H_{mix} \sim \varphi_1 \varphi_2 z \Delta w$, with Δw being the exchange energy per intermolecular contact. The product of φ_1 and φ_2 and z (z= the number of nearest neighbors) corresponds to the number of polymer-solvent contacts. The theory introduces the interaction parameter (χ) into as ΔH_{mix} in the following:[222]

$$\Delta H_{\mathrm{mix}} = nk_{\mathrm{B}}T\chi\varphi_1\varphi_2 \qquad \textbf{\textit{Equation A-2}}$$

The equation for the Gibbs free energy of mixing can thus be written as:[222]

$$\Delta G_{\mathrm{mix}} = nk_{\mathrm{B}}T\left(\frac{\varphi_1}{r}\ln\varphi_1 + \varphi_2\ln\varphi_2 + \chi\varphi_1\varphi_2\right) \qquad \textbf{\textit{Equation A-3}}$$

As the molecular weight of the polymer increases, the negative value inherent with the combinatorial entropy part becomes very small and therefore the enthalpy of mixing term determines the solubility behavior of the polymer.[229] Specific interactions between the polymer and the solvent lower the exchange energy of interacting segments *(*Δw), therefore also the ΔH_{mix}. The value of χ thus indicates the strength of energetic interaction between the components, in other words, the quality of the solvent for the polymer.[55] Typically, with an increase in the interaction parameter, the concentration of polymer in the solvent phase rapidly approaches a negligible value. The solvent will, however, be soluble in the polymer even at large values of χ. This contrasting behavior of the two components, i.e. the size originated differences in entropy, explains the high swelling capacity of polymer chains accompanied by a negligible solubility.[228]

Appendix B: On Phase Diagrams

As introduced in the fundamentals section, the change in free energy of mixing (ΔG_{mix}) defines the change in the free energy of a two-component system when going from an unmixed state to a mixed one. Since equilibrium always favours the lowest energy state, ΔG_{mix} must be smaller than zero for the miscibility of one component (solute) in the other (solvent). Although this is the necessary condition, if the curvature of free energy curve is negative then the phase diagram will display regions where the mixture separates into two phases.[229] The phase behaviour of a mixture can be understood from the shape of composition *vs*. free energy curves.

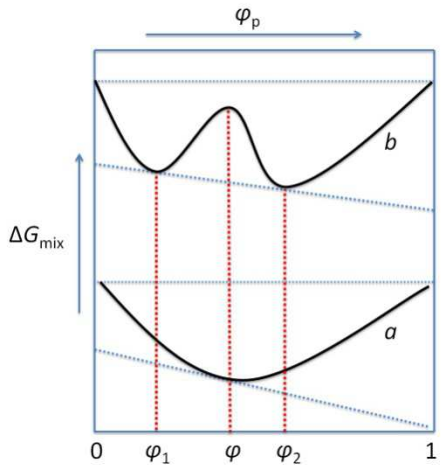

Figure B-1: The free energy of mixing as a function of the polymer fraction (φ_p) for one phase (*a*) or two phase (*b*) mixtures. The typical phase diagram shown in Figure 2-2 is constructed based on these generalized curves. An initial composition of φ is phase separated into two phases φ_1 and φ_2.[55]

Figure B-1 shows two curves; one has a single minimum (curve *a*), and the second one (curve *b*) has two minima and a maximum. Starting with a polymer fraction (φ_p=φ), if the system is identified with curve *a*, a homogenous mixture occur. However, if there is any region of composition in which the curve is a convex, the system will phase separate into two phases containing the polymer with a fraction of φ_1 and φ_2 in order to lower its energy.[55] These compositions are found by drawing a double tangent to the φ_p *vs*. ΔG_{mix} curve and are known as coexisting compositions. These are the polymer fractions that lie on the binodal curve for a certain temperature (see the phase diagram in Figure 2-2). If the free energy is a

symmetric function of composition, meaning that the components have the same size, the coexistence curve (binodal) is $\partial \Delta G_{\mathrm{mix}} / \partial \Delta \varphi_{\mathrm{p}} = 0$.

Within the region between φ_1 and φ_2, depending on the sign of the curvature, there are compositions promoting local stability with respect to small changes in composition.[55] The mixture at this region is metastable and its composition/temperature limits are defined by the spinodal curve. This is defined as the curvature of the free energy function at the position where:

$$\left(\frac{\partial^2 \Delta G_{\mathrm{mix}}}{\partial \Delta \varphi_{\mathrm{p}}{}^2}\right)_{T,P} = 0 \qquad \textbf{\textit{Equation B-1}}$$

The spinodal and the binodal curves merge at the critical point which separates the one phase and two phase region and is defined by the condition:

$$\left(\frac{\partial^3 \Delta G_{\mathrm{mix}}}{\partial \Delta \varphi_{\mathrm{p}}{}^3}\right)_{T,P} = 0 \qquad \textbf{\textit{Equation B-2}}$$

List of Publications

Parts of this Ph.D. thesis were published in scientific journals and were presented in oral presentations as well as on posters at several occasions by the author of this thesis.

Manuscripts peer-reviewed:

- S. Inal, L. Chiappisi, J. D. Kölsch, M. Kraft, M-S. Appavou, U. Scherf, M. Wagner, M. R. Hansen, M. Gradzielski, A. Laschewsky, D. Neher, "Temperature Regulated Fluorescence and Association of an Oligo(ethyleneglycol)methacrylate-based Copolymer with a Conjugated Polyelectrolyte-The Effect of Solution Ionic Strength", *the Journal of Physical Chemistry B* **2013** DOI: 10.1021/jp408864s
- S. Inal, J. D. Kölsch, F. Sellrie, J. A. Schenk, E. Wischerhoff, A. Laschewsky, D. Neher, "A Water Soluble Fluorescent Polymer as a Dual Colour Sensor for Temperature and a Specific Protein", *Journal of Materials Chemistry B* **2013** DOI: 10.1039/c3tb21245a
- S. Inal, J. D. Kölsch, L. Chiappisi, D. Janietz, M. Gradzielski, A. Laschewsky, D. Neher, "Structure-Related Differences in the Temperature-Regulated Fluorescence Response of LCST-type Polymers", *Journal of Materials Chemistry C* **2013**, *1*, 6603.
- S. Inal, J. D. Kölsch, L. Chiappisi, M. Kraft, A. Gutacker, D. Janietz, U. Scherf, M. Gradzielski, A. Laschewsky, D. Neher, "Temperature-Regulated Fluorescence Characteristics of Supramolecular Assemblies Formed By a Smart Polymer and a Conjugated Polyelectrolyte", *Macromolecular Chemistry and Physics* **2013**, *214*, 435.

Other Manuscripts:

- M. Shalom, S. Inal, C. Fettkenhauer, D. Neher, M. Antonietti, "Improving Carbon Nitride Photocatalysis by Supramolecular Preorganization of Monomers", *Journal of the American Chemical Society* **135**, 7118 (2013).
- S. Albrecht, S. Janietz, W. Schindler, J. Frisch, J. Kurpiers, J. Kniepert, S. Inal, P. Pingel, K. Fostiropoulos, N. Koch, D. Neher, "Fluorinated Copolymer PCPDTBT with Enhanced Open-Circuit Voltage and Reduced Recombination for Highly Efficient Polymer Solar Cells", *Journal of the American Chemical Society* **134**, 14932 (2012).

- S. Inal, M. Schubert, A. Sellinger, D. Neher, "The Relationship between the Electric Field-Induced Dissociation of Charge Transfer Excitons and the Photocurrent in Small Molecular/Polymeric Solar Cells", *the Journal of Physical Chemistry Letters* **1**, 982 (2010).
- S. Inal, M. Castellani, A. Sellinger, D. Neher, "Relationship of Photophysical Properties and the Device Performance of Novel Hybrid Small-Molecular/Polymeric Solar Cells", *Macromolecular Rapid Communications* **30**, 1263 (2009).

Selected Conference Contributions:

- S. Inal, J. D. Kölsch, D. Janietz, A. Laschewsky, D. Neher, "The Role of Chemical Structure on the Efficiency of Optical Sensing based on Responsive Copolymers", contributed talk at the *5th Potsdam Days on Bioanalysis,* 8th November **2013**, Potsdam, Germany.
- S. Inal, J. D. Kölsch, L. Chiappisi, M. Gradzielski, A. Laschewsky, D. Neher, "Evaluation of Fluorophore-functionalized Thermoresponsive Copolymers for Sensing Applications", contributed talk at the *Polymers for Advanced Technologies Conference*, 29th September-2nd October **2013**, Berlin, Germany.
- S. Inal, L. Chiappisi, J. D. Kölsch, M. Gradzielski, U. Scherf, M. R. Hansen, A. Laschewsky, D. Neher, "Supramolecular Assemblies of a Conjugated Polyelectrolyte and a Smart Polymer: a Novel Route to Temperature/Chemical Sensing", contributed talk at the *International Symposium on Functional Electron Systems*, 2nd- 7th June **2013**, Arcachon, France.
- S. Inal, L. Chiappisi, J. D. Kölsch, D. Janietz, M. Gradzielski, A. Laschewsky, D. Neher, "Evaluation of Fluorophore-functionalized Thermoresponsive Copolymers for Sensor Applications", contributed talk at the *DPG Spring Meeting*, 10th-15th March **2013**, Regensburg, Germany.
- S. Inal, J. D. Kölsch, D. Janietz, M. Gradzielski, A. Laschewsky, D. Neher, "Supramolecular Complexes of a Thermoresponsive Polymer and a Conjugated Polyelectrolyte for Sensing Applications", Poster at the *Polydays*, 30th September-2nd October **2012**, Berlin, Germany.
- S. Inal, J. D. Kölsch, D. Janietz, A. Laschewsky, D. Neher, "Fluorophore-functionalized Thermoresponsive Copolymers for Sensor Applications", Poster at the *Smart Polymers*, 7th-9th October **2012**, Mainz, Germany.
- S. Inal, J. D. Kölsch, D. Janietz, A. Laschewsky, D. Neher, "Visualization of the Coil-Globule Transition of a Thermoresponsive Polymer: Probing Interactions with a Conjugated Polyelectrolyte", Poster at the at *DPG Spring Meeting*, 26th-30th March **2012**, Berlin, Germany.

Acknowledgements

First and foremost, I would like to thank Prof. Dr. Dieter Neher who allowed me to undertake this research topic with a lot of freedom and responsibility. Without his continual support, guidance, ideas, and trust, this work could not have been completed and I would have never had the courage to go further.

Throughout my time in Taschentuchlabor project, I have had the chance to collaborate with wonderful scientists and received their valuable help for my demanding problems. Prof. Dr. André Laschewsky has always kept his doors open for discussions; his contribution in this work is undeniable and I am extremely grateful for that. I am also grateful to Dr. Dietmar Janietz and to Dr. Erik Wischerhoff for providing very useful comments. I have appreciated our nice cooperation and fruitful discussions with Jonas D. Kölsch. For the laser light scattering studies, I am extremely grateful to Prof. Dr. Michael Gradzielski and Leonardo Chiappisi who has never refused doing further experiments and always taken the calls about my data analysis dramas. Dr. Michael R. Hansen and Dr. Manfred Wagner are greatly appreciated for the NMR work; special thanks to Michael for his help in answering a lot of challenging questions on that topic. I would like to thank Prof. Ullrich Scherf and Mario Kraft who supplied me with their freshly synthesized conjugated polymers. I would like to thank Dr. Frank Sellrie and Dr. Jörg A. Schenk for their antibodies and interest in my work. I thank Sandor Dippel for not saying no to numerous transmission measurements. I also thank Sina Reiter for her enthusiasm in fluorescent solutions. Besides their friendship, I have appreciated all the help from my colleagues living on the other side of the train tracks (Martin Sütterlin, Jens Buller, Robert Bernin, Anne Enzenberg, Frank Stahlhut, Laura Vogel, Viet Hoang, and Jean-Philippe Couturier).

I have always considered myself very lucky owing to the colleagues that I have. Each person in PWM (Andreas Horka, Andreas Pucher, Burkhard Stiller, Daniel Pinkal, Elke Derling, Harry Weigt, Ilja Lange, Jan Heidbrink, Juliane Kniepert, Jona Kurpiers, Marcel Schubert, Patrick Parnow, Peter Brückner, Robert Steyrleuthner, Riccardo di Pietro, Steffen Roland, Thomas Brenner…) has made my life much nicer each day and Golm a second home to me. Their help in the lab, the enjoyable times in lunch breaks and in all other activates that

we had together for the last five years will be in my memories. I would specifically thank Patrick and Steve for being great office-mates, to Dr. Frank Jaiser for educating me and helping me just with everything.

Special thanks go to my beloved family, Kim Joppen, and Inka Löck for their support and to Robert Lehmann for being there in all of my good and bad times.

Declaration

I hereby certify that the work presented in this thesis has not been submitted to any other university or higher education institute and that this work is my own and that all sources and aids used are listed within. Any results not of my own creation are clearly indicated as such.

Potsdam, October 2013

_____

Sahika Inal